

## ABSTRACT

Title of dissertation: BEAMFORMING ALGORITHMS FOR INFORMATION RELAYING IN DENSE WIRELESS NETWORKS

Mohamed Abdallah, Doctor of Philosophy, 2006

Dissertation directed by: Assistant Professor Haralabos C. Papadopoulos  
Department of Electrical and Computer Engineering

In this dissertation we develop a class of bandwidth-efficient algorithms for information relaying in large-scale wireless ad-hoc networks. The settings we consider involve a single source communicating its data to a destination via the aid of low-power low-cost relay nodes. In its simplest two-hop relaying form, data directly broadcasted to the relays from the source are directly relayed to the destination through a shared fading channel. We assume that the relays employ decode-and-forward or amplify-and-forward preprocessing prior to forwarding their data to the destination via beamforming. The beamforming weights are formed at the destination and feedback to the relays via broadcasting. They are constructed using knowledge of the relay-destination channel coefficients and an  $m$ -bit description of each source-relay channel state information (CSI).

For both relay data preprocessing models, we present methods for optimizing the  $m$ -bit quantizer employed at each relay for encoding its source-relay channel

quality level, and for choosing the beamforming weights at the destination, so as to optimize the destination uncoded bit error rates ( $\Pr(e)$ ). We also study the effect of the relative source-relay relay-destination distances on the  $\Pr(e)$  for both relay preprocessing models. We use our findings to develop locally-optimized adaptive data-preprocessing algorithms at the relays. We also develop extensions involving multi-hop networks with hierarchical cluster-based relaying. At each hop of these relay networks, each of the receiving relays obtains a beamformed version of the data of a distinct subset of the transmitting relays. As our simulations and analysis reveal, making available at each cluster head (CH) an optimized one-bit description of the effective source-relay CSIs associated with the transmitting relays in its cluster is sufficient. Specifically, not making fully available to the CHs, the source-relay CSIs, results in only a minimal loss in the  $\Pr(e)$ .

BEAMFORMING ALGORITHMS FOR INFORMATION RELAYING IN  
DENSE WIRELESS NETWORKS

by

Mohamed Abdallah

Dissertation submitted to the Faculty of the Graduate School of the  
University of Maryland, College Park in partial fulfillment  
of the requirements for the degree of  
Doctor of Philosophy  
2006

Advisory Committee:

Professor Haralabos C. Papadopoulos, Chair

Professor Prakash Narayan

Professor Steven Tretter

Professor Amr Baz

Professor Min Wu

© Copyright by

Mohamed Abdallah

2006

# ACKNOWLEDGEMENTS

First, this great achievement and success is all due to Allah. I thank Allah for HIS great blessings that I have experienced during this long journey.

My deep thanks goes to my advisor Babis Papadopoulos. I am so grateful for his endless support and advise. Babis has spared no time in discussing and suggesting a lot of exciting research ideas. I also would like to thank Babis for evaluating, correcting and organizing this dissertation in order to be understandable and presentable.

I also thank my dissertation committee: Prof. Prakash Narayan, Prof. Steven Tretter, Prof. Amr Baz and Prof. Min Wu, for their invaluable feedback and accepting to serve in my committee. Special thanks goes to Prof. Prakash Narayan for his invaluable comments and discussions that provide a lot of insights to the work presented in this dissertation.

I am grateful to my family who were beside me all the time giving me endless patience and love. I am especially grateful to my father; he was always encouraging me to the best. I also would like to thank my mom for her continuous support and prayers. Deep thanks goes to my younger brother Ahmed and my dear younger sister Sarah. I love you all so much.

Special and deep thanks to my soul mate; my wife Aya. She was always surrounding me with her care and love. I will never forget her nice words to me while I am depressed. Also, I would like to thank my children Jannah and Omar

and I ask for their forgiveness for not spending a good amount of time with them especially at the end phase of this journey.

I am also grateful to all my friends and my colleagues in my department. They are all great and kind persons. I would like to thank my group and office mates: Pham Tien (The God father), DZuls and Yeong-Sun. I will never forget our nice discussions on every aspect in life.

I would like to thank my close friends that helped me emotionally during this process; Adel Youssef, Mohamed Shawky, Tamer ElSharnouny, Moustafa Youssef, Abdel-hameed and Mohamed Zahran. Also special thanks goes to Ahmed Sadek for our research discussions. I would like also thank my dear friend in Egypt; Amr Saad for his continuous asking about me. I hope that our friendship will remain forever.

# DEDICATION

*To my Parents*

*To my Wife Aya*

*To my Children Jannah and Omar*

# Contents

<b>1</b>	<b>Introduction</b>	<b>1</b>
1.1	Thesis outline . . . . .	9
<b>2</b>	<b>Beamforming Algorithms for Ad-hoc Networks: System Model</b>	<b>13</b>
2.1	Signal and Channels Models . . . . .	14
2.2	Relay Preprocessing Model . . . . .	15
2.3	Relay-destination Processing Model . . . . .	19
2.4	Quantizer Model . . . . .	20
<b>3</b>	<b>Beamforming Algorithms for Amplify-and-Forward Relay Model</b>	<b>24</b>
3.1	Beamforming Algorithms . . . . .	25
3.1.1	Full Source-Relay CSI Lower Bound . . . . .	25
3.1.2	Partial Source-Relay CSI Beamforming Algorithm . . . . .	29
3.2	Simulations . . . . .	35
3.2.1	Quantizer Threshold Design . . . . .	36
3.2.2	Performance Analysis . . . . .	37



3.2.3	Optimal Relay Location . . . . .	45
<b>4</b>	<b>Beamforming Algorithms for Decode-and-Forward Relay Model</b>	<b>48</b>
4.1	Beamforming Algorithms . . . . .	50
4.1.1	High Relay-Destination SNR Bounds . . . . .	50
4.1.2	SNR maximizing Beamforming Algorithms . . . . .	53
4.1.3	Beamforming via Equivalent Amplify-and-Forward Relay Model	55
4.2	Simulations . . . . .	58
4.2.1	Quantizer Threshold Design . . . . .	59
4.2.2	Performance Analysis . . . . .	61
4.3	Location-optimized Preprocessing Relay Strategy . . . . .	68
<b>5</b>	<b>Location-Optimized Adaptive Beamforming Algorithms</b>	<b>73</b>
5.1	Adaptive Beamforming Algorithms for Hybrid Networks . . . . .	77
5.1.1	High Average Relay-Destination SNR Beamformers . . . . .	78
5.1.2	Equivalent Amplify-and-forward Beamformers for Hybrid Net- works . . . . .	80
5.2	Destination-based Relay Processing Selection Strategy . . . . .	83
5.2.1	Optimal Selection Strategy for Homogenous Networks . . . . .	85
5.2.2	Equivalent-channel Relay Selection Strategy . . . . .	89
5.2.3	Node-by-Node Basis Relay Selection Strategy . . . . .	93
5.3	Relay-based Preprocessing Selection Strategy . . . . .	97

<b>6</b>	<b>Beamforming Algorithms for Multi-hop Networks</b>	<b>101</b>
6.1	System Model . . . . .	103
6.2	Beamforming algorithms . . . . .	107
6.3	Performance Analysis and Power Allocation Strategy . . . . .	110
6.4	Relay Location Strategy . . . . .	122
<b>7</b>	<b>Conclusion and Future Directions</b>	<b>125</b>
7.1	Future Directions . . . . .	127
<b>A</b>	<b><math>\Pr(e)</math> Analysis for Decode-and-forward Relay Model</b>	<b>130</b>
<b>B</b>	<b><math>\Pr(e)</math> Analysis for Decode-and-Forward Relay Model at High Relay-destination Average SNR</b>	<b>132</b>

# List of Figures

1.1	Block diagram of a wireless ad-hoc network with feedback . . . . .	2
2.1	System block diagram including data model, relay model and source-relay and relay-destination channel models. . . . .	16
2.2	Block diagrams of the relays and the destination processors for the amplify-and-forward relay model. . . . .	17
2.3	Block diagrams of the relays and the destination processors for the decode-and-forward model. . . . .	18
3.1	Optimal quantizer threshold, $\gamma_t^{\text{opt}}$ , as a function of $\bar{\gamma}_s$ . The solid curve depicts $\gamma_t^{\text{opt}}$ obtained using numerical methods while the dashed curve depicts $\mathcal{C}_{\text{AF}}(\bar{\gamma}_s)$ in (3.37). . . . .	37
3.2	The successively lower solid curves and the successively lower dash curves depicts the destination $\Pr(e)$ for $L = \{2, 3\}$ obtained using simulations and $\Pr(e)$ expression (3.15), respectively, as a function of $\bar{\gamma}_{\text{sd}}$ assuming the destination has full knowledge of the source-relay CSI, $\gamma_{s_i}$ . . . . .	39

3.3	The successively lower solid curves marked by 'x', the successively lower curves marked by 'o', the successively lower curves marked by '∇' depict the destination $\Pr(e)$ for $L = \{2, 4\}$ as a function of $\bar{\gamma}_{sd}$ assuming the destination has full knowledge of the source-relay CSI, $\gamma_{s_i}$ , optimized <i>one-bit</i> descriptions of $\gamma_{s_i}$ , and average value of $\gamma_{s_i}$ , respectively. . . . .	41
3.4	The successively lower solid curves marked by 'x' and the successively lower curves marked by 'o' depicts the destination $\Pr(e)$ for $\bar{\gamma}_{sd} = \{5\text{dB}, 10\text{dB}, 15\text{dB}\}$ as a function of $\mu$ assuming the destination has full knowledge of the source-relay CSI, $\gamma_{s_i}$ , and optimized <i>one-bit</i> descriptions of $\gamma_{s_i}$ , respectively. . . . .	43
3.5	The solid and the dashed curves depict the destination $\Pr(e)$ performance of the <i>one-bit</i> beamforming algorithms as a function of $\gamma_t/\gamma_t^{\text{opt}}$ (in dB) for $L = 4$ and $6$ , respectively, and $\bar{\gamma}_{sd} = 10$ dB. . . . .	44
3.6	The successively lower solid curves marked by 'x' and the successively lower solid curves marked by 'o' depicts the destination $\Pr(e)$ for $L = \{5, 10, 15\}$ as a function of $\tau$ for the decode-and-forward relay model and the amplify-and-relay model, respectively. . . . .	46
4.1	The dashed curve depicts the SNR-maximizing beamforming weight in (4.22) for high average relay-destination SNR while the solid curve depicts the optimal weights in (4.7). . . . .	55

4.2	Pr( $e$ ) of the optimal linear detector (4.1), (B.1), (B.2) as a function of the quantizer threshold assuming $\bar{p}_s = 0.1$ , for $L = 10$ (dash), and $L = 15$ (solid). . . . .	60
4.3	Optimal quantizer threshold, $p_t^{\text{opt}}$ , as a function of $\bar{p}_s$ . The dashed, dotted, and dash-dot curves show $p_t^{\text{opt}}$ for $L = 5, 15$ , and $25$ , respectively, while the solid curve depicts $\mathcal{C}_{\text{DF}}(\bar{p}_s)$ in (4.32). . . . .	62
4.4	The successively lower solid, dashed, and dash-dot curves depict the destination Pr( $e$ ) for $L = \{2, 4\}$ as a function of $\bar{\gamma}_{\text{sd}}$ assuming the destination has full knowledge of the source-relay CSI, $p_{s_i}$ , optimized <i>one-bit</i> descriptions of $q_i$ , and average source-relay CSI $\bar{p}_s$ , respectively. . . . .	64
4.5	The successively lower solid curves marked by 'x' and the successively lower curves marked by 'o' depicts the destination Pr( $e$ ) for $\bar{\gamma}_{\text{sd}} = \{5\text{dB}, 10\text{dB}, 15\text{dB}\}$ as a function of $\mu$ assuming the destination has full knowledge of the source-relay CSI, $p_{s_i}$ , and optimized <i>one-bit</i> descriptions $q_i$ , respectively. . . . .	65
4.6	The solid curves marked by 'x' and 'o' depict the destination Pr( $e$ ) performance of the <i>one-bit</i> beamforming algorithms as a function of $p_t/p_t^{\text{opt}}$ for $L = 4$ and $6$ , respectively, and $\bar{\gamma}_{\text{sd}} = 7$ dB. . . . .	66
4.7	The figure depicts the destination Pr( $e$ ) performance of the beamforming algorithms formed based on $p_{s_i}$ as function of $\frac{D}{4}$ for $L = 3$ and $\bar{\gamma}_{\text{sd}} = 19$ dB. . . . .	67

4.8	The successively lower solid curves marked by 'x' and the successively lower dash curves marked by 'o' depicts the destination $\Pr(e)$ for $L = \{3, 4\}$ as a function of $\bar{\gamma}_{sd}$ for the SNR-maximizing beamformers and the equivalent-channel beamformers, respectively, when the destination knows the values of $\{p_{s_i}\}'s$ . . . . .	69
4.9	The successively lower solid curves marked by 'x' and the successively lower solid curves marked by 'o' depicts the destination $\Pr(e)$ for $L = \{5, 10, 15\}$ as a function of $\tau$ for the decode-and-forward relay model and the amplify-and-relay model, respectively. . . . .	70
5.1	The solid curves marked by 'x' and marked by 'o' depicts the destination $\Pr(e)$ for $L = 8$ and $\bar{\gamma}_{sd} = 5\text{dB}$ as a function of $\tau$ assuming the destination has full knowledge of the source-relay CSI. The solid curves marked by '∇' depicts the $\Pr(e)$ provided with the optimal selection strategy developed in Sec. 5.2.1 for homogenous networks. . . . .	87
5.2	The solid curves marked by 'x' depicts the probability that the selection strategy chooses decode-and-forward model, $\Pr_{DF}$ , as a function of $\tau$ . . . . .	88
5.3	The solid curves marked by 'x' and marked by 'o' depicts the destination $\Pr(e)$ for $L = 8$ and $\bar{\gamma}_{sd} = 5\text{dB}$ as a function of $\tau$ for the case of optimal selection strategy and equivalent-channel selection strategy, respectively. . . . .	91

5.4	The solid curves marked by 'x' and 'o' depict the probability of employing decode-and-forward relaying, $\Pr_{\text{DF}}$ , as a function of $\tau$ for the case of optimal selection strategy and equivalent-channel selection strategy, respectively . . . . .	92
5.5	The solid curves marked by 'x' and marked by 'o' depicts the destination $\Pr(e)$ for $L = 8$ and $\bar{\gamma}_{\text{sd}} = 5\text{dB}$ as a function of $\tau$ for the case of optimal selection strategy and node-by-node selection strategy, respectively. . . . .	95
5.6	The solid curves marked by 'x' and 'o' depict the probability of employing decode-and-forward relaying, $\Pr_{\text{DF}}$ , as a function of $\tau$ for the case of optimal selection strategy and node-by-node selection strategy, respectively . . . . .	96
5.7	The solid curves marked by 'x', 'o' '∇' depict the destination $\Pr(e)$ for $L = 10$ and $\bar{\gamma}_{\text{sd}} = 5\text{dB}$ as a function of $\tau$ for the case of relay-based selection strategy, employing AFB relay model, and employing DFB relay model, respectively. . . . .	99
5.8	The solid curve depicts the probability of employing decode-and-forward relaying, $\Pr_{\text{DF}}$ , as a function of $\tau$ for the case of relay-based selection strategy. . . . .	100
6.1	A system model for a three-hop network. . . . .	104

6.2	The exponential probability density function of the SNR at the first hop. . . . .	115
6.3	The probability density function of the aggregate SNR at each hop for an amplify-and-forward relaying system that employs optimized one-bit quantizers at the relays. . . . .	116
6.4	The successively lower solid curves and the dashed curves depict the destination $\Pr(e)$ performance of the optimized <i>one-bit</i> and infinite-bit amplify-and-forward beamforming algorithms, respectively, at the first, second, third and fourth hop. . . . .	117
6.5	The probability density function of the aggregate SNR at each hop for an decode-and-forward relaying system that employs optimized one-bit quantizers at the relays. . . . .	119
6.6	The successively lower solid curves and the dashed curves depict the destination $\Pr(e)$ performance of the optimized <i>one-bit</i> and infinite-bit decode-and-forward beamforming algorithms, respectively, at the first, second, third and fourth hop. . . . .	120
6.7	The successively lower solid curves and the dashed curves depict the destination $\Pr(e)$ performance of using amplify-and-forward and decode-and-forward relaying algorithms, respectively, at the first, second, third hop and destination. . . . .	121



6.8 The destination  $\Pr(e)$  as a function of  $1 - \tau_d$  assuming three hop networks and full knowledge of aggregate SNR available at the CHs. The solid curve represents the amplify-and-forward model while the dash curve represents the decode-and-forward model. . . . . 124

# List of Tables

6.1	The optimal quantizer thresholds normalized to the mean of the aggregate SNR, $\gamma_{t_{i\zeta}}/\bar{\gamma}_{i\zeta}^{\text{agg}}$ , computed via Monte-Carlo simulations at each hop for a four multi-hop network employing amplify-and-forward relaying. . . . .	114
6.2	The optimal quantizer thresholds normalized to the mean of the aggregate SNR, $p_{t_{i\zeta}}/\bar{p}_{i\zeta}$ , computed via Monte-Carlo simulations at each hop for a four multi-hop network employing decode-and-forward relaying. . . . .	115

# Chapter 1

## Introduction

In this dissertation we present algorithmic techniques for information relaying in a class of wireless multi-hop networks. The setting of interest involve a network setting whereby a source is communicating its data to a destination via the aid of a large-set of low-power low-cost relay nodes, and is depicted in its simplest form in Fig. 1.1. Aside from conventional multi-hop wireless networks, these type of problems arise in applications that involve the use of wireless sensor networks for data collection [1]. Indeed, these types of networks are becoming increasingly attractive in many military and civilian applications, including target tracking and identification, and environmental monitoring [2–6].

The abundance of low-cost and low-power nodes in large-scale wireless networks, coupled with limitations in the available bandwidth, place constraints on the type of processing and signaling that can be employed for relaying information across the network. Given that a source can efficiently convey its messages to

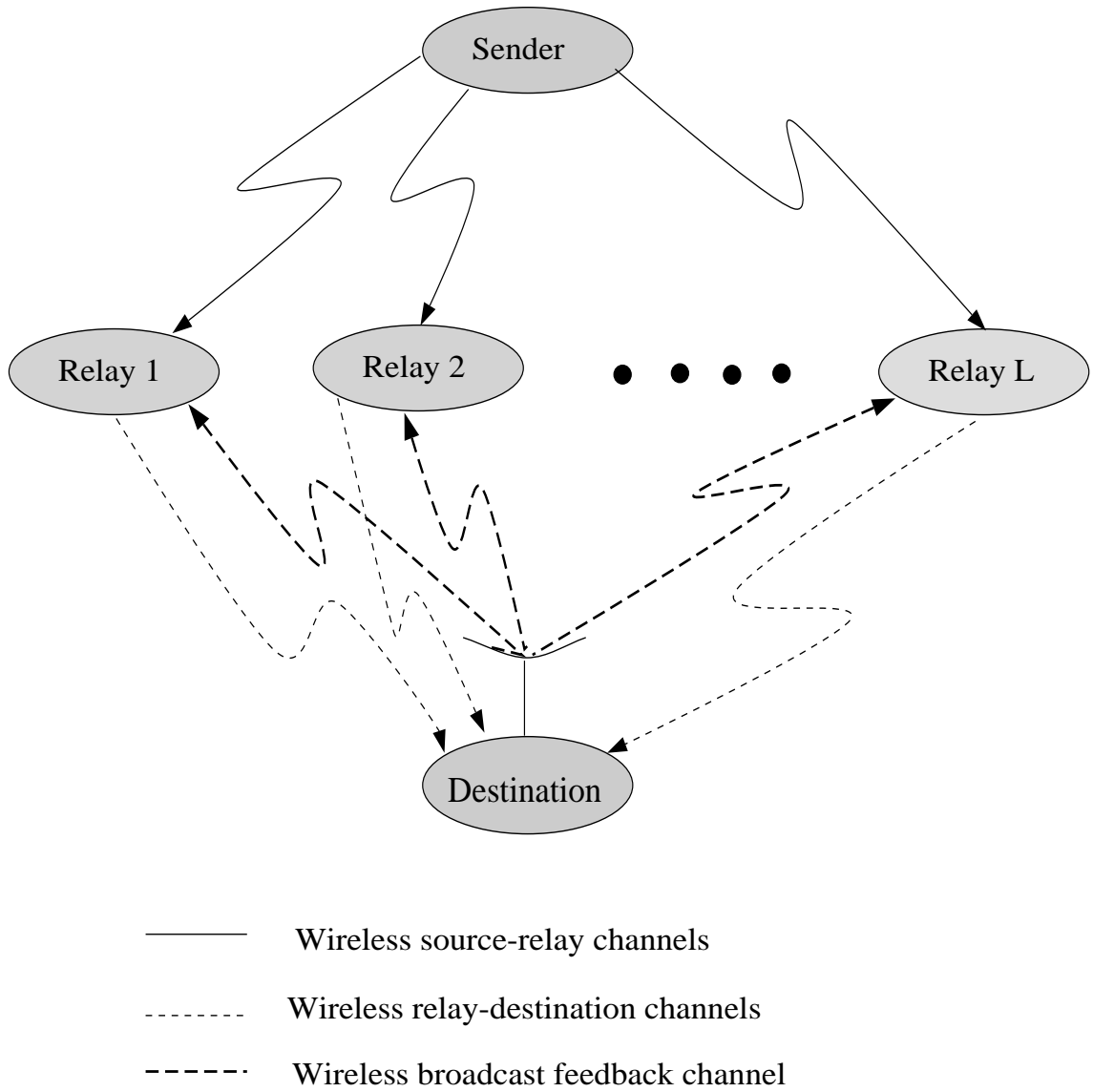


Figure 1.1: Block diagram of a wireless ad-hoc network with feedback

multiple neighboring relay nodes at the expense of no extra power or bandwidth via broadcasting, there is an inherent need for relay-signaling techniques that can provide spatial diversity benefits, while maintaining similar bandwidth efficiency.

Capacity of large-scale relaying wireless networks received considerable attention in the information theory community. In their landmark paper Cover and El Gamal [7] obtained the capacity of degraded, reversely degraded and feedback non-faded relay channels. In [8], Gupta and Kumar considered  $n$  nodes network with uniform traffic pattern and point to point coding. They showed that the aggregate capacity grows by  $O(\sqrt{n})$  in bits-meters per second for large  $n$  suggesting that the throughput per node goes to zero as the number of nodes increases. Grossglauser and Tse in [9] considered a modified version of the model in [8] that includes node mobility. They showed that the aggregate capacity increases to  $O(n)$  bits per second assuming unbounded delay allowed between a sender and a destination. Gaspar and Vetterli [10] considered extensions for same model in [8], that allow for relay traffic pattern and network coding. They showed that capacity of such  $n$  node wireless network improves to  $O(\log(n))$  bits per second. Gupta and Kumar [11] developed an information-theoretic scheme to develop the achievable rate region for wireless ad-hoc networks with arbitrary size and topology.

Motivated by the large-scale economics of wireless ad-hoc networks as well as promising information-theoretic results, there has been recently research efforts to develop communication algorithms that exploit the spatial diversity provided by

these networks. It is mainly based on the idea that a set of relay nodes with correlated versions of an information bearing signal can collaboratively provide diversity benefits at the destination when viewed as a virtual antenna array. The resulting concept of cooperative transmission was originally explored in [12] in the context of CDMA and [13–15] in the context of TDMA. Collectively, the works present cooperative protocols and methods for evaluating their performance limits for various relay strategies. In the case where the set of relays is small, it was shown that cooperative transmission can provide spatial diversity gains as well as energy and bandwidth savings. In dense networks with large numbers of relay nodes, however, there is an even greater need for neighboring nodes to share the wireless medium in relaying their messages, in a way that the total bandwidth employed by the relays does not increase appreciably with the number of relays employed per hop in the network.

Another class of applications in which dense networks are utilized for information relaying involves large-scale wireless sensor networks. One class of research activities of interest in this area, focus on the problem of resource-efficient data fusion based on large collections of coarse encodings of measurements collected by sensors in the networks. In [5, 16], optimal data fusion algorithms have been developed in the case where the sensor encodings are made available to the fusion algorithm through orthogonal and noise-free channels. Recently, in [17], the fusion algorithms have been generalized to the case where the sensor encodings are

transmitted to the fusion center over fading channels.

In this dissertation we focus on achieving reliable information relaying in dense relay networks subject to limited bandwidth constraints. The majority of the research efforts in the area of relay networks have focused on system models where signaling from the relays to a destination is over orthogonal channels, and assume, with the exception of [18], full knowledge at the destination of the channel state information (CSI) of all channels involved in communication. The main potential drawbacks associated with these two assumptions is the considerable additional bandwidth required to establish relay-orthogonal communication and the amount of signaling overhead and bandwidth needed for making available to the destination the CSI vector of the associated source-relay channels.

The settings we consider involve a single source communicating its data to a destination via the aid of low-power low-cost relay nodes. In its simplest two-hop relaying form, data directly broadcasted to the relays from the source are directly relayed to the destination through a shared fading channel. To account for the inherent bandwidth limitations in these relay networks, we focus on the case that the relays communicate their received versions of the source data over a shared fading channel. In this context, the destination receives a linear superposition of the signals transmitted by relays over nonselective fading channels. We also assume that there is no direct link between the source and the destination and in general there may be multi-hop connection between the source and the destination.

For the proposed relay-destination channel model, we consider relay-destination beamforming algorithms whereby the processed signal at each relays is scaled by a (complex) beamforming factor prior to transmission to the destination. Beamforming has proved an efficient method for data transmission over fading channels as proper selection of the beamforming weights used by the relays can yield spatial diversity gains and energy savings [19, 20]. Beamforming has also proved to be an efficient method for source localization; *cf.*, [21] for detailed surveys on source localization and beamforming. We consider two different relay pre-processing strategies: i) Amplify-and-forward via beamforming (AFB), and ii) Decode-and-forward via beamforming (DFB). Specifically, the received signals at the relays are either amplified or decoded prior to forwarding to the destination.

We assume that the beamforming weights are computed at the destination and feedback to the relays over a broadcast channel. We remark that despite the fact that the feedback channel incurs an additional overhead bandwidth, it is still relatively small compared to that required by orthogonal channels. This is due to the relatively large network size addressed in our problems and the slowly time-variations of the quasi-static non-selective fading channels involved in communications.

The quality of the beamforming algorithms depends on the composite relays-destination channel and the quality of the CSI that is available at the destination about the individual source-relay channels. We assume that the CSI of the composite relays-destination channel is available at the destination; for instance, estimates of



the individual relay-destination fading coefficients can be obtained via pilot-assisted techniques. As the CSI of the individual (slowly time-varying) source-relay channels, however, is *not* directly observable at the destination, these schemes require that the CSI information of the source-relay channels is communicated to the destination by the relays. In particular, we focus on the case where each relay broadcasts to the destination its individual source-relay CSI at various levels of precision.

In this dissertation we develop beamforming algorithms for the two relaying preprocessing strategies that optimize the destination uncoded bit error rates ( $\Pr(e)$ ). The beamforming weights are formed based on the relays-destination composite CSI and quantized descriptions of the source-relay CSI. Several key challenges arise in developing beamforming algorithms that exploit partial CSI of the source-relay channels at the destination. Due to the complex dependence of the  $\Pr(e)$  on the beamforming weights and the available CSI, developing closed form expressions and iterative algorithms to find the optimal beamforming weights appears intractable. Most of the research approaches used in the literature amount to choosing the beamforming weights so as to minimize the received signal-to-noise (SNR) ratio at the destination [12, 13]. Increasing (the notion of) SNR, however, does not translate to lower  $\Pr(e)$  performance. As we show beamformers can be developed for some relay data-preprocessing models that outperform the SNR-maximizing beamformers in terms of destination  $\Pr(e)$ . Another related challenging aspect of the problem involves designing optimal  $m$ -bit quantizer of the source-relay CSI exploited at the

relays so as to optimize the destination  $\Pr(e)$ . The choice of the data relay models at the relays can also affect the achievable  $\Pr(e)$  performance. One key question in this context is how to select the data preprocessor at each relay to locally optimize the performance.

Scaling these approaches to multi-hop setting raises additional challenges. So first, it is important to determine how approaches developed for the two-hop setting can be efficiently extended to multi-hop settings. These include the selection of the beamforming weights at each receiving relay (destination) as well as the CSI information provided by the associated transmitting relays. In particular, as multi-hop networks become large, joint optimization design of the beamforming weights and the CSI provided becomes impractical. Alternatively, we can consider locally optimized selection for the CSI quality at the relays and the beamforming weights that exploit extensions of the two-hop settings.

To this end, we first develop beamformers for a two-hop network formed based on the relay-destination CSI and  $m$ -bit quantized descriptions of the source-relay CSI. We develop methods for optimizing the quantizer design at each relay and selecting the associated beamforming weights that optimize the destination  $\Pr(e)$ . We show that the beamformers based on an optimized one-bit source-relay CSI provide most of the benefits in terms of the destination  $\Pr(e)$  assuming full knowledge of source-relay CSI is available at the destination.

We also determine the optimal relative relay location with respect to the

source and the destination associated with each relay preprocessing strategy. Assuming the node locations are not available, we develop adaptive beamforming algorithms. In these algorithms, the type of the preprocessing at each relay is selected based on each relay source-relay and relay-destination CSI so as to optimize the destination  $\Pr(e)$  given any relative location.

We next provide extensions by considering the problem of finding the  $\Pr(e)$ -optimized beamforming weights for multi-hop networks. We consider a hierarchical clustering approach in processing the information from the source to the destination. At each hop, we assume that the nodes are grouped into clusters. Each cluster is composed of transmitting relays and one receiving cluster head (CH). In this context, we addressed the problem of finding the beamforming weights as well as the  $m$ -bit source-relay CSI quantizer employed at the relays of each cluster. We develop a systematic way to select the beamforming weights locally at each cluster as the data flows from the source to the destination. In addition, we develop a power allocation strategy for these multi-hop networks that optimize the  $\Pr(e)$  values attained per hop which in turn optimize the destination  $\Pr(e)$ .

## 1.1 Thesis outline

In this dissertation, we develop bandwidth-efficient beamforming algorithms for information relaying in wireless ad-hoc multi-hop networks.

In Chapter 2, we present the main components of the system model including

source signal and channel models, preprocessing relaying strategies as well as the relay-destination model.

In Chapter 3, we consider the amplify-and-forward via beamforming (AFB) relay model in a two-hop ad-hoc network setting. We develop beamformers based on the relay-destination CSI and an  $m$ -bit quantized versions of the source-relay CSI. We develop methods for optimizing the  $m$ -bit source-relay CSI quantizer so as to minimize the destination  $\Pr(e)$ . Our simulations show that the  $\Pr(e)$  performance loss attained using only a one-bit source-relay CSI quantizer is negligible compared to the  $\Pr(e)$  values attained using full source-relay CSI. We then determine the optimal relative relay location with respect to the source and destination that optimizes the  $\Pr(e)$  values.

In Chapter 4, we consider the decode-and-forward via beamforming (DFB) relaying strategies whereby the relays decode their received signals in a two-hop network setting. We present a class of beamforming algorithms based on an "equivalent" amplify-and-forward relay model of the decode-and-forward source relay model. Furthermore, we present a framework for quantizing the source-relay CSI so as to minimize the data  $\Pr(e)$  at the destination. The algorithms we develop outperform in terms of  $\Pr(e)$  the SNR maximizing beamformers and are only slightly inferior to beamformers that exploit perfect CSI knowledge of the source-relay channels at the destination. We then determine the  $\Pr(e)$ -optimized relative relay location for the DFB model. We then develop a method for determining the preprocessing type

at the relays that optimizes the  $\Pr(e)$  for a given location.

In Chapter 5, we develop location-optimized adaptive beamforming algorithms whereby the preprocessing strategy at each relay is selected based on its source-relay and relay-destination CSI so as to optimize the destination  $\Pr(e)$  at any given relative relay location. We first develop beamforming algorithms for hybrid networks where a subset of the nodes is employing decode-and-forward and the other subset is employing amplify-and-forward. We next develop node-by-node basis destination-based and relay-based selection strategies. We explore the tradeoffs between the selection strategies in terms of the  $\Pr(e)$  performance and the bandwidth required for each strategy.

In Chapter 6, we develop beamforming algorithms for multi-hop networks based on the beamformers developed in Chap. 3 and Chap. 4. We first develop a system model that involves hierarchical clustering approach for aggregating the information from the source to the destination. We develop a systematic way for constructing the beamforming weights locally at each hop. For the case of using one-bit source-relay CSI quantizer, we design the quantizers at each hop that optimize the  $\Pr(e)$  performance at each clustering level for both the amplify-and-forward and the decode-and-forward relay models. We finally present algorithms for determining the relative relay locations as well as the relay strategy at each hop that optimize the  $\Pr(e)$  at the destination.

Finally, a summary of the main contributions is presented in chapter 7 as

well as future directions for the research problems considered in this dissertation.

## Chapter 2

# Beamforming Algorithms for Ad-hoc Networks: System Model

In this chapter, we present the system model of the two-hop ad-hoc relay network for which beamforming algorithms are developed in Chap. 3, 4, & 5. In addition, the model serves as the basic building block for the multi-hop relay networks presented in Chap. 6. In particular, we consider two types of models for processing the received data signals at the relays (which, in the case of sensor networks, may also represent the measurements observed at the sensor “relays”) prior to forwarding them via beamforming to the destination. In the first relay model, referred to as amplify-and-forward via beamforming (AFB), the relays scale their received versions of the source signal prior to transmission to the destination. In the second relay model, referred to as decode-and-forward via beamforming (DFB), the relay data is first decoded and then scaled via a beamforming weight prior to transmission to the destination. For both relay models, we assume that the beamforming weights are constructed at the

destination and subsequently fed back to the relays via a broadcast feedback channel. We also suppress any timing/synchronization issues, *i.e.*, we assume that the signals transmitted from the relays arrive at the destination “fully synchronized” [22].

In the subsequent sections, we present the source signal, source-relay and relay-destination channels model, as well as the relay and destination process models.

## 2.1 Signal and Channels Models

The setting we consider in this dissertation for a two-hop network is depicted in Fig. 2.1 and involves a source communicating its data sequence,  $x[n]$ , to a destination via the aid of  $L$  intermediate relay nodes. We assume that  $x[n]$  is a zero-mean independent and identically distributed (IID) binary-valued sequence  $x[n]$ , with  $x[n] \in \{1, -1\}$ . We adopt frame-by-frame processing, according to which for the duration of any frame, the source-relay and relay-destination channels are assumed to remain constant. In particular, as shown in Fig. 2.1, the source-relay channels are modeled as quasi-static mutually independent channels whereby the  $n$ th observation in a given frame at the  $i$ th relay is given by

$$y_{s_i}[n] = \sqrt{P_s} \alpha_{s_i} x[n] + v_i[n], \quad (2.1)$$

where  $P_s$  is the source transmit power, the source-relay channel fading coefficients  $\{\alpha_{s_i}\}$  are zero-mean mutually IID circularly symmetric (CS) Gaussian random variables with variance  $E[|\alpha_{s_i}|^2] = \sigma_s^2$ , and the  $v_i[n]$ 's are zero-mean mutually IID CS



Gaussian random processes, each with variance  $\sigma_v^2$ , and independent of the  $\alpha_{s_i}$ 's and  $x[n]$ . The quality of each source-relay channel can be expressed in terms of its SNR, defined as

$$\gamma_{s_i} = \frac{P_s |\alpha_{s_i}|^2}{\sigma_v^2} \quad (2.2)$$

with average value

$$\bar{\gamma}_s = \frac{P_s \sigma_s^2}{\sigma_v^2}. \quad (2.3)$$

Similarly, as shown in Fig. 2.1, the sequences  $y_{r_i}[n]$ , corresponding to processed versions of the associated received relay sequences,  $y_{s_i}[n]$ , are communicated by the relays to the destination via a composite quasi-static fading channel, *i.e.*, the  $n$ th observation at the destination is given by

$$y_d[n] = \sum_{i=1}^L \alpha_{r_i} y_{r_i}[n] + w[n] \quad (2.4)$$

where the relay-destination channel fading coefficients  $\{\alpha_{r_i}\}$  are mutually IID zero-mean CS Gaussian random variables with variance  $\sigma_r^2$ , while  $w[n]$  is a zero-mean IID CS Gaussian random process with variance  $\sigma_w^2$ . We further assume that  $x[n]$ , the  $\{\alpha_{s_i}\}$ 's, the  $\{v_i[n]\}$ 's, the  $\{\alpha_{r_i}\}$ 's, and  $w[n]$  are mutually independent.

## 2.2 Relay Preprocessing Model

In this section, we consider two types of front-end processing at the relays: (i) the amplify-and-forward via beamforming (AFB) relay model, and (ii) the decode-and-forward via beamforming (DFB) relay model. The AFB relay model is shown in

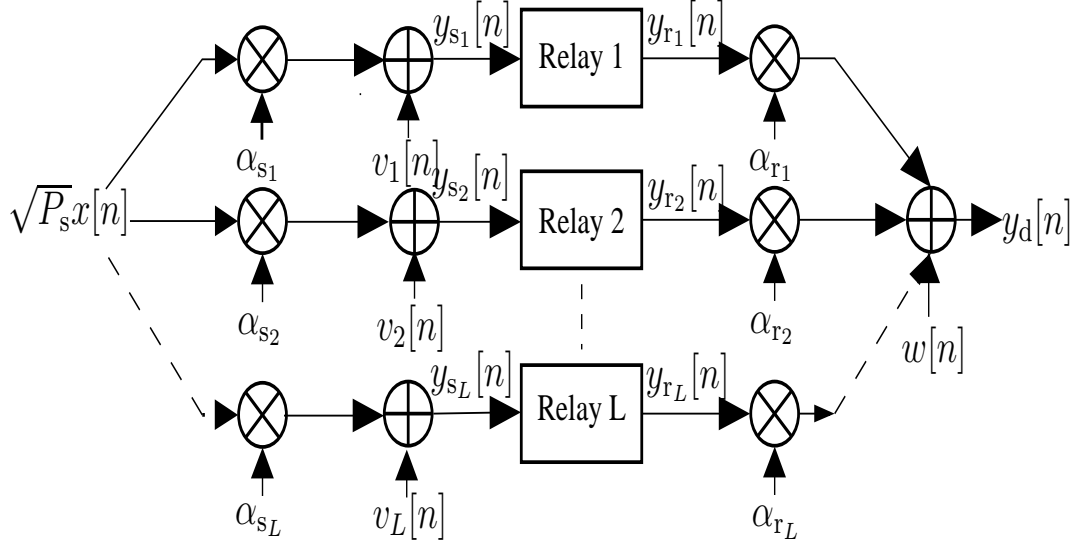


Figure 2.1: System block diagram including data model, relay model and source-relay and relay-destination channel models.

Fig. 2.2 and corresponds to first scaling the received sequences at the relays,  $y_{s_i}$ , to achieve unit-power output signals prior to forwarding the signal to the destination. In particular, without loss of generality, the received relay sequences  $y_{s_i}[n]$  at the  $i$ th relay are scaled by the gain factor

$$G_i = \frac{1}{\alpha_{s_i} \sqrt{P_s (1 + \xi_{s_i})}}, \quad (2.5)$$

resulting in the following unit-power  $n$ th relay output,

$$z_{a_i}[n] = \frac{1}{\sqrt{1 + \xi_{s_i}}} x[n] + \frac{\sqrt{\xi_{s_i}}}{\sqrt{1 + \xi_{s_i}}} \bar{v}_i[n] \quad (2.6)$$

where  $\xi_{s_i}$  is the inverse of  $\gamma_{s_i}$  and the  $\bar{v}_i[n]$ 's are independent CS IID Gaussian random processes, independent of  $x[n]$  and with  $\bar{v}_i[n] \sim \mathcal{N}(0, 1)$ .

As shown in Fig. 2.3, in the DFB relay model the received sequences  $y_{s_i}[n]$

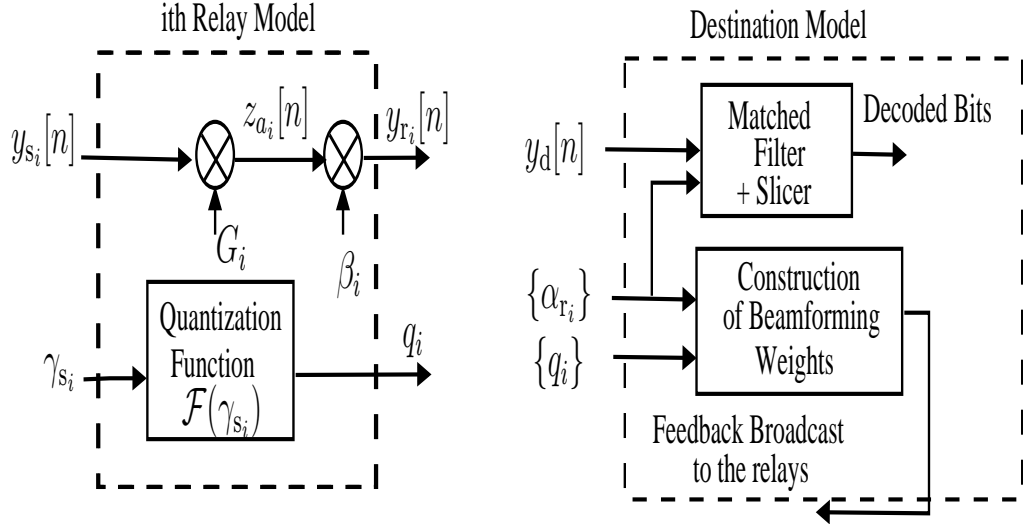


Figure 2.2: Block diagrams of the relays and the destination processors for the amplify-and-forward relay model.

are first decoded (using a matched filter followed by a slicer) prior to forwarding via beamforming to the destination. The  $n$ th decoded output at the  $i$ th relay can be modeled as,

$$z_{d_i}[n] = \epsilon_i[n] x[n] \quad (2.7)$$

where  $\epsilon_i[n]$  denotes a set of mutually independent IID error sequences, satisfying

$$\epsilon_i[n] = \begin{cases} 1, & \text{with probability } 1 - p_{s_i} \\ -1, & \text{with probability } p_{s_i} \end{cases}, \quad (2.8)$$

and where  $p_{s_i}$  denotes the “instantaneous” BER associated with the given frame channel realization and can be viewed as a metric of the individual source-relay CSI quality. Specifically,  $p_{s_i}$  can be expressed in terms of the instantaneous SNR,  $\gamma_{s_i}$ , as

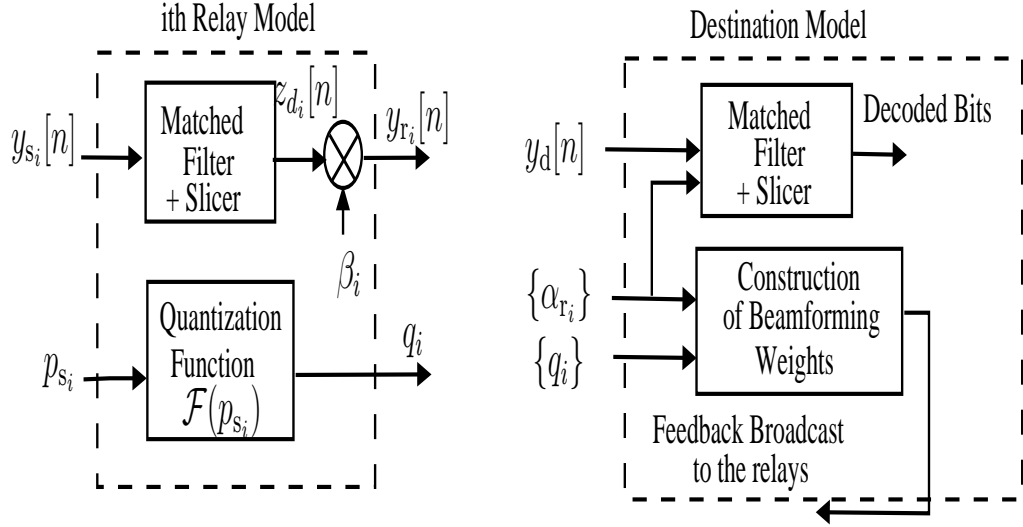


Figure 2.3: Block diagrams of the relays and the destination processors for the decode-and-forward model.

follows

$$p_{s_i} = Q(\sqrt{2\gamma_{s_i}}) . \quad (2.9)$$

Similarly the frame-averaged BER,  $\bar{p}_s$ , is given by

$$\bar{p}_s = E [p_{s_i}] = 0.5 \left( 1 - \sqrt{\frac{\bar{\gamma}_s}{1 + \bar{\gamma}_s}} \right) , \quad (2.10)$$

where  $\bar{\gamma}_s$  is given by (2.3). For both relay processing models, it is assumed that each relay has full knowledge of its own source-relay CSI, *i.e.*, the relay knows  $p_{s_i}$  (or, equivalently, either  $\gamma_{s_i}$ , or  $\xi_{s_i}$ ).

## 2.3 Relay-destination Processing Model

In light of the composite channel (2.4), we consider employing relay-destination beamforming where the output of the  $i$ th relay is scaled by a complex beamforming weight  $\beta_i$  prior to transmission over the shared channel. As a result,  $y_d[n]$  in (2.4) is given by

$$y_d[n] = \sum_{i=1}^L \alpha_{r_i} \beta_i z_i[n] + w[n], \quad (2.11)$$

where the sequence  $z_i[n]$  represents  $z_{a_i}[n]$  in the AFB relay model and  $z_{d_i}[n]$  in the DFB relay model, and where we assume a total transmit power constraint at the relays

$$\sum_i^L |\beta_i|^2 = P_d. \quad (2.12)$$

In light of (2.11)–(2.12), the quality of the  $i$ th relay-destination channel can be expressed in terms of the  $i$ th relay-destination channel SNR  $\gamma_{r_i} = P_d |\alpha_{r_i}|^2 / \sigma_w^2$ , or, equivalently, its inverse,  $\xi_{r_i} = \gamma_{r_i}^{-1}$ .

Also shown in Figs. 2.2 and 2.3 is the processing performed at the destination for the AFB and DFB relay models, respectively. In addition to implementing a straightforward matched filter detector, the destination computes and broadcasts back subject to (2.12) a set of beamforming weights,  $\{\beta_i\}$ , that are to be used by the relays for signaling, according to (2.11). In computing the  $\{\beta_i\}$ 's we assume that the  $\{\alpha_{r_i}\}$ 's (and, thus, the associated  $\{\xi_{r_i}\}$ 's) are known at the destination, and consider various levels of knowledge available at the destination regarding the source-relay CSIs. Aside from the case of perfect CSI available (the destination

knows  $\{\gamma_{s_i}\}$  or,  $\{p_{s_i}\}$ ), we also consider the case where the  $i$ th relay sends to the destination a quantized representation of the source-relay CSI (represented by  $\gamma_{s_i}$  and  $p_{s_i}$  for the AFB and DFB relay models, respectively), obtained using a quantizer,  $\mathcal{F}(\cdot)$ .

We also consider adaptive beamforming strategies whereby the destination can select, based on the available knowledge of the source-relay and relay-destination CSIs, the type of processing to be performed at each relay. In particular, the destination sends over its feedback channel  $L$  bits to the  $L$  relays informing each one whether to use the AFB relay model or the DFB relay model. In Chap. 5, we develop these adaptive beamforming algorithms and examine its  $\Pr(e)$  performance against using only AFB or DFB relay models.

## 2.4 Quantizer Model

Letting  $\{\varrho_k\}_{k=1}^{\mathcal{K}}$ , with  $\mathcal{K} = 2^m$ , denote the set of quantizer levels of an  $m$ -bit quantizer, we focus on quantizers for which the individual quantizer-level preimages,  $I_k = \mathcal{F}^{-1}(\varrho_k)$ , are contiguous regions of the nonnegative real axis for all  $k$ . We remark that any two such  $m$ -bit quantizers with the same set of individual quantizer-level preimages  $\{I_k\}$  provide the *same* information about the source-relay channels, provided the quantization levels (*i.e.*, the  $\varrho_k$ 's) are distinct for each quantizer. As a result, such quantizers are effectively fully described via the set of their quantization

thresholds. Without loss of generality, we thus set the quantization levels as follows,

$$q_k = k, \quad \text{for } k = 0, 1, 2, \dots, \mathcal{K}. \quad (2.13)$$

Although the quantizer can be applied to either the  $\{\gamma_{s_i}\}$ 's or the  $\{p_{s_i}\}$ 's, in order to easily distinguish between the quantizer designs for the two distinct relay models of interest, we consider quantizing the  $\{\gamma_{s_i}\}$ 's for the AFB model and the  $\{p_{s_i}\}$ 's for the DFB relay model. As a result, we use  $\{\gamma_{t_k}\}$  and  $\{p_{t_k}\}$  to denote the quantizer thresholds for the AFB and DFB relay models, respectively. In summary, we focus on quantizers described via their preimages as follows

$$I_k = \mathcal{F}^{-1}(k) \quad \text{for } k \in \{1, 2, \dots, \mathcal{K}\} \quad (2.14)$$

whereby for the AFB relay model,

$$I_k = [\gamma_{t_k}, \gamma_{t_{k+1}}) \quad (2.15)$$

with quantizer thresholds satisfying  $\gamma_{t_0} = 0 < \gamma_{t_1} < \dots < \gamma_{t_{\mathcal{K}+1}} = \infty$ , while for the DFB relay model,

$$I_k = [p_{t_k}, p_{t_{k+1}}) \quad (2.16)$$

with quantizer thresholds satisfying  $p_{t_0} = 0 < p_{t_1} < \dots < p_{t_{\mathcal{K}+1}} = \infty$ .

As a result, in the AFB relay model shown in Fig. 2.2, the output of the  $i$ th source-relay CSI quantizer (with input the  $i$ th source-relay CSI  $\gamma_{s_i}$ ) is given by

$$q_i = \mathcal{F}(\gamma_{s_i}) = k, \quad \text{if } \gamma_{s_i} \in I_k, \quad (2.17)$$

with  $I_k$  given by (2.15). Similarly, in the DFB relay model shown in Fig. 2.3, the output of the  $i$ th source-relay CSI quantizer (with input the  $i$ th source-relay CSI  $p_{s_i}$ ) is given by

$$q_i = \mathcal{F}(p_{s_i}) = k, \text{ if } p_{s_i} \in I_k, \quad (2.18)$$

with  $I_k$  given by (2.16). As shown in Fig. 2.2 and Fig. 2.3, the destination uses its knowledge of the relay-destination channel coefficients  $\{\alpha_{r_i}\}$  and the available source-relay CSI  $\{q_i\}$  to compute the beamforming weights to be broadcasted to the relays.

In this thesis, our objectives can be summarized as follows:

- Given full knowledge of the relay-destination CSI and an  $m$ -bit description of each source-relay CSI at the destination, select the  $m$ -bit description (*i.e.*, the  $2^M$ -level quantizer, or, equivalently the  $\{\gamma_{t_k}\}$ 's for the AFB relay model and the  $\{p_{t_k}\}$ 's for the DFB relay model) and the associated beamforming algorithms subject to (2.12), so as to minimize the destination  $\Pr(e)$ .
- Develop adaptive beamforming algorithms that exploit feedback information from the destination which determines for each relay its processing type. In addition, examine the tradeoff between the feedback information and the  $\Pr(e)$  performance if the relay processing is locally decided at each relay rather than being determined by the destination.
- Develop beamforming algorithms for multi-hop relay networks. In particular,



we determine bandwidth-efficient methods for selecting the weights at each hop using the beamforming algorithms developed for the two-hop networks.

## Chapter 3

# Beamforming Algorithms for Amplify-and-Forward Relay Model

In this chapter, we develop relay-destination beamforming algorithms for information relaying for the amplify-and-forward relay model under bandwidth constraints. We consider the system model developed in Chap. 2. In particular, we develop relay-destination beamforming algorithms for the amplify-and-forward model whereby the beamforming weights are formed via the composite relays-destination CSI and  $m$ -bit descriptions of the individual source-relay CSIs. We present methods for choosing the source-relay CSI quantizer so as to minimize the data bit error rates (BERs) at the destination. The algorithms we develop, even in the case when only a single bit is used to describe the source relay CSI, are only slightly inferior to beamformers that exploit perfect CSI knowledge of the source-relay channels at the destination [23,24].

The outline of this chapter is as follows. In Sec. 3.1, we present a class of beamforming algorithms for the amplify-and-forward relay model assuming full and

partial knowledge of the source-relay CSI is available at the destination, respectively. We also present a method for designing the source relay CSI quantizer. In Sec. 3.2, we present a performance evaluation of the proposed beamforming algorithms.

## 3.1 Beamforming Algorithms

In this section, we present beamforming algorithms for the AFB relay model that are based on the individual relay-destination channel coefficients and various levels of source-relay channel CSI at the destination. We first determine lower bounds on  $\Pr(e)$  at the destination by considering the case where full knowledge of the  $\{\gamma_{s_i}\}$ 's is available at the destination. We then develop beamforming algorithms for the case that only their quantized versions from (2.17) are available at the destination.

### 3.1.1 Full Source-Relay CSI Lower Bound

We first develop beamforming algorithms that minimize the  $\Pr(e)$  at the destination by considering the case that the  $\{\gamma_{s_i}\}$ 's are fully known at the destination. The  $\Pr(e)$  at the destination can be expressed in terms of the (instantaneous) destination SNR,  $\gamma_d$ , as follows,

$$\Pr(e) = E_{\gamma_d} \left[ \mathcal{Q}(\sqrt{2\gamma_d}) \right] \quad (3.1)$$

where  $\mathcal{Q}(x) \triangleq \frac{1}{2\pi} \int_x^\infty \exp(-y^2) dy$  and where, given a set of relay-destination channel coefficients,  $\{\alpha_{r_i}\}$ , a set of source-relay CSI,  $\{\gamma_{s_i}\}$ , and using (2.6) and (2.11), the

SNR,  $\gamma_d$ , at the destination can be represented as follows,

$$\gamma_d = \frac{|\sum_i (\alpha_{r_i} \beta_i / \sqrt{1 + \xi_{s_i}})|^2}{\sum_i (|\beta_i|^2 |\alpha_{r_i}|^2 [\xi_{s_i}/(\xi_{s_i} + 1)]) + \sigma_w^2}. \quad (3.2)$$

Since minimizing the right-hand side of (3.1), is equivalent to maximizing (3.2), we focus our attention on beamforming algorithms that maximize the instantaneous  $\gamma_d$ , attained at the destination subject to the constraint (2.12). Under this constraint, the SNR expression  $\gamma_d$  in (3.2) can be rewritten as follows,

$$\gamma_d = \frac{|\sum_i (\alpha_{r_i} \beta_i / \sqrt{1 + \xi_{s_i}})|^2}{\sum_i (|\beta_i|^2 [\xi_{s_i}/(\xi_{s_i} + 1) + \xi_{r_i}])}. \quad (3.3)$$

By applying the Cauchy-Schwartz inequality defined as,

$$E[X Y] \leq \sqrt{|E[X]|^2 |E[Y]|^2} \quad (3.4)$$

where the equality occurs when  $X \propto Y$ , on the SNR expression (3.3) by setting

$$X = \beta_i \left[ \sqrt{[\xi_{s_i}/(\xi_{s_i} + 1) + \xi_{r_i}]} \right], \quad (3.5)$$

and

$$Y = \frac{\alpha_{r_i}}{[(\xi_{s_i} + 1)(\xi_{r_i} + 1) - 1]}. \quad (3.6)$$

The SNR-maximizing beamformers for the amplify-and-forward relay model subject to the constraint (2.12) are given by

$$\beta_i \propto \frac{\sqrt{\xi_{s_i} + 1}}{\alpha_{r_i} [(\xi_{s_i} + 1)(\xi_{r_i} + 1) - 1]}, \quad (3.7)$$

yielding a maximum SNR at the destination

$$\gamma_{d,\max} = \sum_i \frac{1}{[(\xi_{s_i} + 1)(\xi_{r_i} + 1) - 1]}. \quad (3.8)$$

We then develop a closed form expression for the destination  $\Pr(e)$  performance of the beamformers in (3.7) at high average source-relay and relay-destination SNR values. The destination  $\Pr(e)$  performance for such case provides a lower bound on the destination  $\Pr(e)$  of the beamforming algorithms formed based on quantized source-relay channel CSI. The  $\Pr(e)$  expression defined in (3.1) can be rewritten in the following expanded form

$$\Pr(e) = \int_0^\infty Q(\sqrt{2\gamma}) p_{\gamma_{d,\max}}(\gamma) d\gamma, \quad (3.9)$$

where  $p_{\gamma_{d,\max}}(\cdot)$  denotes the probability density function of  $\gamma_{d,\max}$  defined in (3.10). At high values of average SNR  $\bar{\gamma}_s$  and  $\bar{\gamma}_r$ , the maximum SNR  $\gamma_{d,\max}$  defined in (3.8) can be reduced to,

$$\begin{aligned} \gamma_{d,\max} &= \sum_i^L \frac{1}{\xi_{s_i} + \xi_{r_i}} \\ &= \sum_i^L \frac{\gamma_{s_i} \gamma_{r_i}}{\gamma_{s_i} + \gamma_{r_i}}. \end{aligned} \quad (3.10)$$

As it will be shown later via simulations, that the above expression of the maximum SNR at the destination approximates well the  $\Pr(e)$  performance even at moderate average SNR values. To obtain an expression for the  $\Pr(e)$  at the destination, we use the method developed in [15, 25]. This method depends on the observation that as the average SNR values increase, the  $\Pr(e)$  values are mainly dictated by the values of the probability density function,  $p_{\gamma_{d,\max}}(\cdot)$  around zero. This is due to the fact that the effect of the values of  $Q(\cdot)$  function in (3.9) away from zero, decreases significantly as the average SNR increases. As a result, a closed form

of  $\Pr(e)$  expression (3.9) that almost captures the exact values of the  $\Pr(e)$  can be obtained by approximating the behavior of the probability density function of  $p_{\gamma_{d,\max}}(\cdot)$  around zero. In [25], the authors develop a close approximations of the probability density function of  $p_{\gamma_{d,\max}}(\cdot)$  using McLaurin series. Given that the first non-zero term of the series is the  $k$ th term, the McLaurin series representation of  $p_{\gamma_{d,\max}}(\cdot)$  can be given as follows,

$$p_{\gamma_{d,\max}}(\gamma) = \frac{\partial^k p_{\gamma_{d,\max}}(0)}{\partial \gamma^k} \gamma^k + o(\gamma^k), \quad (3.11)$$

where we assume that  $\lim_{\gamma \rightarrow 0} o(\gamma)/\gamma = 0$ . By applying the expression (3.11) in the  $\Pr(e)$  expression (3.9) and perform simple integration, we can deduce the  $\Pr(e)$  expression as the average SNR goes to infinity is given by [25],

$$\Pr(e) \rightarrow \frac{\prod_{i=1}^{k+1} (2i-1)}{(k+1)2^{(k+2)}} \cdot \frac{1}{k!} \frac{\partial^k p_{\gamma_{d,\max}}(0)}{\partial \gamma^k}. \quad (3.12)$$

To evaluate the  $\Pr(e)$  expression, we need to calculate the first non-zero McLuarin coefficient  $\frac{\partial^k p_{\gamma_{d,\max}}(0)}{\partial \gamma^k}$ . As shown in [15], the first non-zero coefficient McLaurin coefficient is the  $L$ th term and was found by using initial value theorem and Laplace transformation to be equal to

$$\frac{\partial^k p_{\gamma_{d,\max}}(0)}{\partial \gamma^k} = \prod_{i=1}^L [p_{\gamma_{s_i}}(0) + p_{\gamma_{r_i}}(0)]. \quad (3.13)$$

where  $p_{\gamma_{s_i}}(0)$  and  $p_{\gamma_{r_i}}(0)$  are the zero value of the probability density function of the source-relay and relay-destination channel, respectively. Given the Rayleigh distribution model assumed for the source-relay and relay-destination channels, the

values of  $p_{\gamma_{s_i}}(0)$  and  $p_{\gamma_{r_i}}(0)$  are given by,

$$p_{\gamma_{s_i}}(0) = \frac{1}{\bar{\gamma}_s} \quad p_{\gamma_{r_i}}(0) = \frac{1}{\bar{\gamma}_r}, \quad (3.14)$$

which by applying to the  $\Pr(e)$  expression in (3.12) and performing simple algebraic simplifications, the asymptotic  $\Pr(e)$  of the amplify-and-forward model (as average SNR goes to infinity) can be expressed as follows,

$$\Pr(e) \rightarrow \frac{\prod_{i=1}^{L+1} (2i-1)}{(L+1)2^{(L+2)}} \cdot \frac{1}{L!} \left[ \frac{1}{\bar{\gamma}_s} + \frac{1}{\bar{\gamma}_r} \right]^L. \quad (3.15)$$

The destination  $\Pr(e)$  of the beamformers in (3.7) provides a lower bound on the destination  $\Pr(e)$  of the beamforming algorithms that exploit quantized source-relay channel CSIs.

### 3.1.2 Partial Source-Relay CSI Beamforming Algorithm

In this section, we develop beamforming algorithms in the case that only the  $\{q_i\}$ 's from (2.17) (*i.e.*, only quantized values of the source-relay channels coefficients) are available at the destination. To this end, we first obtain a closed-form expression for the  $\Pr(e)$  at the destination that is valid when the number of relays becomes large, and use it to construct methods for selecting the beamforming weights and the source-relay CSI quantizer thresholds so as to minimize the destination  $\Pr(e)$ .

The optimal detector at the destination is simply a matched filter followed by a slicer. Omitting for convenience the dependence of random sequences on the

time index  $n$ , we note that

$$E[y_d|x, \{\alpha_{r_i}\}, \{\xi_{s_i}\}, \{\beta_i\}] = xAe^{j\theta}, \quad (3.16)$$

for some  $A \geq 0$  and some  $-\pi \leq \theta < \pi$ , which may depend on the  $\{\alpha_{r_i}\}$ 's, the  $\{\xi_{s_i}\}$ 's, and the set of beamforming vectors  $\{\beta_i\}$ . Letting  $\mathcal{R}(t)$  denote the real part of a complex number  $t$ , the optimal detector in this case selects  $\hat{x} = 1$ , if  $\mathcal{R}(y_d e^{-j\theta})$  is positive and  $\hat{x} = -1$  otherwise. Without loss of generality, we shall assume that  $\theta = 0$ , since, choosing any set of  $\beta_i$ 's yielding a nonzero  $\theta = \theta_o$  is equivalent (in terms of performance) to choosing beamforming weights  $\beta_i e^{-j\theta_o}$ , yielding  $\theta = 0$ . With this assumption the optimal detector is given by,

$$\mathcal{R}(y_d) \underset{\hat{x}=-1}{\overset{\hat{x}=1}{\geq}} 0 \quad (3.17)$$

where  $y_d$ , using (2.4) and (2.6), is given by

$$y_d = \sum_i^L \frac{\beta_i \alpha_{r_i}}{\sqrt{\xi_{s_i} + 1}} x + \sum_i^L \frac{\beta_i \alpha_{r_i} \xi_{s_i}}{\sqrt{\xi_{s_i} + 1}} \bar{v}_i + w. \quad (3.18)$$

As a prelude to designing beamforming methods that exploit knowledge of the quantized source-relay CSIs

$$\mathbf{q} = \begin{bmatrix} q_1 & q_2 & \cdots & q_L \end{bmatrix}^T \quad (3.19)$$

with  $q_i$  given by (2.17), and the relay-destination channel CSIs

$$\boldsymbol{\alpha}_r = \begin{bmatrix} \alpha_{r_1} & \alpha_{r_2} & \cdots & \alpha_{r_L} \end{bmatrix}^T \quad (3.20)$$



it is instructive to consider the destination  $\Pr(e)$  conditioned on  $\mathbf{q}$  and  $\boldsymbol{\alpha}_r$  in the following form

$$\Pr(e|\boldsymbol{\alpha}_r, \mathbf{q}) = \Pr(\mathcal{R}(y_d) < 0|\boldsymbol{\alpha}_r, \mathbf{q}) . \quad (3.21)$$

Computing  $\Pr(e|\boldsymbol{\alpha}_r, \mathbf{q})$  via (3.21) requires knowledge of the probability density function (p.d.f) of  $y_d$  in (3.18) given  $\boldsymbol{\alpha}_r$ , and  $\mathbf{q}$ , which, as (3.18) reveals, is not Gaussian. Consequently, for finite  $L$ , (3.21) does not provide a computationally efficient algorithm for obtaining the  $\Pr(e)$ -minimizing beamforming vectors. In the large  $L$  ( $L \rightarrow \infty$ ) case, however, the right hand side of (3.18) converges to a Gaussian random variable, yielding the following limit on the  $\Pr(e|\boldsymbol{\alpha}_r, \mathbf{q})$  in (3.21)

$$\lim_{L \rightarrow \infty} \Pr(e|\boldsymbol{\alpha}_r, \mathbf{q}) = \mathcal{Q}(\sqrt{2\gamma_{dq}}), \quad (3.22)$$

where the SNR  $\gamma_{dq}$  at the destination is given by

$$\gamma_{dq} = \gamma_d(\boldsymbol{\beta}, \mathbf{q}, \boldsymbol{\alpha}_r) = \frac{|E[y_d|\boldsymbol{\alpha}_r, \mathbf{q}]|^2}{E[|y_d - E[y_d|\boldsymbol{\alpha}_r, \mathbf{q}]|^2|\boldsymbol{\alpha}_r, \mathbf{q}]}, \quad (3.23)$$

and

$$\boldsymbol{\beta} = \boldsymbol{\beta}(\mathbf{q}, \boldsymbol{\alpha}_r) = \left[ \beta_1 \quad \beta_2 \quad \dots \quad \beta_L \right]^T, \quad (3.24)$$

is the vector of beamforming weights.

We next determine the choice of the beamforming vector  $\boldsymbol{\beta}$  that maximizes the SNR expression  $\gamma_{dq}$  in (3.23). Using (2.6) and (2.11), the signal power quantity  $|E[y_d|\boldsymbol{\alpha}_r, \mathbf{q}]|^2$  can be expressed as follows,

$$|E[y_d|\boldsymbol{\alpha}_r, \mathbf{q}]|^2 = \left| \sum_i \alpha_{r_i} \beta_i E \left[ (1/\sqrt{1 + \xi_{si}}) \middle| \mathbf{q} \right] \right|^2 . \quad (3.25)$$

Similarly, the denominator in (3.23) represents the noise power which, after performing algebraic manipulations, can be represented as follows,

$$E [|y_d - E[y_d | \boldsymbol{\alpha}_r, \mathbf{q}]|^2 | \boldsymbol{\alpha}_r, \mathbf{q}] = \sum_i |\alpha_{r_i}|^2 \left[ |\beta_i|^2 \left( 1 - \left| E \left[ \frac{1}{\sqrt{1 + \xi_{s_i}}} \middle| q_i \right] \right|^2 \right) \right] + \sigma_w^2. \quad (3.26)$$

Combining (3.25)-(3.26), the SNR in (3.23) can be represented as follows,

$$\gamma_{dq} = \frac{\left| \sum_i \alpha_{r_i} \beta_i E \left[ \frac{1}{\sqrt{1 + \xi_{s_i}}} \middle| q_i \right] \right|^2}{\sum_i |\alpha_{r_i}|^2 \left( |\beta_i|^2 \left[ 1 - \left| E \left[ \frac{1}{\sqrt{1 + \xi_{s_i}}} \middle| q_i \right] \right|^2 \right] \right) + \sigma_w^2}. \quad (3.27)$$

Also, by letting

$$a_k = \int_{\gamma^{t_k}}^{\gamma^{t_{k+1}}} \frac{1}{\sqrt{1 + (1/\mu)}} \frac{1}{\bar{\gamma}_s} \exp\left(-\frac{\mu}{\bar{\gamma}_s}\right) d\mu, \quad (3.28)$$

and

$$c_k = \int_{\gamma^{t_k}}^{\gamma^{t_{k+1}}} \frac{1}{\bar{\gamma}_s} \exp\left(-\frac{\mu}{\bar{\gamma}_s}\right) d\mu, \quad (3.29)$$

we obtain

$$E \left[ \frac{1}{\sqrt{1 + \xi_{s_i}}} \middle| q_i = k \right] = \frac{a_k}{c_k}. \quad (3.30)$$

Using (3.28)-(3.30) in (3.27) yields

$$\gamma_{dq} = \frac{\left| \sum_i \alpha_{r_i} \beta_i a_i c_i^{-1} \right|^2}{\sum_i |\alpha_{r_i}|^2 |\beta_i|^2 \left( 1 - \frac{a_i^2}{c_i^2} \right) + \sigma_w^2}. \quad (3.31)$$

Finally, by using the Cauchy-Schwartz inequality in (3.31), the beamforming weights,  $\beta_i$ , that maximize the SNR,  $\gamma_{dq}$ , subject to the constraint (2.12) can be expressed as

$$\beta_i \propto \frac{\alpha_{r_i}^{-1} \left( \frac{a_i}{c_i} \right)}{1 + \xi_{r_i} - \left( \frac{a_i}{c_i} \right)^2}, \quad (3.32)$$

yielding a maximum value of  $\gamma_{\text{dq}}$  given by

$$\gamma_{\text{dq,max}} = \sum_i \frac{\left(\frac{a_i}{c_i}\right)^2}{1 + \xi_{r_i} - \left(\frac{a_i}{c_i}\right)^2}. \quad (3.33)$$

We remark that as the quality of the source-relay CSI information available at the destination improves towards the case where the  $\{\gamma_{s_i}\}$ 's are available at the destination, the maximum SNR (3.33) converges to the one in (3.8). This can be readily verified by considering a sequence of  $\mathcal{K}$ -level quantizers with thresholds  $\gamma_{t_k} = k/\sqrt{\mathcal{K}}$ , and exploiting the fact that as  $\mathcal{K} \rightarrow \infty$ ,  $\gamma_{\text{dq,max}} \rightarrow \gamma_{\text{d,max}}$ , with  $\gamma_{\text{dq,max}}$  and  $\gamma_{\text{d,max}}$  given by (3.8) and (3.33), respectively.

We next focus our attention on finding the source-relay CSI quantizer thresholds that optimize the  $\text{Pr}(e)$  at the destination. As suggested by (3.33), finding the set of thresholds that maximize the SNR,  $\gamma_{\text{dq,max}}$ , is equivalent to finding the thresholds that maximize the individual terms in  $\gamma_{\text{dq,max}}$ . Each term in  $\gamma_{\text{dq,max}}$  can be maximized by finding the optimal value of the ratio  $\left(\frac{a_i}{c_i}\right)^2$  for a given  $q_i$ .

Although in principle this method can be used in finding the set of quantizer thresholds that maximize the SNR expression in (3.33), it has the disadvantage of providing a set of thresholds that depend on the instantaneous relay-destination SNR,  $\xi_{r_i}$ , and the quantized descriptions of the source-relay CSI received at the destination. Alternatively, we consider choosing the thresholds that maximize the value of  $\left(\frac{a_i}{c_i}\right)^2$  over all the realizations of the quantization levels,  $q_i$ , and at high relay-destination SNR, *i.e.*  $\xi_{r_i} = 0$ . In particular, we focus on finding the set of

thresholds that maximize the following

$$\Lambda_{\text{q}} = \sum \left( \frac{a_i}{c_i} \right)^2 \Pr(q_i) \quad (3.34)$$

where  $\Pr(q_i)$  is the probability of the occurrence of one realization of  $\{q_i\}$  and is given by

$$\Pr(q_i) = c_i \quad (3.35)$$

where  $c_i$  given by (3.29). Using (3.33)-(3.35), and letting  $\xi_{r_i} \rightarrow 0$ , the average term in (3.34) can be expressed as

$$\Lambda_{\text{q}} = \sum_{k=1}^{\mathcal{K}} \frac{a_k^2}{c_k}. \quad (3.36)$$

where  $a_k$  and  $c_k$  are given by (3.28) and (3.29), respectively. As shown Sec. 3.2.1, the set of quantizer thresholds that maximizes (3.36) can be readily obtained using offline numerical optimization techniques.

As is verified via simulations in Sec. 3.2, even when a two-level quantizer is used (i.e., a single-bit is used to describe each source-relay CSI to the destination), the optimized quantizer threshold and the associated beamforming weights obtained based on the methods developed in this section yield destination bit error rates that are a small fraction higher than those obtained assuming full knowledge of the instantaneous values of the source-relay SNRs,  $\{\xi_{s_i}\}$ , at the destination.

## 3.2 Simulations

In this section, we conduct a performance analysis of the beamforming algorithms developed for the AFB relay model in Sec. 3.1. We focus our attention on *one-bit* quantizers employed at the relays, *i.e.*, the destination receives only a *one-bit* representation of the CSI of each source-relay channel. Although, the case of the  $m$ -bit quantized source-relay CSI of each source-relay channel can be similarly analyzed, as our simulations suggest, a *one-bit* source-relay CSI quantizer provides destination  $\Pr(e)$  sufficiently close to the one obtained when the quality of each source-relay channel is precisely known at the destination.

We first develop rule-of-thumb expression for the one-bit quantizer threshold that optimizes the  $\Pr(e)$  at the destination for the AFB relay model. Based on these optimized quantizer thresholds, we then present a performance evaluation of the beamforming algorithms presented in Sec. 3.1, and comparison against beamforming algorithms that exploit full source-relay CSIs at the destination. Finally, we study the effect of the relative location of the relays with respect to the source and the destination on the destination  $\Pr(e)$  performance at the destination for the AFB relay model. Based on these simulations, we derive a rule-of-thumb expressions for the optimal relative relay locations considering the case of the AFB relay model.

### 3.2.1 Quantizer Threshold Design

In this section, we investigate the effect of the choice of the threshold of the *one*-bit source-relay CSI quantizer  $\mathcal{F}(\cdot)$  defined in (2.17) on the destination  $\Pr(e)$ .

As shown in Sec. 3.1, our objective is to find the quantizer threshold, defined as  $\gamma_t^{\text{opt}}$ , that maximizes the value  $\Lambda_q$ , defined in (3.36) assuming a *one*-bit source-relay CSI quantizer ( $\mathcal{K} = 2$ ). Inspection of (3.36) reveals that  $\gamma_t^{\text{opt}}$  is only a function of the average source-relay channel SNR,  $\bar{\gamma}_s$ , which is convenient in terms of system design as the threshold can be conveniently computed offline. As it will be shown later via simulations, that obtained threshold  $\gamma_t^{\text{opt}}$  minimizes the  $\Pr(e)$  performance for the *one*-bit quantizer.

Numerical threshold optimization can be used to obtain rule-of-thumb expressions that provide an estimate of the value of  $\gamma_t^{\text{opt}}$  as a function of  $\bar{\gamma}_s$ . In particular, We develop rule-of-thumb expression via numerical techniques that determines the value of  $\gamma_t^{\text{opt}}$  as a function of  $\bar{\gamma}_s$ . In particular, Fig. 3.2.1 depicts the dependence of the threshold,  $\gamma_t^{\text{opt}}$  on the source-relay average CSI,  $\bar{\gamma}_s$ . The solid curve represents  $\gamma_t^{\text{opt}}$  computed by numerically finding the value of  $\gamma_t$  that maximizes the expression  $\Lambda_q$  defined in (3.36), while the dashed curve depicts the following rule-of-thumb function,

$$\mathcal{C}_{\text{AF}}(\bar{\gamma}_s) = -\left(\frac{\bar{\gamma}_s}{10}\right)^2 + 0.5483 \bar{\gamma}_s - 3.48, \quad (3.37)$$

obtained via curve-fitting techniques. As the figure reveals, the function  $\mathcal{C}_{\text{AF}}(\bar{\gamma}_s)$  approximates remarkably well the numerically obtained value of  $\gamma_t^{\text{opt}}$  for all values

of  $\bar{\gamma}_s$  in the range 1-20 dB.

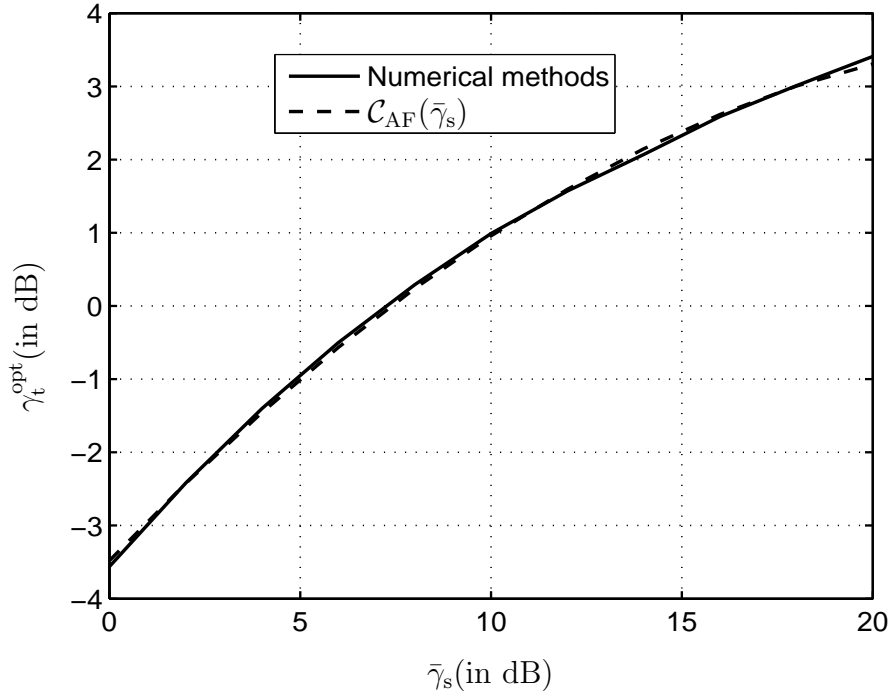


Figure 3.1: Optimal quantizer threshold,  $\gamma_t^{\text{opt}}$ , as a function of  $\bar{\gamma}_s$ . The solid curve depicts  $\gamma_t^{\text{opt}}$  obtained using numerical methods while the dashed curve depicts  $\mathcal{C}_{\text{AF}}(\bar{\gamma}_s)$  in (3.37).

We remark that this optimal threshold does not necessarily minimize the  $\Pr(e)$  at the destination, however, as our simulations reveal, the threshold obtained by minimizing,  $\Lambda_q$ , provides the minimum  $\Pr(e)$  at the destination.

### 3.2.2 Performance Analysis

In this section, we study the performance of the beamforming algorithms developed in Sec. 3.1 based on Monte-Carlo simulations. We consider the performance of

the beamforming algorithms formed assuming the destination has available *one-bit* descriptions of the individual source-relay channel CSIs and where the associated binary quantizer threshold is obtained using the techniques developed in Sec. 3.2.1. In particular, we consider a two-hop network setting with a single source and a destination communicating via  $L$  relays, whereby the average source-relay channel CSI  $\sigma_s^2 = 1$  and the average relay-destination channel CSI  $\sigma_r^2 = 1$ .

We first consider the case where full knowledge of source-relay CSI SNR is available at the destination where fig. 3.2 compares the  $\Pr(e)$  values obtained using simulations and the  $\Pr(e)$  expression (3.15) developed for high average SNR case. In particular, the figure depicts the destination  $\Pr(e)$  for various number of relay nodes  $L = \{2, 3\}$ , as a function of the total average SNR  $\bar{\gamma}_{sd} = \bar{\gamma}_s + \bar{\gamma}_r$ . We define the parameter  $\mu$  as the ratio of the power allocated to the source node to the total power *i.e.*,

$$\mu = \frac{\bar{\gamma}_s}{\bar{\gamma}_{sd}}. \quad (3.38)$$

In fig. 3.2 we consider the case of equal power distribution;  $\bar{\gamma}_s = \bar{\gamma}_r$  or equivalently  $\mu = 0.5$ . As the figure reveals, the  $\Pr(e)$  values obtained using the expression (3.15) accurately approximates the behavior of the  $\Pr(e)$  function at the destination for high average SNR.

We next study the performance of the quantized beamforming algorithms for the case where only optimized *one-bit* quantized descriptions of the source-relay CSIs are available at the destination. Fig. 3.3 depicts the  $\Pr(e)$  at the destination



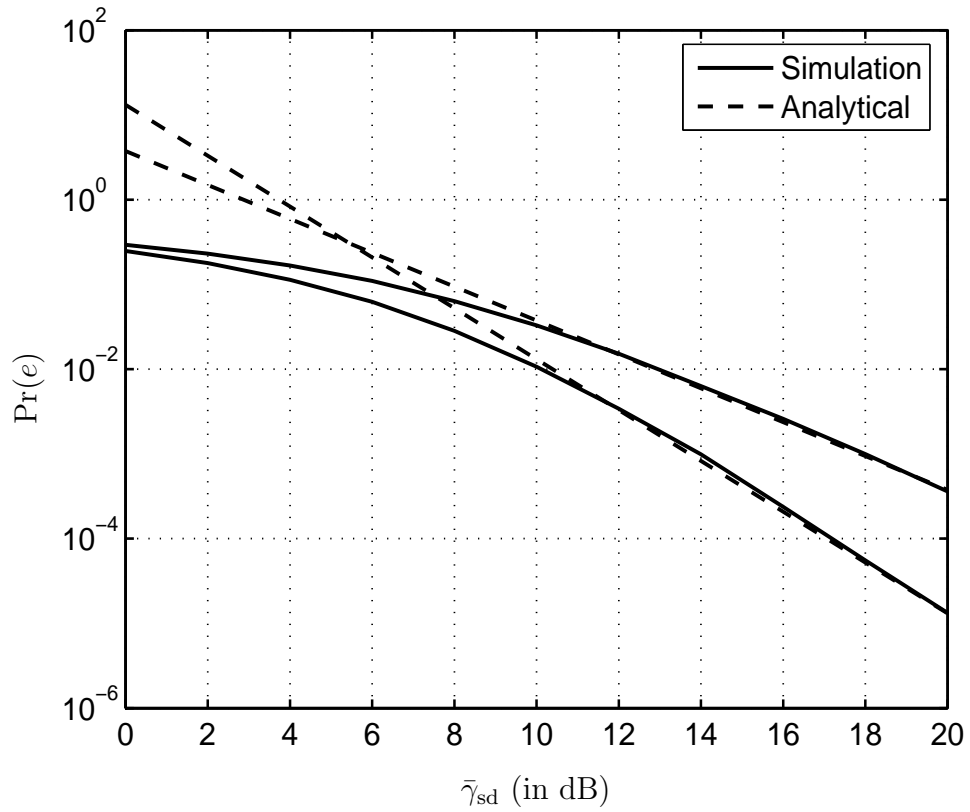


Figure 3.2: The successively lower solid curves and the successively lower dash curves depicts the destination  $\Pr(e)$  for  $L = \{2, 3\}$  obtained using simulations and  $\Pr(e)$  expression (3.15), respectively, as a function of  $\bar{\gamma}_{sd}$  assuming the destination has full knowledge of the source-relay CSI,  $\gamma_{s_i}$

for  $L = 2$  and  $4$ , as a function of the total average SNR  $\bar{\gamma}_{sd}$ . The successively lower solid curves marked by 'x' depict the destination  $\Pr(e)$ , assuming the destination has full knowledge of the source-relay channel CSI  $\gamma_{s_i}$  (or equivalently infinite bit description of  $\gamma_{s_i}$ ) for  $L = 2$  and  $4$ . The successively solid curves marked by 'o' depict the destination  $\Pr(e)$  assuming the destination has an *one-bit* description of the each source-relay CSI, for networks with  $L = 2$ , and  $4$  relay nodes, respectively. The source-relay CSI quantizer threshold is selected in each case according to (3.37). Finally, the successively solid curves marked by '∇' depict the destination  $\Pr(e)$  assuming that destination has only the average of each source-relay CSI. As the figure reveals, using these threshold-optimized *one-bit* source-relay CSIs at the destination results in a small loss in  $\Pr(e)$  performance (and no apparent loss in diversity order) with respect to an AFB relay system that exploits precise source-relay CSI knowledge at the destination. In particular, in the  $\bar{\gamma}_s$  range 0–20 dB, the SNR loss does not exceed 1dB. In contrast, the  $\Pr(e)$  performance (in addition to the diversity order) degrades considerably if only the destination has the average of each source-relay CSI.

We next determine the optimal power allocation among the source and the relay nodes that minimizes  $\Pr(e)$  at the destination or equivalently, we need to determine the optimal value of  $\mu$ . Based on the  $\Pr(e)$  expression (3.15), we can deduce that equal power distribution among the source and the relays provides the minimum  $\Pr(e)$  distribution for the case of full knowledge of source-relay SNR is

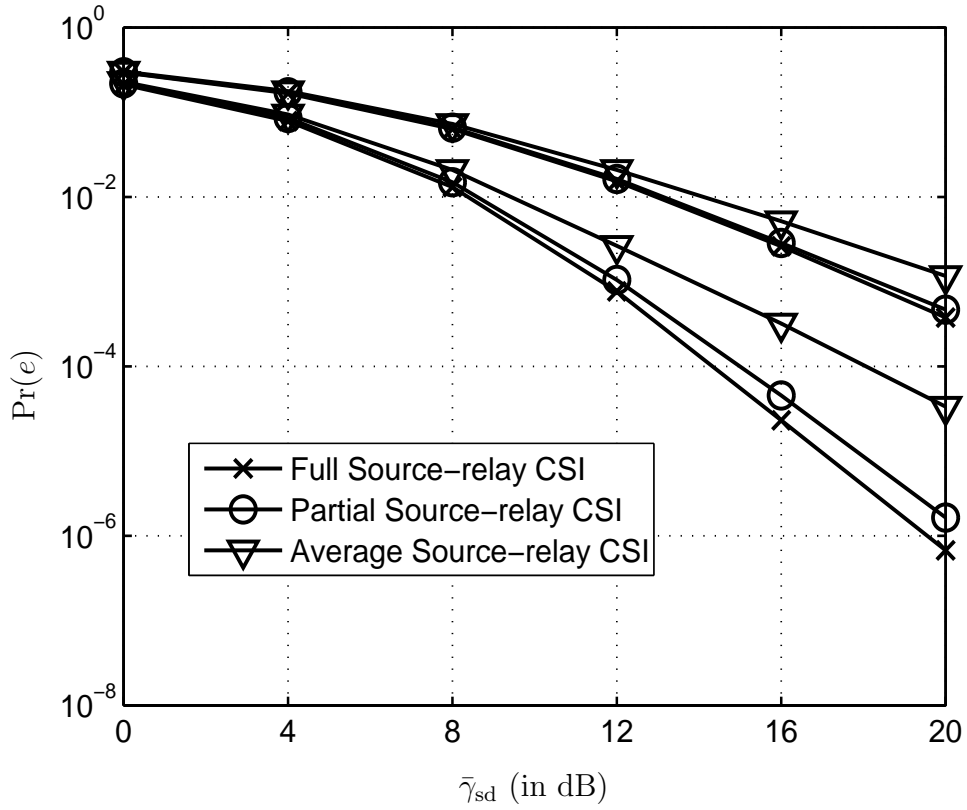


Figure 3.3: The successively lower solid curves marked by 'x', the successively lower curves marked by 'o', the successively lower curves marked by 'v' depict the destination  $\Pr(e)$  for  $L = \{2, 4\}$  as a function of  $\bar{\gamma}_{sd}$  assuming the destination has full knowledge of the source-relay CSI,  $\gamma_{s_i}$ , optimized *one-bit* descriptions of  $\gamma_{s_i}$ , and average value of  $\gamma_{s_i}$ , respectively.

available at the destination. For the case of only *one*-bit quantized versions of the source-relay SNR is available at the destination, fig. 3.4 depicts the  $\Pr(e)$  at the destination as a function of  $\mu$  for various values of  $\bar{\gamma}_{sd} = \{5\text{dB}, 10\text{dB}, 15\text{dB}\}$  and  $L = 3$ . As the figure reveals, that equal power distribution provides the minimum  $\Pr(e)$  for the case of *one*-bit quantizers. In addition, it is shown that the  $\Pr(e)$  values provided by using the optimized *one*-bit quantizers almost close to those obtained by using the exact values of source-relay SNR as mentioned before.

To verify that the quantizer threshold,  $\gamma_t^{\text{opt}}$ , developed in Sec. 3.2.1 optimize the  $\Pr(e)$  at the destination, fig. 3.5 depicts the  $\Pr(e)$  performance of the beamforming algorithms formed based on the optimized *one*-bit quantizers as a function of the normalized quantizer threshold  $\gamma_t/\gamma_t^{\text{opt}}$  (in dB) for different values of  $L = 4$  and  $6$ , respectively and  $\bar{\gamma}_{sd} = 10$  dB. As the figure reveals, the threshold  $\gamma_t^{\text{opt}}$  obtained using (3.37) minimizes the destination  $\Pr(e)$  for various values of  $L$ . In addition, the figure suggests that the destination  $\Pr(e)$  enhancement by selecting the optimal  $\gamma_t^{\text{opt}}$  provides increases considerably as the number of nodes increase. Finally, we remark that the destination  $\Pr(e)$  is not sensitive to the optimal selection of the threshold. For instance, as the figure reveals, the loss in the  $\Pr(e)$  performance is negligible within 2 dB range from the optimal threshold.

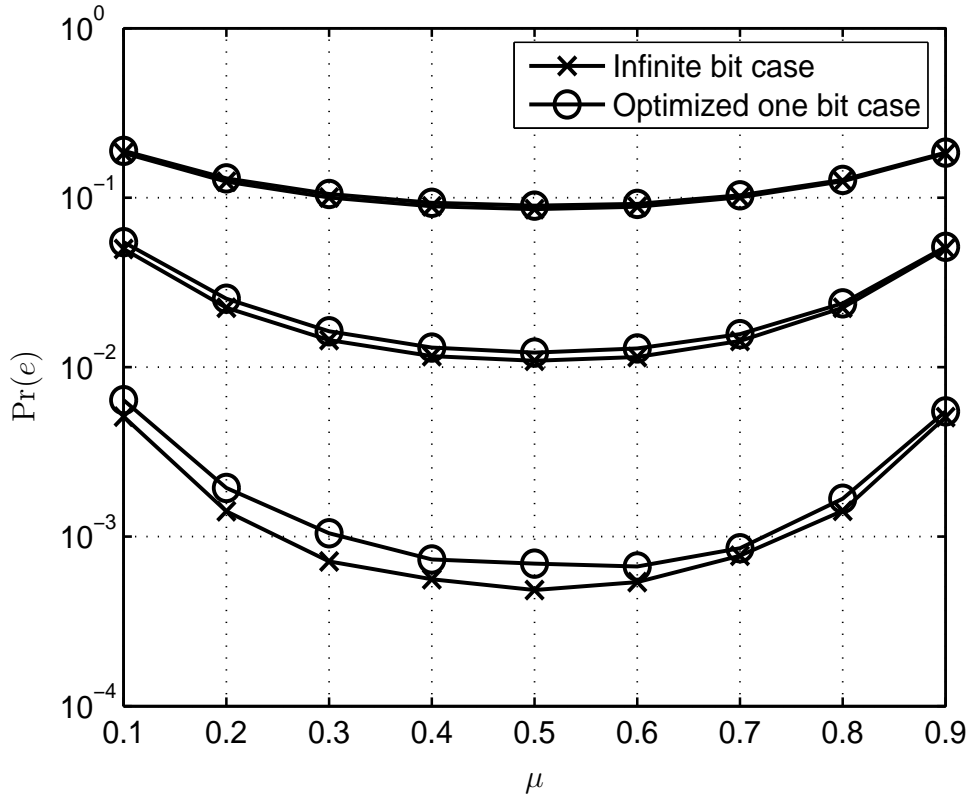


Figure 3.4: The successively lower solid curves marked by 'x' and the successively lower curves marked by 'o' depicts the destination  $\Pr(e)$  for  $\bar{\gamma}_{sd} = \{5\text{dB}, 10\text{dB}, 15\text{dB}\}$  as a function of  $\mu$  assuming the destination has full knowledge of the source-relay CSI,  $\gamma_{s_i}$ , and optimized *one-bit* descriptions of  $\gamma_{s_i}$ , respectively.

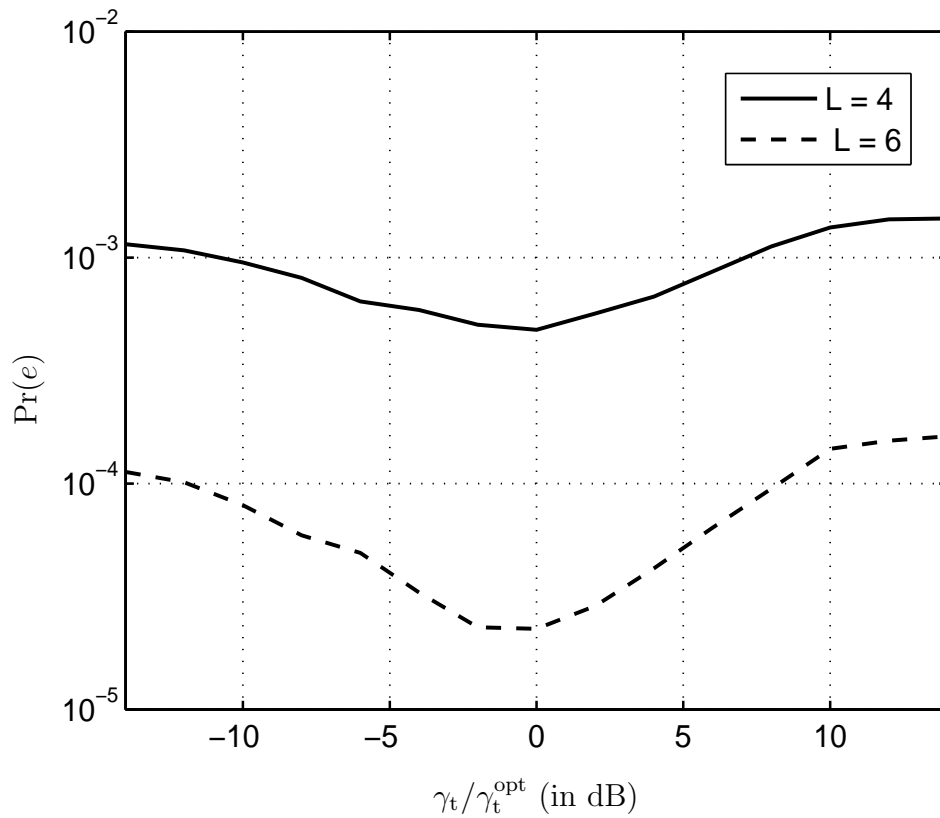


Figure 3.5: The solid and the dashed curves depict the destination  $\Pr(e)$  performance of the *one-bit* beamforming algorithms as a function of  $\gamma_t/\gamma_t^{\text{opt}}$  (in dB) for  $L = 4$  and 6, respectively, and  $\bar{\gamma}_{\text{sd}} = 10$  dB.

### 3.2.3 Optimal Relay Location

In this section, our objective is to determine the optimal relative relay location with respect to the source and the destination that minimizes destination the  $\Pr(e)$ . We focus on the case where single-bit source-relay CSI descriptions are available at the destination, and assume that all the inter-relay distance is much smaller than the source-destination distance, and that the relays are effectively within a small distance from the straight line connecting the source and the destination.

Letting  $d_{sd}$  and  $d_{sr}$  denote the source-destination and source-relay distances, respectively, we define the relative source-relay proximity index as

$$\tau = \frac{d_{sr}}{d_{sd}}, \quad (3.39)$$

and focus on quantifying the effect of  $\tau$  on the destination  $\Pr(e)$ . To this end, we define the average source-relay channel SNR and the average relay-destination channel SNR,  $\sigma_s^2$  via

$$\sigma_s^2 = \frac{|K|^2}{d_{sr}^\nu}, \quad \sigma_r^2 = \frac{|K|^2}{(d_{sd} - d_{sr})^\nu} \quad (3.40)$$

respectively, and where  $K$  is a constant that depends on the antenna design and  $\nu$  denotes the path loss exponent. In all our simulations we set  $K = 1$  and  $\nu = 3$ .

Fig. 3.6 depicts the  $\Pr(e)$  of the proposed beamformers as a function of  $\tau$ , and where  $\bar{\gamma}_s = \bar{\gamma}_r = 5$  dB. The successively lower solid curves represents the destination  $\Pr(e)$  for networks with  $L = 5, 10,$  and  $15$  nodes employing the AFB relay model. As the figure reveals, the optimal source-relay proximity index is weakly dependent

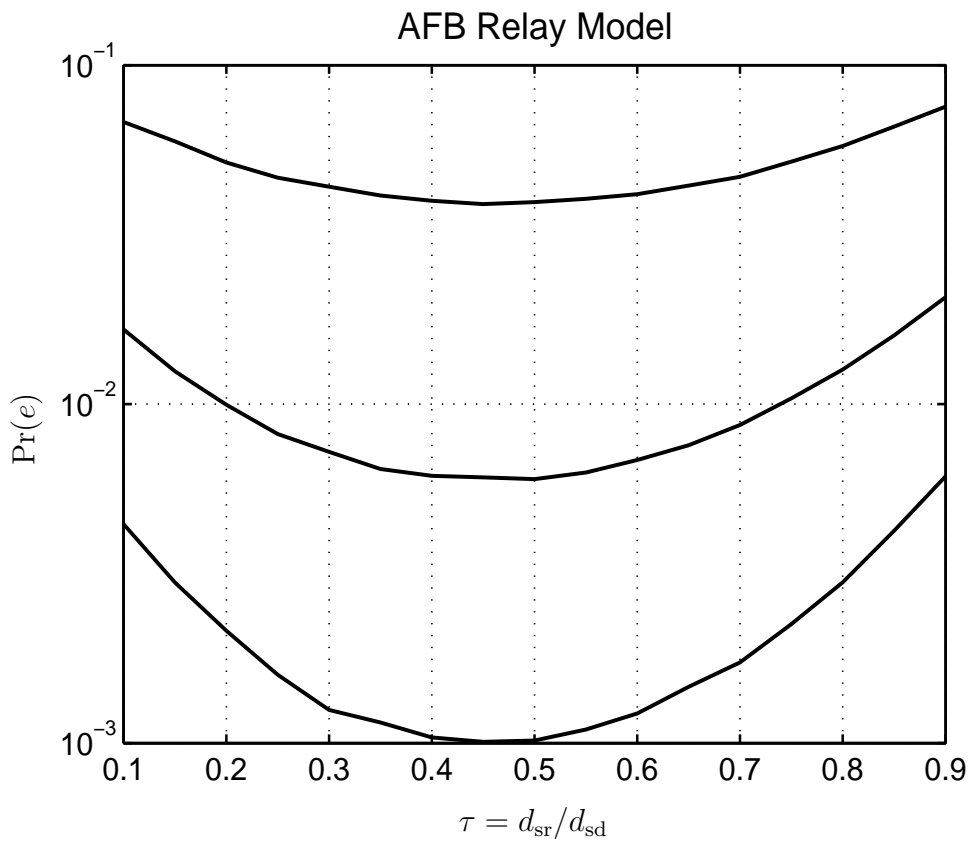


Figure 3.6: The successively lower solid curves marked by 'x' and the successively lower solid curves marked by 'o' depicts the destination  $\Pr(e)$  for  $L = \{5, 10, 15\}$  as a function of  $\tau$  for the decode-and-forward relay model and the amplify-and-relay model, respectively.



on  $L$ . In addition, the optimal relative source-relay proximity indexes is  $\tau \approx 0.5$  for the AFB relay model.

## Chapter 4

# Beamforming Algorithms for Decode-and-Forward Relay Model

In this chapter, we develop information relaying algorithms via beamforming for the case of decode-and-forward relay model. Given the system model developed in Chapter 2, we consider a network setting whereby data broadcasted by a source are decoded at multiple relays and forwarded via beamforming to a destination over a shared channel. The beamforming weights broadcasted by the destination to the relays are formed based on the individual relay-destination fading channel coefficients and a coarse description of the quality of the decoded data at each relay. We present a class of beamformers that are formed via an "equivalent" amplify-and-forward source-relay model of the decode-and-forward model. As our simulations and analysis reveal, the resulting beamformers provide uncoded bit-error-rates that outperform the SNR maximizing beamformers for the decode-and-forward setting [24, 26].

The problem of finding the optimal beamforming weights for a decode-and-forward relay model that minimize the  $\Pr(e)$  at the destination has been addressed in [13], [27]. It was assumed in [13], [27] that the decoded relay data are transmitted to the destination over orthogonal fading channels. At the destination, the beamformers are constructed knowing the average  $\Pr(e)$  of the source-relay channels. In [27], it was shown that the problem of finding optimal weights that minimize the  $\Pr(e)$  at the destination is mathematically intractable. As a result, a  $\lambda$  maximal ratio combiner ( $\lambda$ -MRC) is introduced for a single relay channel setting according which a constant  $\lambda$ , employed to scale the received decoded relay data, is numerically optimized. In [13], the SNR maximal ratio combiner that performs directly on the decode-and-forward relay channel model is proposed.

In this chapter, we develop relay-destination beamforming algorithms whereby the beamforming weights are formed via the composite relays-destination CSI and quantized one-bit descriptions of the individual source-relay CSIs. In particular, we present a class of beamforming algorithms based on an "equivalent" amplify-and-forward relay model of the decode-and-forward source relay model. Furthermore, we present a framework for quantizing the source-relay CSI so as to minimize the data  $\Pr(e)$  at the destination. The algorithms we develop outperform in terms of  $\Pr(e)$  the SNR maximizing beamformers and are only slightly inferior to beamformers that exploit perfect CSI knowledge of the source-relay channels at the destination.

## 4.1 Beamforming Algorithms

In this section, we develop beamforming algorithms for the decode-and-forward relay model assuming various level of knowledge of the source-relay channel CSI  $p_{s_i}$ . In App. A, we develop an analytical expression for the destination  $\Pr(e)$  in (A.1) at the destination assuming full knowledge of the source-relay CSIs at the destination. Although the resulting expression can in principle be used to determine the  $\Pr(e)$  for a given set of beamforming weights, it is only useful in determining the beamforming weights that maximize the  $\Pr(e)$  numerically for small  $L$ , as the number of terms in (A.8) grows exponentially with  $L$ .

In the subsequent subsections, we consider an alternative approach that constructs SNR-maximizing beamformers for an “equivalent” amplify-and-forward via beamforming model. As shown via simulations in Sec. 4.2, the proposed beamforming algorithms can outperform the SNR maximizing beamformers introduced in [13] that perform optimization directly on the decode-and-forward model. In addition, the  $\Pr(e)$  performance of the proposed algorithms is proved to be optimal in high average relay-destination SNR region.

### 4.1.1 High Relay-Destination SNR Bounds

In this section we develop lower bounds on the  $\Pr(e)$  of the proposed beamforming algorithms. In particular, we present lower bounds on the destination  $\Pr(e)$ , by considering the best linear detectors (linear combiners followed by thresholding) in

the presence of infinite relay-destination SNR, *i.e.*, assuming that the decoded relay data  $\{z_i[n]\}$  is available at the destination. The minimum- $\Pr(e)$  linear detector of  $x[n]$  based on  $\{z_i[n]\}$ , assuming knowledge of the  $p_{s_i}$ 's and high average relay-destination SNR (*i.e.*  $\bar{\gamma}_r \rightarrow \infty$ ), takes the form

$$\ell = \sum_i \lambda_i z_{d_i} \underset{\hat{x}=-1}{\overset{\hat{x}=1}{\geq}} 0 \quad (4.1)$$

where the weights  $\lambda_i$  are chosen to minimize the  $\Pr(e)$  at the destination. The weights  $\lambda_i$  can be found by developing an expression for the  $\Pr(e)$  similar to that developed in App. A then choosing  $\lambda_i$  that minimize  $\Pr(e)$ . This approach can be shown to be mathematically hard. An alternative yet a simple method for computing the optimal  $\lambda_i$  is to consider finding the maximum likelihood detector for a given vector  $\mathbf{z}_d$ . As we next show, the  $\lambda_i$ 's can be obtained by noting that the minimum- $\Pr(e)$  detector of  $x[n]$  based on  $\{z_i[n]\}$  is a linear detector. In particular, omitting for convenience the dependence of  $x[n]$  and  $z_i[n]$  on the time-index,  $n$ , the maximum likelihood detector of  $x$  based on the vector  $\mathbf{z}_d$  is given by

$$\Pr(\mathbf{z}_d | \{p_{s_i}\}, x = 1) \underset{\hat{x}=-1}{\overset{\hat{x}=1}{\geq}} \Pr(\mathbf{z}_d | \{p_{s_i}\}, x = -1) \quad (4.2)$$

where

$$\Pr(\mathbf{z}_d | \{p_{s_i}\}, x) = \prod_{i=1}^L \Pr(z_{d_i} | p_{s_i}, x) \quad (4.3)$$

and

$$\Pr(z_{d_i} | p_{s_i}, x) = (1 - p_{s_i})^{\left(\frac{1+z_{d_i}x}{2}\right)} p_{s_i}^{\left(\frac{1-z_{d_i}x}{2}\right)}. \quad (4.4)$$

Alternatively, the maximum likelihood detector can be represented as follows,

$$\prod_{i=1}^L (1 - p_{s_i})^{\left(\frac{1+z_{d_i}}{2}\right)} p_{s_i}^{\left(\frac{1-z_{d_i}}{2}\right)} \underset{\hat{x}=-1}{\overset{\hat{x}=1}{\geq}} \prod_{i=1}^L (1 - p_{s_i})^{\left(\frac{1-z_{d_i}}{2}\right)} p_{s_i}^{\left(\frac{1+z_{d_i}}{2}\right)} \quad (4.5)$$

Using simple algebraic implications, the above expression reduces to,

$$\sum_i \log \left( \frac{1 - p_{s_i}}{p_{s_i}} \right) z_{d_i} \underset{\hat{x}=-1}{\overset{\hat{x}=1}{\geq}} 0. \quad (4.6)$$

By comparing (4.1) and (4.6), the  $\lambda_i$ 's for the best linear detector satisfy

$$\lambda_i \propto \log \left( \frac{1 - p_{s_i}}{p_{s_i}} \right). \quad (4.7)$$

Evidently, the  $\Pr(e)$  performance of this detector provides a lower bound on the  $\Pr(e)$  achievable at the destination based on (2.11) in the case that the  $p_{s_i}$ 's are known to the destination. Similarly, a lower bound on the  $\Pr(e)$  in the case that only the quantized values  $\{q_i = \mathcal{F}(p_{s_i})\}$  are available at the destination is provided by the  $\Pr(e)$  of the optimal linear detector of  $x[n]$  based on  $\{z_i[n]\}$  assuming the detector knows  $q_i$ 's. Similarly, the weights  $\lambda_i$  can be obtained by considering the maximum likelihood detector for a given vector  $\mathbf{z}_d$  and set of  $q_i$ 's which can be expressed as follows,

$$\Pr(\mathbf{z}_d | \mathbf{q}, x = 1) \underset{\hat{x}=-1}{\overset{\hat{x}=1}{\geq}} \Pr(\mathbf{z}_d | \mathbf{q}, x = -1) \quad (4.8)$$

where

$$\Pr(\mathbf{z}_d | \mathbf{q}, x) = \prod_{i=1}^L \Pr(z_{d_i} | q_i, x). \quad (4.9)$$

Using Bayes' rule, the term  $\Pr(z_{d_i} | q_i, x)$  can be represented as follows,

$$\Pr(z_{d_i} | q_i, x) = \Pr(z_{d_i} | p_{s_i} \in I_k, x) = (1 - f_i)^{\left(\frac{1+z_{d_i}x}{2}\right)} f_i^{\left(\frac{1-z_{d_i}x}{2}\right)}, \quad (4.10)$$

where

$$f_i = E_{q_i} [p_{s_i}] = E [p_{s_i} | p_{s_i} \in I_k]. \quad (4.11)$$

Hence, the maximum likelihood detector can be represented as follows,

$$\prod_{i=1}^L (1 - f_i)^{\left(\frac{1+z_{d_i}}{2}\right)} f_i^{\left(\frac{1-z_{d_i}}{2}\right)} \underset{\hat{x}=-1}{\overset{\hat{x}=1}{\geq}} \prod_{i=1}^L (1 - f_i)^{\left(\frac{1-z_{d_i}}{2}\right)} f_i^{\left(\frac{1+z_{d_i}}{2}\right)} \quad (4.12)$$

Using simple algebraic implications, the above expression reduces to,

$$\sum_i \log \left( \frac{1 - f_i}{f_i} \right) z_{d_i} \underset{\hat{x}=-1}{\overset{\hat{x}=1}{\geq}} 0. \quad (4.13)$$

Hence, the optimal detector in this case is given by (4.1) with

$$\lambda_i \propto \log \left( \frac{1 - f_i}{f_i} \right). \quad (4.14)$$

Finally an upper bound on  $\Pr(e)$  in the case the destination knows only the average source-relay SNR, is provided by the  $\Pr(e)$  of the detector given by (4.1) with

$$\lambda_i \propto \log \left( \frac{1 - \bar{p}_s}{\bar{p}_s} \right). \quad (4.15)$$

### 4.1.2 SNR maximizing Beamforming Algorithms

In this section, we review the SNR maximizing beamformers performed directly on the decode-and-forward relay model developed in [13]. Assuming a set of relay-destination channel fading coefficients,  $\alpha_{r_i}$  and a set of source-relay channel quality levels,  $p_{s_i}$ , the instantaneous SNR at the destination  $\gamma_{d_i}$  can be computed using (2.8), (2.11) and (2.8) as follows,

$$\gamma_d = \frac{|E[y_d]|^2}{E[|y_d|^2] - |E[y_d]|^2}. \quad (4.16)$$

Using

$$E [z_{d_i}] = 1 - 2p_{s_i} \quad (4.17)$$

and

$$E [|z_{d_i}|^2] - |E [z_{d_i}]|^2 = 4 p_{s_i} (1 - p_{s_i}), \quad (4.18)$$

we can deduce that

$$E [y_d] = \sum \alpha_{r_i} \beta_i (1 - 2p_{s_i}), \quad (4.19)$$

and

$$E [|y_d|^2] - |E [y_d]|^2 = \sum |\beta_i|^2 |\alpha_{r_i}|^2 (4 p_{s_i} (1 - p_{s_i})) + \sigma_w^2. \quad (4.20)$$

Hence the instantaneous SNR,  $\gamma_d$ , can be expressed as follows,

$$\gamma_d = \frac{|\sum \alpha_{r_i} \beta_i (1 - 2p_{s_i})|^2}{\sum |\beta_i|^2 |\alpha_{r_i}|^2 (4 p_{s_i} (1 - p_{s_i})) + \sigma_w^2}. \quad (4.21)$$

Using Cauchy-Schwartz inequality, the SNR-maximizing beamformers for the decode-and-forward relay model subject to the constraint (2.12) are then given by,

$$\beta_i \propto \frac{(1 - 2 p_{s_i})}{\alpha_{r_i} [4 p_{s_i} (1 - p_{s_i}) + \xi_{r_i}]}. \quad (4.22)$$

As comparison of (4.7) and (4.22), the SNR maximizing beamformers are suboptimal at high relay-destination SNR, since  $\lim_{\xi_{r_i} \rightarrow 0} \beta_i \neq \lambda_i$ . Fig. 4.1.2 depicts the functions  $\log \left( \frac{1-p_{s_i}}{p_{s_i}} \right)$  and  $\frac{(1-2p_{s_i})}{[4p_{s_i}(1-p_{s_i})]}$  defining the behavior of the optimal beamforming weights and the SNR-maximizing beamforming weights. As the figure reveals, the two weights are not equal and in addition the SNR-maximizing beamforming weights provides much more weight to the nodes with lower  $p_{s_i}$  than the optimal



$\lambda_i$ . As it will be shown by simulations that the  $\Pr(e)$  values obtained by using SNR-maximizing beamforming weights is much higher than those obtained by our proposed beamforming algorithms developed in the next section.

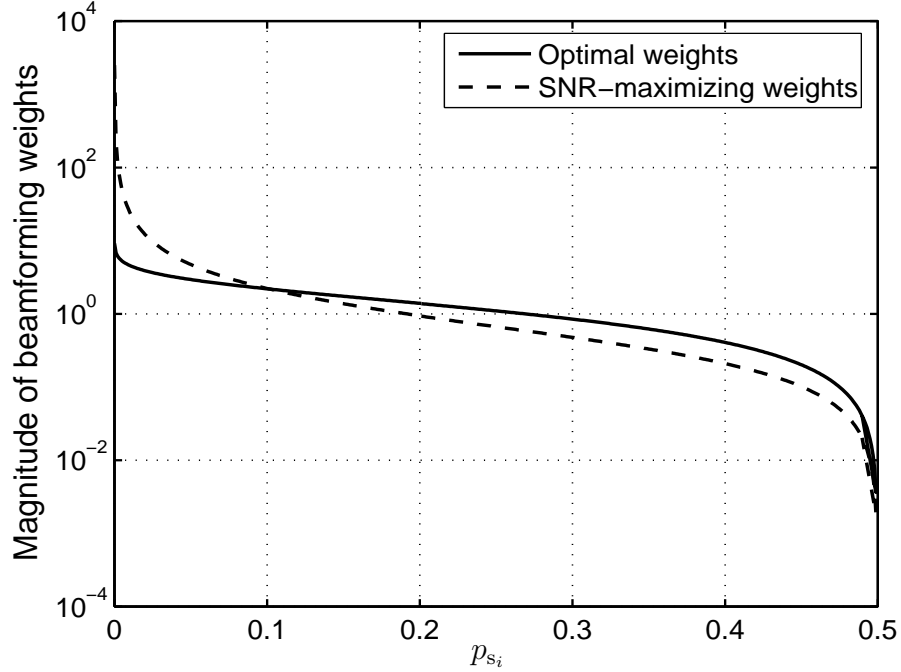


Figure 4.1: The dashed curve depicts the SNR-maximizing beamforming weight in (4.22) for high average relay-destination SNR while the solid curve depicts the optimal weights in (4.7).

### 4.1.3 Beamforming via Equivalent Amplify-and-Forward Relay Model

In this section we develop beamformers for the decode-and-forward relay setting by viewing the problem as one of finding the SNR-maximizing beamformers for an

“equivalent” amplify-and-forward relay setting. We develop an equivalent amplify-and-forward source-relay model for the decode-and-forward model, and use it to develop beamforming algorithms for the decode-and-forward setting.

Given a DFB relay model of interest, we first develop an “equivalent” AFB relay model and then employ the model to develop beamforming algorithms for the decode-and-forward setting. The approach amounts to selecting the source-relay and relay-destination inverse SNRs  $\{\xi_{s_i}^{\text{eff}}\}$  and  $\{\xi_{r_i}\}$ , respectively, in the AFB relay model so that the model is in some sense “equivalent” to the DFB relay model of interest. As a prelude, we first present the SNR maximizing beamformers for an equivalent amplify-and-forward setting with source-relay and relay-destination inverse SNRs  $\{\xi_{s_i}^{\text{eff}}\}$  and  $\{\xi_{r_i}\}$ , respectively. Without loss of generality, after proper scaling, the measurements at the relays can be considered in their unit-power form as follows

$$x_i[n] = \frac{1}{\sqrt{\xi_{s_i}^{\text{eff}} + 1}}x[n] + \frac{\sqrt{\xi_{s_i}^{\text{eff}}}}{\sqrt{\xi_{s_i}^{\text{eff}} + 1}}\bar{v}_i[n] \quad (4.23)$$

where  $\bar{v}_i[n]$  is an IID Gaussian random process with  $\bar{v}_i[n] \sim \mathcal{N}(0, 1)$  and  $\xi_{s_i}^{\text{eff}}$  is the effective inverse SNR of the equivalent amplify-and-forward relay model. The SNR-maximizing beamformers subject to the constraint (2.12) are given by

$$\beta_i \propto \frac{\sqrt{\xi_{s_i}^{\text{eff}} + 1}}{\alpha_{r_i} [(\xi_{s_i}^{\text{eff}} + 1)(\xi_{r_i} + 1) - 1]}. \quad (4.24)$$

The equivalent AFB relay model is chosen based on comparison of the optimal linear detectors based on the relay data in the two relay model settings. Since the optimal detector of  $x[n]$  based on the AFB model relay data is linear, the optimal

linear detector based on the relay data from the equivalent model is given by (4.1)

with

$$\lambda_i \propto \frac{\sqrt{\xi_{s_i}^{\text{eff}} + 1}}{\xi_{s_i}^{\text{eff}}} . \quad (4.25)$$

Comparison of (4.7) and (4.25) suggests that we may view the linear fusion rule arising from a decode-and-forward operation (2.8) as one arising from an amplify-and-forward rule on the model (4.23) where the  $\xi_{s_i}$ 's in the equivalent amplify-and-forward setting are chosen so as to satisfy

$$\log\left(\frac{1 - p_{s_i}}{p_{s_i}}\right) = D \frac{\sqrt{\xi_{s_i}^{\text{eff}} + 1}}{\xi_{s_i}^{\text{eff}}} . \quad (4.26)$$

for some arbitrary  $D > 0$ . An alternative interpretation that also provides the proper choice of  $D$  involves comparison of the log-likelihood functions for the two settings. In particular, for the source-relay setting (2.7) we have

$$\ln \Pr[z_i|x] = C_1 + z_i x \frac{1}{2} \log\left(\frac{1 - p_{s_i}}{p_{s_i}}\right) \quad (4.27)$$

while for the amplify and forward setting (4.23)

$$\ln f(x_i|x) = C_2 + x_i x 2 \frac{\sqrt{\xi_{s_i}^{\text{eff}} + 1}}{\xi_{s_i}^{\text{eff}}} \quad (4.28)$$

and where  $C_1$  and  $C_2$  are independent of  $x$ . Eqns (4.27)-(4.28) suggest modeling a decode-and-forward channel with source-relay CSI  $p_{s_i}$  via an equivalent amplify-and-forward channel with  $\xi_{s_i}^{\text{eff}}$  chosen so as to satisfy equation (4.26) with  $D = 4$ . Solving the resulting quadratic equation in  $\xi_{s_i}^{\text{eff}}$  yields the following positive root for the inverse SNR of an equivalent amplify-and-forward source-relay channel

$$\xi_{s_i}^{\text{eff}} = 4B_i \left[ 2B_i + \sqrt{4B_i^2 + 1} \right] , \quad (4.29)$$

with

$$B_i = \left[ \log \left( \frac{1 - p_{s_i}}{p_{s_i}} \right) \right]^{-1} . \quad (4.30)$$

The preceding equivalent amplify-and-forward channel approach readily suggests a simple yet attractive class of beamforming algorithms for various cases of CSI information at the relays. In particular, in the case that the  $p_{s_i}$ 's are available at the destination, the equivalent-channel SNR-maximizing beamformers are given by (4.24) with  $\xi_{s_i}^{\text{eff}}$  given by (4.29)-(4.30). In the case that the destination only knows the average source-relay SNR the equivalent-channel SNR-maximizing beamformers are given by (4.24) with  $\xi_{s_i}^{\text{eff}} = \bar{\xi}_s^{\text{eff}}$ , where  $\bar{\xi}_s^{\text{eff}}$  is given by (4.29)-(4.30), with  $p_{s_i}$  replaced by  $\bar{p}_s$ . Finally, in the case that the destination possesses an one-bit description of  $p_{s_i}$  via  $\mathcal{F}$  in (2.17), the equivalent-channel SNR-maximizing beamformers are given by (4.24), (4.29), and

$$B_i = \left[ \log \left( \frac{1 - f_i}{f_i} \right) \right]^{-1} . \quad (4.31)$$

Finally, in Sec. 3.2.1, we present a method for determining the quantizer thresholds in (2.17) so as to minimize the destination  $\Pr(e)$  of the proposed beamforming algorithms.

## 4.2 Simulations

In this section, we conduct a performance analysis of the beamforming algorithms developed Sec. 4.1. We first determine the optimal quantizer to be employed at the relay for the case of *one-bit* quantizers. Then we perform Monte-Carlo simulations

to study the performance of the beamforming algorithms based on the optimized quantizers. Finally, we study the effect of the relative location of the relays with respect to the source and the destination on the destination  $\Pr(e)$  for the DFB relay models. Based on these simulations, we derive rule-of-thumb expressions for choosing the relay preprocessing model based on the relative relay locations.

### 4.2.1 Quantizer Threshold Design

For the decode-and-forward via beamforming model, we focus on selecting the thresholds assuming an infinite relays-destination SNR. In particular, we are interested in the quantizer threshold,  $p_t$ , that minimizes the  $\Pr(e)$  of the linear detector of  $x[n]$  based on the relay data  $\{z_{d_i}[n]\}$ , assuming the destination has available one-bit descriptions of the individual source-relay CSIs. In App. B, a closed-form expression is derived for the  $\Pr(e)$  of the detector given by (4.1) and (4.7). The set of equations (2.17), (B.7), (B.5)-(B.9) developed in App. B provides a closed-form expression for the  $\Pr(e)$  of the optimal linear combiner of the relay decodings assuming the  $\mathcal{F}(p_{s_i})$ 's are available at the destination. It can therefore serve as a basis for numerically approximating the value of  $p_t$  that minimizes the destination  $\Pr(e)$ . Fig. 4.2 depicts this  $\Pr(e)$  as a function of the threshold  $p_t$  for a fixed average source-relay BER,  $\bar{p}_s = 0.1$ . The figure suggests the existence of an optimum non-zero threshold  $p_t = p_t^{\text{opt}}$  that minimizes the  $\Pr(e)$  Fig. 4.2.1 depicts the dependence of  $p_t^{\text{opt}}$  on the source-relay average BER,  $\bar{p}_s$ , for various numbers of relay nodes,  $L$ .

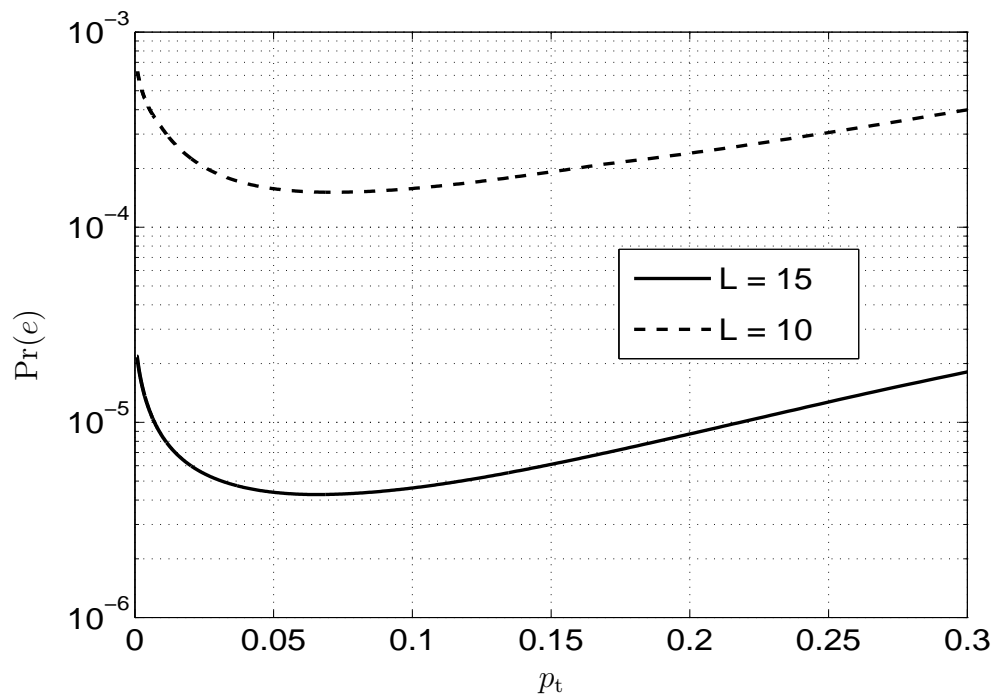


Figure 4.2:  $\Pr(e)$  of the optimal linear detector (4.1), (B.1), (B.2) as a function of the quantizer threshold assuming  $\bar{p}_s = 0.1$ , for  $L = 10$  (dash), and  $L = 15$  (solid).

The dashed, dotted, and dash-dot curves depict the optimum  $p_t$  for  $L = 5$ ,  $L = 15$  and  $L = 25$ . Interestingly, as the figure suggests, the optimum  $p_t$  is very weakly dependent on  $L$ .

Also shown in the figure is a solid curve representing the following function

$$\mathcal{C}_{\text{DF}}(\bar{p}_s) = 1.929\bar{p}_s^2 + 0.5\bar{p}_s - 0.003841 \quad (4.32)$$

obtained via a curve-fitting algorithm. As shown in the figure, the quadratic function in (4.32) accurately approximates the numerically obtained  $p_t^{\text{opt}}$  values as a function of  $\bar{p}_s$  for all the values of  $L$  in the figure.

## 4.2.2 Performance Analysis

In this section, we study the performance of the beamforming algorithms developed in Sec. 4.1 via Monte-Carlo Simulations. We consider the case of the beamformers developed based on full knowledge of  $p_{s_i}$  and the one-bit quantized versions of  $p_{s_i}$  where the quantizer threshold is selected based on the expression (4.32).

Fig. 4.4 depicts the  $\Pr(e)$  performance of the beamforming algorithms based on the equivalent-channel model as a function of  $\bar{\gamma}_{\text{sd}}$  where we assume equal power distribution or equivalently  $\mu$  defined in (3.38) is equal to 0.5. In particular, the successively lower solid curves depict the destination  $\Pr(e)$  of the beamforming algorithms formed based on full knowledge of the values  $p_{s_i}$  for  $L = 2$  and 4. The successively lower dashed curves depicts the  $\Pr(e)$  assuming the destination knows an *one-bit* descriptions of the source-relay CSI, for  $L = 2$ , and 4. Finally, the succes-

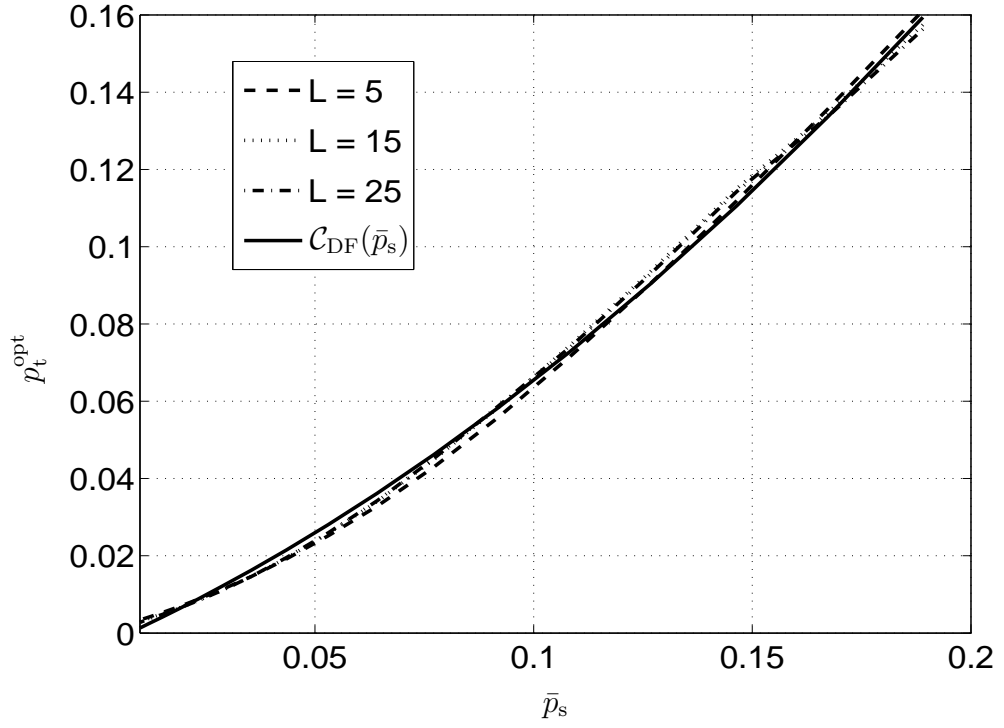


Figure 4.3: Optimal quantizer threshold,  $p_t^{\text{opt}}$ , as a function of  $\bar{p}_s$ . The dashed, dotted, and dash-dot curves show  $p_t^{\text{opt}}$  for  $L = 5$ , 15, and 25, respectively, while the solid curve depicts  $\mathcal{C}_{\text{DF}}(\bar{p}_s)$  in (4.32).



sively lower dash-dot curves depict the  $\Pr(e)$  assuming the destination knows only the average source-relay CSI  $\bar{p}_s$ . As the figure reveals, the quantized beamforming weights provide most of the benefits in terms of  $\Pr(e)$  and diversity order attained by using full knowledge of source-relay channel CSI, provided the quantizer threshold is properly chosen. In addition, we note that employing the quantized beamforming weights incurs a slight increase in SNR loss compared to the amplify-and-forward model. In addition, the SNR loss increases as the total average SNR  $\bar{\gamma}_{sd}$  increases which is due to the fact that the  $\Pr(e)$  for low SNR region is mainly dominated by the relay-destination SNR. Finally, as shown in the figure, the destination  $\Pr(e)$  degrades considerably compared to the one-bit case as well as the diversity order for the case that the destination knows only the average source-relay CSI.

We next determine the optimal power distribution among the source and relays or equivalently the optimal  $\mu$  defined in (3.38). Fig. 4.5 depicts the  $\Pr(e)$  at the destination as a function of  $\mu$  for different values of the total average SNR  $\bar{\gamma}_{sd} = \{5\text{dB}, 10\text{dB}, 15\text{dB}\}$ . The successively lower solid curves marked by 'x' and the successively lower curves marked by 'o' depicts the  $\Pr(e)$  for the case of full knowledge of  $p_{s_i}$  and optimized *one-bit* descriptions  $q_i$ , respectively, are available at the destination. As it is shown by the figure, the equal power distribution (equivalently  $\mu = 0.5$ ) is the optimal strategy for the decode-and-forward relay model. This result was also verified in [15] for amplify-and-forward model and [18] for decode-and-forward model at high SNR values.

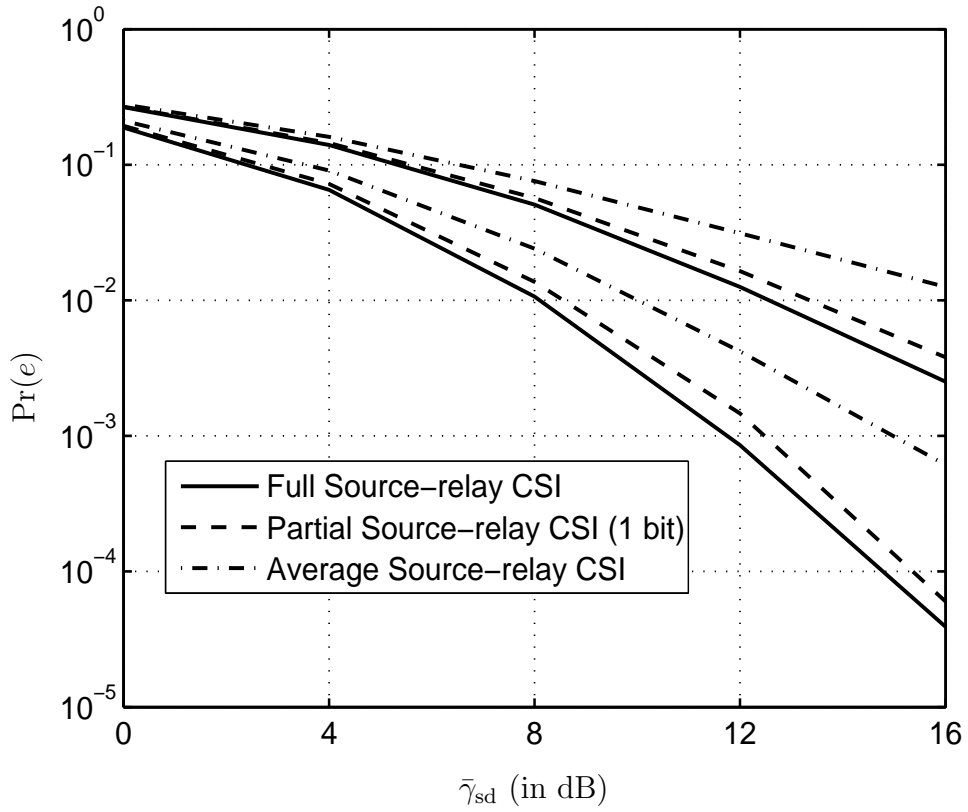


Figure 4.4: The successively lower solid, dashed, and dash-dot curves depict the destination  $\Pr(e)$  for  $L = \{2, 4\}$  as a function of  $\bar{\gamma}_{sd}$  assuming the destination has full knowledge of the source-relay CSI,  $p_{s_i}$ , optimized *one-bit* descriptions of  $q_i$ , and average source-relay CSI  $\bar{p}_s$ , respectively.

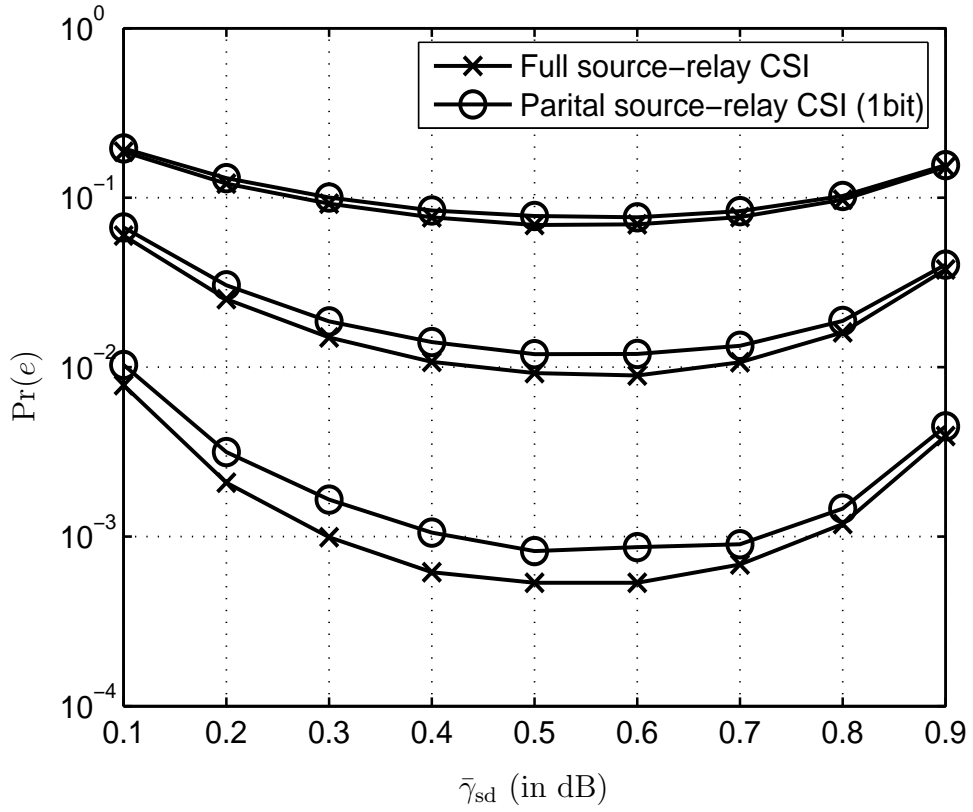


Figure 4.5: The successively lower solid curves marked by 'x' and the successively lower curves marked by 'o' depicts the destination  $\Pr(e)$  for  $\bar{\gamma}_{sd} = \{5\text{dB}, 10\text{dB}, 15\text{dB}\}$  as a function of  $\mu$  assuming the destination has full knowledge of the source-relay CSI,  $p_{s_i}$ , and optimized *one-bit* descriptions  $q_i$ , respectively.

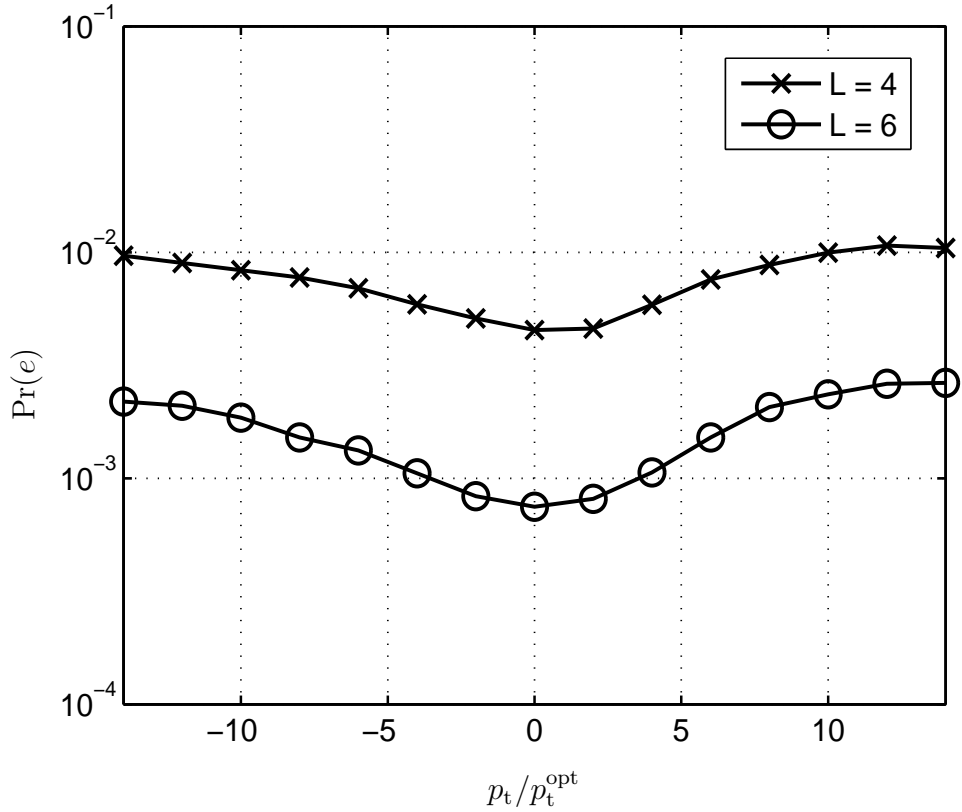


Figure 4.6: The solid curves marked by 'x' and 'o' depict the destination  $\Pr(e)$  performance of the *one-bit* beamforming algorithms as a function of  $p_t/p_t^{\text{opt}}$  for  $L = 4$  and 6, respectively, and  $\bar{\gamma}_{\text{sd}} = 7$  dB.

Similar to the case of the amplify-and-forward model, fig. 4.6 depicts the  $\Pr(e)$  performance of the one-bit quantized beamforming weights as a function of the normalized quantizer threshold  $p_t/p_t^{\text{opt}}$ . In particular, in fig. 4.6, the successively lower curves marked by 'x', 'o' depict the  $\Pr(e)$  performance for  $L = 2$  and 4, respectively. As the figure reveals, the quantizer threshold  $p_t^{\text{opt}}$  given by the function  $\mathcal{C}_{\text{DF}}(\bar{p}_s)$  optimizes the  $\Pr(e)$  compared to other thresholds.

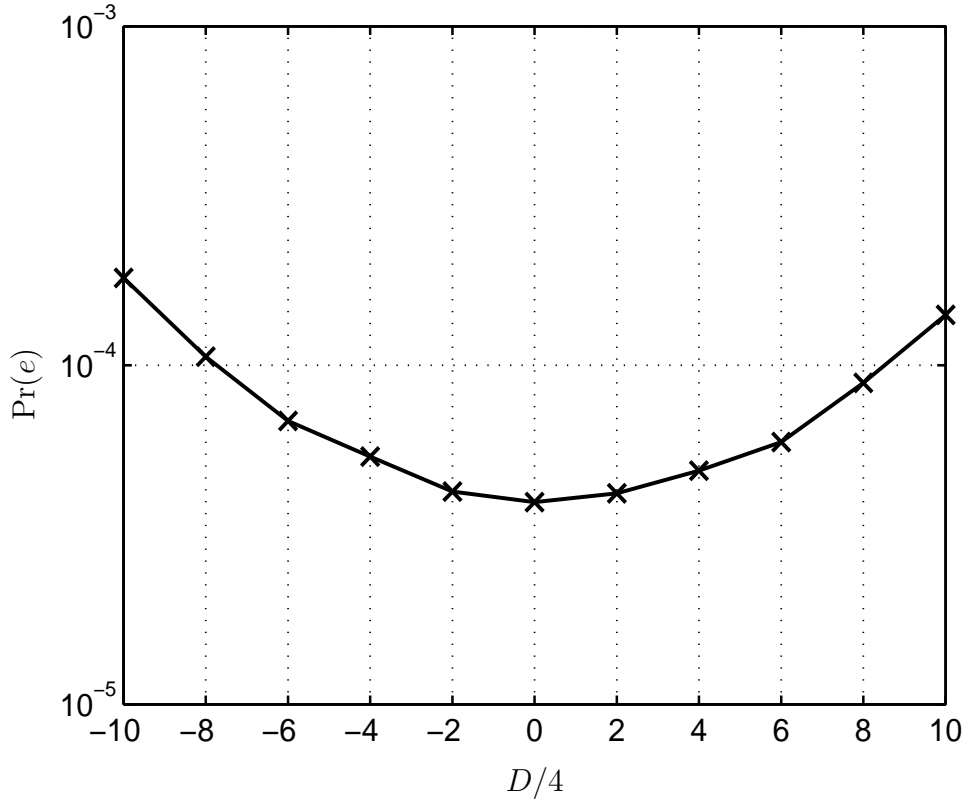


Figure 4.7: The figure depicts the destination  $\Pr(e)$  performance of the beamforming algorithms formed based on  $p_{s_i}$  as function of  $\frac{D}{4}$  for  $L = 3$  and  $\bar{\gamma}_{sd} = 19$  dB.

Fig. 4.7 depicts the effect of varying the constant  $D$  in the expression (4.26) on the  $\Pr(e)$  values at the destination. In particular, the figure depicts the  $\Pr(e)$  for the case of beamformers formed based on  $p_{s_i}$  as a function of a normalized  $\frac{D}{4}$  where  $D = 4$  is the optimal value, for  $L = 3$  and  $\bar{\gamma}_{sd} = 19$  dB. As it was shown in Sec. 4.1, that selecting the optimal value of  $D = 4$  minimizes the  $\Pr(e)$  at the destination.

For comparison purposes, fig. 4.8 depicts the performance of the SNR-maximizing beamformers formed directly on the decode-and-forward model as presented in

Sec. 4.1.2 (solid curves) and the equivalent-channel beamformers (dashed curves), respectively, when the destination knows the  $p_{s_i}$ 's for  $L = 3, 4$ . As the figure reveals, the proposed algorithms outperform the SNR-maximizing algorithms for the decode-and-forward setting especially for high SNR values.

### 4.3 Location-optimized Preprocessing Relay Strategy

In this section, our objective is to determine the relative location of the relays with respect to the source and the destination for the decode-and-forward model. In addition, we compare the  $\Pr(e)$  performance of the AFB and DFB relays at relative relay locations and determine the optimal preprocessing strategy at each relative relay location. We focus our attention on the case where only single bit descriptions of the source-relay CSI are available at the destination.

Fig. 4.9 depicts the  $\Pr(e)$  of the *one-bit* beamformers as a function of  $\tau$  defined in (3.39) and  $\bar{\gamma}_s = \bar{\gamma}_r = 5dB$ . The successively solid curves marked by 'x' and 'o' represent the decode-and-forward relay model and the amplify-and-forward model, respectively, for  $L = 5, 10, 15$ . As the figure reveals, the optimal location of the relays for the decode-and-forward model as well as the amplify-and-forward is weakly dependent on  $L$ . In addition, the optimal location of the relays for the decode-and-forward model is given approximately by  $\tau = 0.35$ . For the amplify-

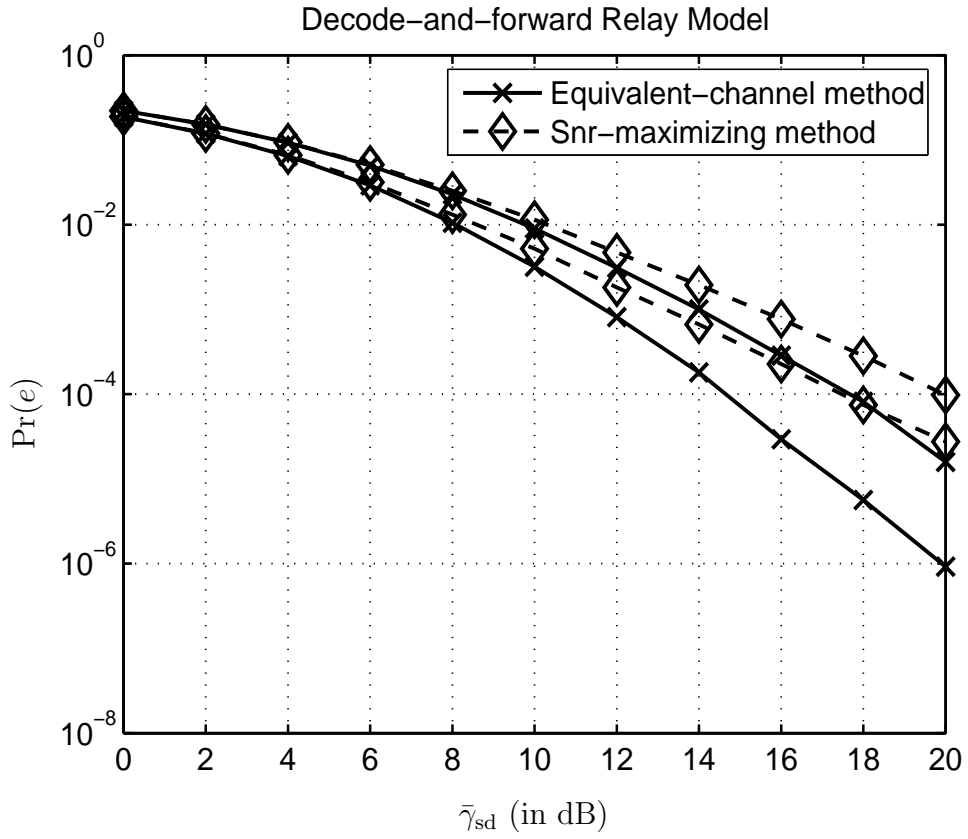


Figure 4.8: The successively lower solid curves marked by 'x' and the successively lower dash curves marked by 'o' depicts the destination  $\Pr(e)$  for  $L = \{3, 4\}$  as a function of  $\bar{\gamma}_{sd}$  for the SNR-maximizing beamformers and the equivalent-channel beamformers, respectively, when the destination knows the values of  $\{p_{s_i}\}'s$

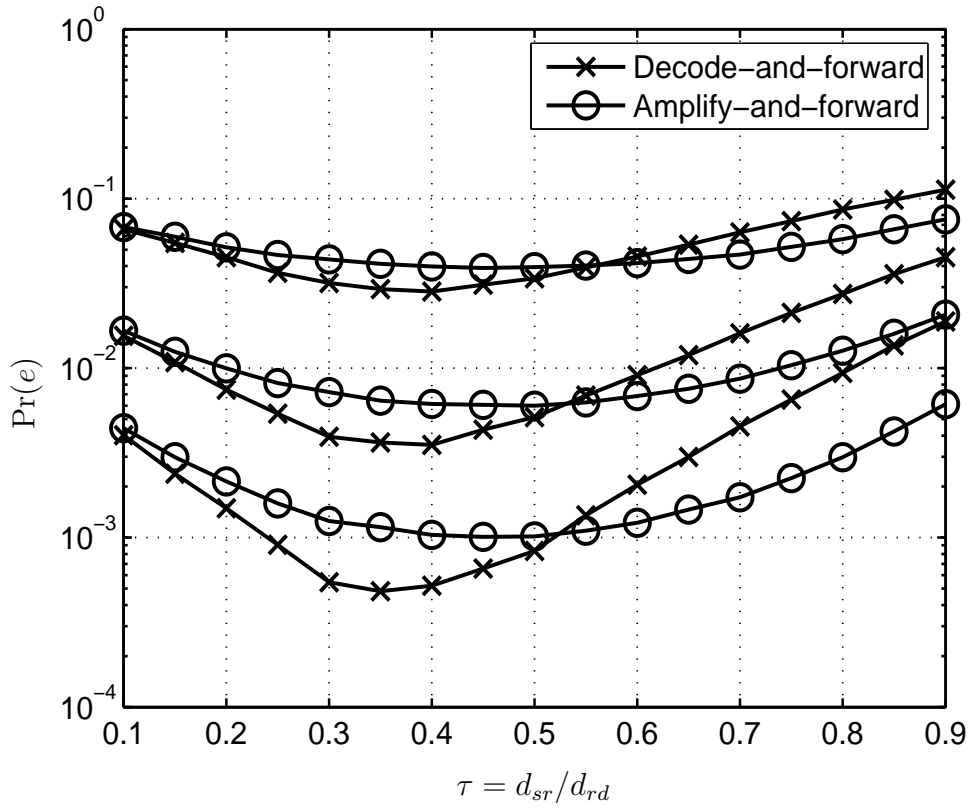


Figure 4.9: The successively lower solid curves marked by 'x' and the successively lower solid curves marked by 'o' depicts the destination  $\Pr(e)$  for  $L = \{5, 10, 15\}$  as a function of  $\tau$  for the decode-and-forward relay model and the amplify-and-relay model, respectively.



and-forward model, the optimal location is half the distance between the source and destination.

The figure also suggests a method for choosing between AFB and DFB relaying based on the relative locations between the relays the source and the destination. Specifically, if the source-relay proximity index is less than 0.5 (the relays are closer to the source than the destination), then it is advantageous in terms of  $\Pr(e)$  to employ DFB relaying, while AFB relaying gives favorable  $\Pr(e)$  performance if the relays are closer to the destination ( $\tau > 0.5$ ). Also, as it is revealed by the figure, the  $\Pr(e)$  benefits by picking the  $\tau$ -optimized relaying strategy become more substantial as the number of relays increases. Such significant  $\Pr(e)$  benefits by picking the right relaying strategy can be especially attractive in dense large-scale sensor network applications, where it is possible to employ large numbers of nodes as relays.

Also, the figure illustrates that the  $\Pr(e)$  performance provided by employing of both the amplify-and-forward and the decode-and-forward relay models model is approximately the same as the relay nodes get closer to the source. This is due to the fact the quality of the source-relay channels increases significantly as the relays gets closer to the source. As a result, the source-relay channels can be effectively viewed as perfect channels in the limit as  $\tau \rightarrow 0$ . This leads to the conclusion that the type of processing employed at the relays has no effect on the  $\Pr(e)$  at the destination as the relay nodes with very high probability can have perfect estimates

of the source signal  $x[n]$ .

On the other side where  $\tau \rightarrow 1$  or equivalently the relays get closer the destination, the  $\Pr(e)$  values at the destination for the amplify-and-forward relay model outperform those attained by employing the decode-and-forward relay model. For the case of  $\tau \rightarrow 1$ , the problem can be viewed as finding the optimal linear detector based on either soft decisions  $z_{a_i}[n]$  defined in (2.6) or hard decisions,  $z_{d_i}[n]$  defined in (2.8) of  $x[n]$  for the case of amplify-and-forward model and decode-and-forward model, respectively. This problem has been solved in the literature [28] and it was shown that the  $\Pr(e)$  performance of system detectors based on soft decodings outperforms those who are based on hard decodings.

Fig. 4.9 also suggests a method for individual relay-dependent relaying in cases where the individual source-relay proximity indexes differ from relay to relay. In particular, due to the weak dependence of the optimal relaying strategy on the number of nodes  $L$ , Fig. 4.9 also suggests that a viable approach is to have each node choose its relaying strategy based on its own source-relay proximity index. Once the relaying strategy is selected for a given relay node, its beamforming weight is readily selected as the one (among the two provided in Secs. 3.1–4.1) corresponding to the chosen relaying strategy. This location-optimized adaptive beamforming algorithms will be shown in the next chapter.

## Chapter 5

# Location-Optimized Adaptive Beamforming Algorithms

In this chapter, we develop adaptive beamforming algorithms that optimize the destination  $\Pr(e)$  for every possible relative location of the relays. In particular, we consider a network setting for which we develop a selection strategy that determines the preprocessing type at each relay whether amplify-and-forward or decode-and-forward so as to minimize the destination  $\Pr(e)$ . In Chaps. 3 and 4, we determine the optimal preprocessing relaying strategy given any relative relay location. This requires that the relay nodes must have the knowledge of its relative location. The problem of determining the exact locations of the nodes is a challenging problem that requires a lot of coordination between the nodes or employing Global positioning system (GPS) at each nodes which are not desired in large-scale networks. Therefore, in this chapter, we consider developing adaptive algorithms that can determine, based on the available source-relay and relay-destination CSI rather than the relative

relay location, the optimal preprocessing to be performed at each relay.

In general, the type of preprocessing relaying selected by each relay must be agreed upon by the relays and the destination. This suggests two scenarios for performing the selection strategy. The first is a destination-based selection strategy where the destination based on the available CSI determines the processing at each relay then feedback the results to each relay. The second is a relay-based selection strategy where each relay determines its processing strategy then informs the destination. Since we assume that destination has the knowledge of the source-relay and relay-destination CSI compared to the relays which only know their source-relay CSI, It is evident that the destination-based selection strategy must outperform the relay-based selection strategy in terms of  $\Pr(e)$ . On the other hand, the destination-based selection strategy requires additional feedback bandwidth to inform the relays of their selected relaying strategies. In this chapter, we determine the tradeoffs in terms of  $\Pr(e)$  and bandwidth of the two selection strategies.

The adaptive beamforming algorithms developed in this chapter is characterized by being performed on a node-by-node basis where for the destination-based strategy the destination selects the processing at each relay in a way that only depends on the channel state information of its source-relay and relay-destination channels. While for the relay-based selection strategy, each relay decides based on its source-relay CSI. This node-by-node basis strategy is computationally efficient and requires minimum overhead bandwidth. For instance, in the case of the destination-

based strategy, the problem of finding the optimal selection strategy requires that the destination, based on the availability of the CSI of the channels involved in communications, computes the instantaneous SNR at the destination for all the possible combinations of the processing that can be selected for each relay. For example, for a number of relay nodes  $L = 2$ , to find the optimal processing for each of the two relays, the destination must compute the instantaneous SNR, for four different cases; amplify-and-forward for both nodes, decode-and-forward for both nodes, and amplify-and-forward for node 1 while decode-and-forward for node 2 or vice versa. Clearly, this process requires a lot of computation by the destination and most importantly that the computation process grows exponentially in  $L$  which is considered a major disadvantage for sensor networks where the number of nodes is in the order of thousands. Therefore, it is desirable that the selection strategy at the destination can be performed on a node-by-node basis by only considering the CSI of the source-relay and relay-destination of each relay node. For the case of relay-based selection strategy, the optimal strategy requires that the relay node has the knowledge of the source-relay and relay-destination CSIs. This has the problem of increasing the overhead bandwidth considerably especially for large scale nodes. As it will be shown in this chapter, that the node-by-node basis selection strategies incur a negligible loss in  $\Pr(e)$  compared to methods that exploit the available CSI of all source-relay and relay-destination channels.

In contrast to Chap. 3 and Chap. 4, we develop beamforming algorithms

for the cases where we assume that the relay nodes are all either amplifying-and-forward or decoding-and-forward. For the case of adaptive beamforming algorithms, this assumption is not necessarily valid. As depending on the node-by-node basis selection strategy used, we can have a hybrid network setting where subset of the relay nodes are selected to employ an amplify-and-forward relaying while decode-and-forward relaying will be selected for the rest of the nodes. Therefore, in this chapter, we develop beamforming algorithms assuming a hybrid network setting that combine the output signals of the relays at the destination so as to minimize the  $\Pr(e)$ .

As it will be shown in this chapter via simulations, the node-by-node basis adaptive beamforming algorithms provide the best  $\Pr(e)$  performance among the decode-and-forward and amplify-and-forward relay model for all possible relative relay locations with respect to the source and the destination. In addition, we show that the location of the relay node relative to the source, if available, defined by  $\tau$  in (3.39) can be considered as a sole key design factor in selecting the optimal relaying strategy for each relay node.

The outline of this chapter is as follows. In Sec. 5.1, we develop hybrid beamforming algorithms for the case where different processing strategies are employed at the relays. Then, in Sec. 5.2, we first develop destination-based selection strategy and its associated adaptive beamforming algorithm. To this end, we first determine the optimal selection strategy assuming that all the nodes can either amplify

or decode. Based on this optimal strategy and by using the equivalent amplify-and-forward model, we develop a node-by-node basis selection strategy where the destination selects the type of processing to be employed at each node as well as its associated beamforming weight based only on the CSI of its source-relay and relay-destination channel. Finally, we develop relay-based selection strategy and determine its  $\Pr(e)$  performance compared to the destination-based selection strategy.

## 5.1 Adaptive Beamforming Algorithms for Hybrid Networks

In this section, we develop adaptive beamforming algorithms for hybrid networks where subset of the nodes are employing amplify-and-forward relaying while the rest are employing decode-and-forward relaying. We first determine lower bounds on  $\Pr(e)$  by finding the beamforming weights for the case of high average relay-destination SNR,  $\bar{\gamma}_r \rightarrow \infty$ . Then based on the equivalent amplify-and-forward relay model presented in Sec. 4.1, we next present a method for constructing the beamforming algorithms for the hybrid networks assuming various levels of information available on the quality of the source-relay CSI.

### 5.1.1 High Average Relay-Destination SNR Beamformers

In this section, we develop beamforming weights for the hybrid case assuming high average relay-destination ( $\bar{\gamma}_r \rightarrow \infty$ ) and full knowledge of source-relay CSI ( $\gamma_{s_i}$  and  $p_{s_i}$ ) is available at the destination. Under these assumptions, the received signal at the destination, based on (2.11) can be represented as follows,

$$y_d = \sum_{i=1}^{L_a} \beta_{a_i} z_{a_i} + \sum_{i=1}^{L_d} \beta_{d_i} z_{d_i} \quad (5.1)$$

where  $z_{a_i}$  and  $z_{d_i}$  is defined in (2.6) and (2.8), respectively. The notations  $L_a$  and  $L_d$  denotes the number of relay nodes that employ amplify-and-forward relaying and decode-and-forward relaying, respectively.

Without loss of generality, we focus our attention on finding the optimal weights for the case of  $L = 2$  where an amplify-and-forward relaying is selected for one node ( $L_a = 1$ ) and the other node is employing decode-and-forward relaying ( $L_d = 1$ ). The extension for the case of any number of relay nodes can be adequately generalized. Under this assumption, the expression,  $y_d$  in (5.1) can be conveniently expressed using (2.6) and (2.8) as follows,

$$y_d = \beta_a \left( \frac{1}{\sqrt{1 + \xi_s}} x + \frac{\sqrt{\xi_s}}{\sqrt{1 + \xi_s}} \bar{v} \right) + \beta_d e x. \quad (5.2)$$

where the subscript  $i$  is dropped for convenience. Our objective is to find the weights,  $\beta_a$  and  $\beta_d$ , so as to minimize the  $\Pr(e)$  at the destination. The  $\Pr(e)$  expression given the values of  $\gamma_s, p_s$  based on (5.2) is given by ,

$$\Pr(e|\gamma_s, p_s) = (1 - p_s) Q \left( \sqrt{2\gamma_s(1 + \chi)^2} \right) + p_s Q \left( \sqrt{2\gamma_s(1 - \chi)^2} \right), \quad (5.3)$$



where  $\chi$  is defined as follows,

$$\chi = \frac{\beta_d}{\beta_a} \sqrt{1 + \xi_s}. \quad (5.4)$$

It is evident from the above  $\Pr(e)$  expression, that our objective is to find the ratio  $\frac{\beta_d}{\beta_a}$  that minimizes the  $\Pr(e)$ . By applying simple algebraic calculation, we can find that the optimal ratio is given by,

$$\frac{\beta_d}{\beta_a} = \left[ \frac{1}{4} \log \left( \frac{1 - p_s}{p_s} \right) \right] \left[ \frac{\xi_s}{\sqrt{\xi_s + 1}} \right] \quad (5.5)$$

yielding a minimum  $\Pr(e|\gamma_s, p_s)$  given by,

$$\begin{aligned} \Pr(e|\gamma_s, p_s) = (1 - p_s) & Q \left( \sqrt{2\gamma_s \left( 1 + \frac{\xi_s}{4} \log \left( \frac{1 - p_s}{p_s} \right) \right)^2} \right) \\ & + p_s Q \left( \sqrt{2\gamma_s \left( 1 - \frac{\xi_s}{4} \log \left( \frac{1 - p_s}{p_s} \right) \right)^2} \right). \end{aligned} \quad (5.6)$$

Since the preceding analysis was performed for the case of  $\bar{\gamma}_r \rightarrow \infty$ , it can only provides an expression for the optimal ratio  $\beta_d/\beta_a$  given by (5.5) rather the optimal individual values of  $\beta_d$  and  $\beta_a$ . However, by comparing the obtained optimal ratio in (5.5) with the beamforming weights obtained for high  $\bar{\gamma}_r$  defined by (3.7) for the amplify-and-forward model and (4.7), we can deduce that,

$$\begin{aligned} \beta_a & \propto \frac{\sqrt{\xi_s + 1}}{\xi_s}, \\ \beta_d & \propto \frac{1}{4} \log \left( \frac{1 - p_s}{p_s} \right). \end{aligned} \quad (5.7)$$

We remark that the above results suggest that the beamforming weights selected for each relay node is independent of the type of the processing performed at the

other relay nodes. As a result, the optimal beamforming weights can be selected remarkably on a node-by-node basis. This is remarkably a desirable design feature especially in the case of sensor nodes where each relay node has the freedom to select its relaying strategy along with its associated beamforming weight without the need to alter the beamforming weights of the remaining nodes. We also remark that expression obtained for the optimal beamforming weight of the decode-and-forward model for the case of hybrid networks verifies that the optimal D defined in Sec. 4.1 is equal to 4.

### 5.1.2 Equivalent Amplify-and-forward Beamformers for Hybrid Networks

In this section, we present beamforming algorithms for the hybrid networks based on the equivalent amplify-and-forward method developed in Sec. 4.1. As shown in Sec. 4.1, we present a method for developing an equivalent amplify-and-forward source relay model to the decode-and-forward relay model by finding the effective SNR of the equivalent model by comparing the optimal linear fusion rules of both model as the average relay-destination  $\bar{\gamma}_r \rightarrow \infty$ . The main advantage of this method is that effective SNR for each source-relay node can be found on a node-by-node basis as the effective SNR of each decode-and-forward model only depends on the CSI of its source-relay and relay-destination channels. Also, it was shown in the previous section that the optimal beamforming weight for a hybrid network as  $\bar{\gamma}_r \rightarrow \infty$

for the decode-and-forward model is equivalent to the one developed for the case where all the nodes employ decode-and-forward model. As a result, the equivalent amplify-and-forward method can be readily used to find the beamforming weights.

In particular, for a network setting where  $L_a$  nodes are employing an amplify-and-forward and  $L_d$  nodes are employing decode-and-forward model whose received sequences at the destination is given by

$$y_d = \sum_i^{L_a} \beta_{a_i} \alpha_{r_i} \left( \frac{1}{\sqrt{1 + \xi_{s_i}}} x + \frac{\sqrt{\xi_{s_i}}}{\sqrt{1 + \xi_{s_i}}} \bar{v} \right) + \sum_i^{L_d} \beta_{d_i} \alpha_{r_i} e_i x + w, \quad (5.8)$$

the equivalent amplify-and-forward model can be represented as follows

$$y_d = \sum_i^{L_a} \beta_{a_i} \alpha_{r_i} \left( \frac{1}{\sqrt{1 + \xi_{s_i}}} x + \frac{\sqrt{\xi_{s_i}}}{\sqrt{1 + \xi_{s_i}}} \bar{v} \right) + \sum_i^{L_d} \beta_{d_i} \alpha_{r_i} \left( \frac{1}{\sqrt{1 + \xi_{s_i}^{\text{eff}}}} x + \frac{\sqrt{\xi_{s_i}^{\text{eff}}}}{\sqrt{1 + \xi_{s_i}^{\text{eff}}}} \bar{v} \right) + w. \quad (5.9)$$

where  $\xi_{s_i}^{\text{eff}}$  is given by the expression (4.29) and (4.31). Similarly, using Cauchy-Schwartz inequality, the beamforming weights that minimize the  $\text{Pr}(e)$  for the equivalent amplify-and-forward model under the power constraint (2.12) can be given by,

$$\beta_{a_i} \propto \frac{\sqrt{\xi_{s_i} + 1}}{\alpha_{r_i} [(\xi_{s_i} + 1)(\xi_{r_i} + 1) - 1]}, \quad (5.10)$$

$$\beta_{d_i} \propto \frac{\sqrt{\xi_{s_i}^{\text{eff}} + 1}}{\alpha_{r_i} [(\xi_{s_i}^{\text{eff}} + 1)(\xi_{r_i} + 1) - 1]}.$$

We next consider developing beamforming algorithms for hybrid networks assuming coarse *one-bit* descriptions of the source-relay channels are available at the destination. We first develop an equivalent amplify-and-forward relay model for the relay nodes employing decode-and-forward relaying by using the method developed

in Sec. 4.1. In particular, the received sequences for the equivalent amplify-and-forward relay model can be represented as follows,

$$y_d = \sum_i^{L_a} \beta_{a_i} \alpha_{r_i} \left( \frac{1}{\sqrt{1 + \xi_{s_i}}} x + \frac{\sqrt{\xi_{s_i}}}{\sqrt{1 + \xi_{s_i}}} \bar{v} \right) + \sum_i^{L_a} \beta_{d_i} \alpha_{r_i} \left( \frac{1}{\sqrt{1 + \xi_{s_i}^{\text{eff}}}} x + \frac{\sqrt{\xi_{s_i}^{\text{eff}}}}{\sqrt{1 + \xi_{s_i}^{\text{eff}}}} \bar{v} \right) + w. \quad (5.11)$$

where  $\xi_{s_i}^{\text{eff}}$  is given by (4.29) and (4.31). By using the Cauchy-Schwartz inequality, the optimal beamforming weights, under the power constraint (2.12), and using the analysis developed in Sec. 3.1.2 are given by

$$\beta_{a_i} \propto \frac{1}{\alpha_{r_i}} \left[ \frac{\left( \frac{a_i}{c_i} \right)}{1 + \xi_{r_i} - \left( \frac{a_i}{c_i} \right)^2} \right], \quad (5.12)$$

$$\beta_{d_i} \propto \frac{\sqrt{\xi_{s_i}^{\text{eff}} + 1}}{\alpha_{r_i} [(\xi_{s_i}^{\text{eff}} + 1)(\xi_{r_i} + 1) - 1]}.$$

where  $\xi_{s_i}^{\text{eff}}$  is given by (4.29) and (4.31).

We finally remark that the threshold for the quantizers employed at the relays are selected according to the function  $\mathcal{C}_{\text{AF}}(\cdot)$  defined in (3.37) and the function  $\mathcal{C}_{\text{DF}}(\cdot)$  defined in (4.32) for the amplify-and-forward model and the decode-and-forward model, respectively. This is due to the fact that employing optimal beamforming algorithm for the equivalent amplify-and-forward model results in the following maximum SNR at the destination

$$\gamma_d^{\text{max}} = \sum_{i=1}^{L_a} \frac{1}{(1 + \xi_{s_i})(1 + \xi_{r_i}) - 1} + \sum_{i=1}^{L_d} \frac{1}{(1 + \xi_{s_i}^{\text{eff}})(1 + \xi_{r_i}) - 1}. \quad (5.13)$$

The above expression can be viewed as the sum of the maximum SNR attained by the amplify-and-forward relay model and that attained by the decode-and-forward

model. This suggests that the problem of finding the optimal threshold for each processing model can be decoupled and solved separately and still the SNR expression defined in (5.13) is maximized. As a result, the optimal threshold functions,  $\mathcal{C}_{\text{AF}}(\cdot)$  and  $\mathcal{C}_{\text{DF}}(\cdot)$  developed in Sec. 4.2.1 and Sec. 3.2.1, respectively, can be readily used to optimize the  $\text{Pr}(e)$  for the case of hybrid networks.

## 5.2 Destination-based Relay Processing Selection Strategy

In this section, we present a destination-based selection strategy for determining the type of information processing to be employed at each relay so as to optimize the  $\text{Pr}(e)$  at the destination. We assume that the selection strategy as well as the associated beamforming weights are processed at the destination then feedback to the relays over a broadcast feedback channel. The main characteristic of this strategy that it can be performed on a node-by-node basis where the preprocessing model at each relay is selected based only the quality of its source-relay and relay-destination channels and independent of the CSI of the channels of the other relays. This node-by-node basis selection feature is advantageous in sensor networks where the number of nodes are relatively large and computing the optimal selection strategy is exponentially large in the number of nodes. In addition, this selection strategy can adapt quickly to networks where the number of operating nodes can vary with

time due to node mobility or nodes leaving the network due to their short battery lifetime.

As it will be shown later, that the optimized selection strategy along with the adaptive beamforming algorithms presented in Sec. 5.1 provide the best of the  $\Pr(e)$  performance achieved by either of the decode-and-forward and amplify-and-forward model without the need for the knowledge of the location of the relays. This feature is attractive in the area of wireless sensor networks where determining the accurate location of the sensor node is difficult especially for large number of nodes [29–31]. Also, for application like target tracking or applications that involves mobility of the nodes, the adaptive beamforming algorithms can adapt quickly to the channel variations. This is definitely is achieved on the expense of increase of overhead bandwidth as the destination has to inform each relay, as the channel varies, its type of relay preprocessing model.

This section is organized as follows. We first consider a homogenous network model where we assume that all the nodes are selected to employ either an amplify-and-forward or decode-and-forward relaying, respectively. Given this network model, we first present an optimal selection strategy that optimizes the  $\Pr(e)$  performance for all possible locations of the relays. Next, for the same network model, we present an alternative selection strategy based on the equivalent amplify-and-forward channel method that provides the same  $\Pr(e)$  performance attained by the optimal selection strategy. Finally, based on this equivalent-channel selection

strategy, we develop a node-by-node basis selection strategy for hybrid network that optimizes destination  $\Pr(e)$  values.

### 5.2.1 Optimal Selection Strategy for Homogenous Networks

In this section, we present an optimal selection strategy to determine the processing type at each relay for homogenous networks where we assume that the all nodes are either amplifying or decoding. We consider the case of full knowledge of the CSI of both source-relay and relay-destination channels are available at the destination.

We develop an optimal selection strategy whereby the destination determines the type of processing employed at the relays based on comparing the  $\Pr(e)$  values for each realization of the destination SNR,  $\gamma_d$ , of the amplify-and-forward model and the decode-and-forward model, respectively. Specifically, given the instantaneous values of the CSI of the source-relay channels,  $\gamma_{s_i}$  and the relay-destination channels,  $\gamma_{r_i}$ , the destination compares the  $\Pr(e)$  expression defined in (A.8) for the decode-and-forward model where  $\beta_i$  is given by (4.24) and (2.12) and the  $\Pr(e)$  expression for the amplify-and-forward model given by

$$\Pr(e|\gamma_{s_i}, \gamma_{r_i}) = Q \left( \sqrt{2 \sum_i \frac{1}{[(\xi_{s_i} + 1)(\xi_{r_i} + 1) - 1]}} \right). \quad (5.14)$$

This strategy is optimal in the sense of minimizing the  $\Pr(e)$  at the destination as comparing the  $\Pr(e)$  expression for a given instantaneous CSI of the source-relay and relay-channels minimizes the average  $\Pr(e)$  at the destination.

We study the performance of the optimal selection strategy via Monte-Carlo

simulations. Fig. 5.1 depicts the  $\Pr(e)$  at the destination as function of the location of the relay nodes defined by  $\tau$  in (3.39) for  $L = 8$  and  $\bar{\gamma}_{sd} = 5dB$ . The solid curves marked by 'x' and 'o' depict the  $\Pr(e)$  values for the case that the relay nodes are always selected to decode-and-forward and amplify-and-forward, respectively. The solid curve marked by '∇' depicts the  $\Pr(e)$  at the destination provided by the optimal selection strategy that utilizes the beamforming weights developed in Sec. 5.1. As the figure reveals, the optimal selection strategy provides the minimum of the  $\Pr(e)$  values provided by the amplify-and-forward and decode-and-forward relay models.

We next study the probability of using the decode-and-forward model versus the amplify-and-forward provided by the optimal selection strategy as a function of the location of the relays. Fig. 5.2 depicts the probability of using the decode-and-forward model defined by  $\Pr_{DF}$  as a function of the location of the relays  $\tau$ . The figure shows that, for values of  $\tau < 0.5$  (equivalently the relays are closer to the source than the destination), the optimal selection strategy chooses the decode-and-forward model with probability  $\Pr_{DF}$  almost equal to one. As the values of  $\tau$  increases above 0.5,  $\Pr_{DF}$  decreases sharply that almost approaches zero for values of  $\tau > 0.7$ . This figure suggests that the destination can select the optimal strategy to be employed at the relays if the location of the relays are known to the destination or equivalently the average SNR values of the source-relay and relay-destination channels. However, this type of information is difficult to obtain especially in the



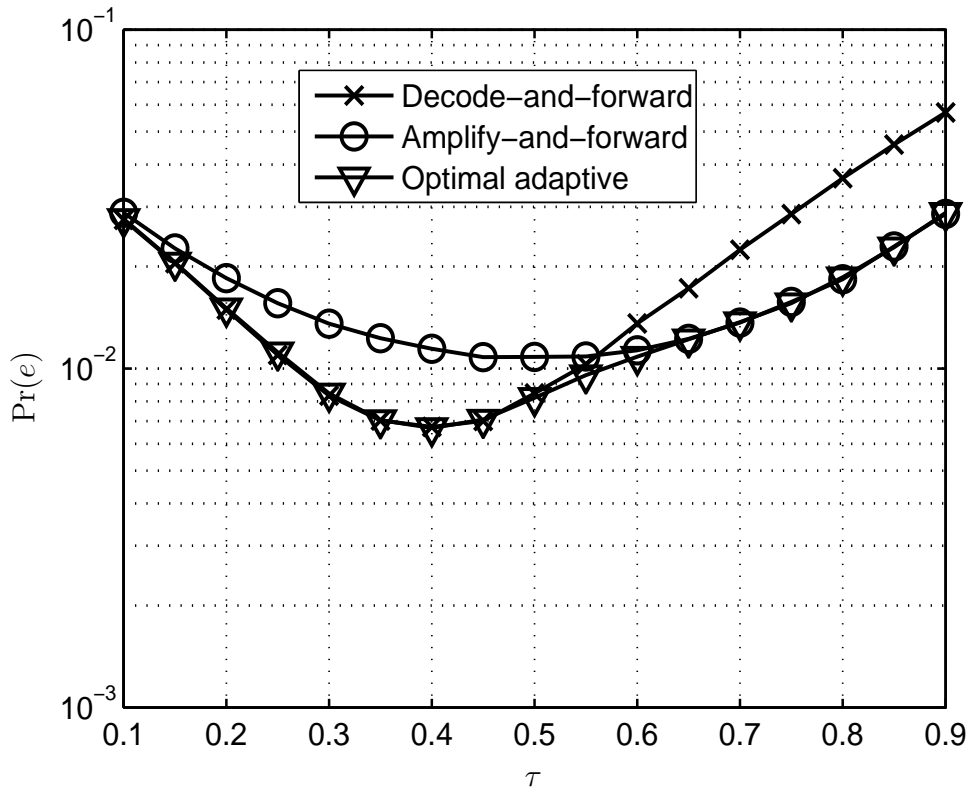


Figure 5.1: The solid curves marked by 'x' and marked by 'o' depicts the destination  $\Pr(e)$  for  $L = 8$  and  $\bar{\gamma}_{sd} = 5\text{dB}$  as a function of  $\tau$  assuming the destination has full knowledge of the source-relay CSI. The solid curves marked by 'v' depicts the  $\Pr(e)$  provided with the optimal selection strategy developed in Sec. 5.2.1 for homogenous networks.

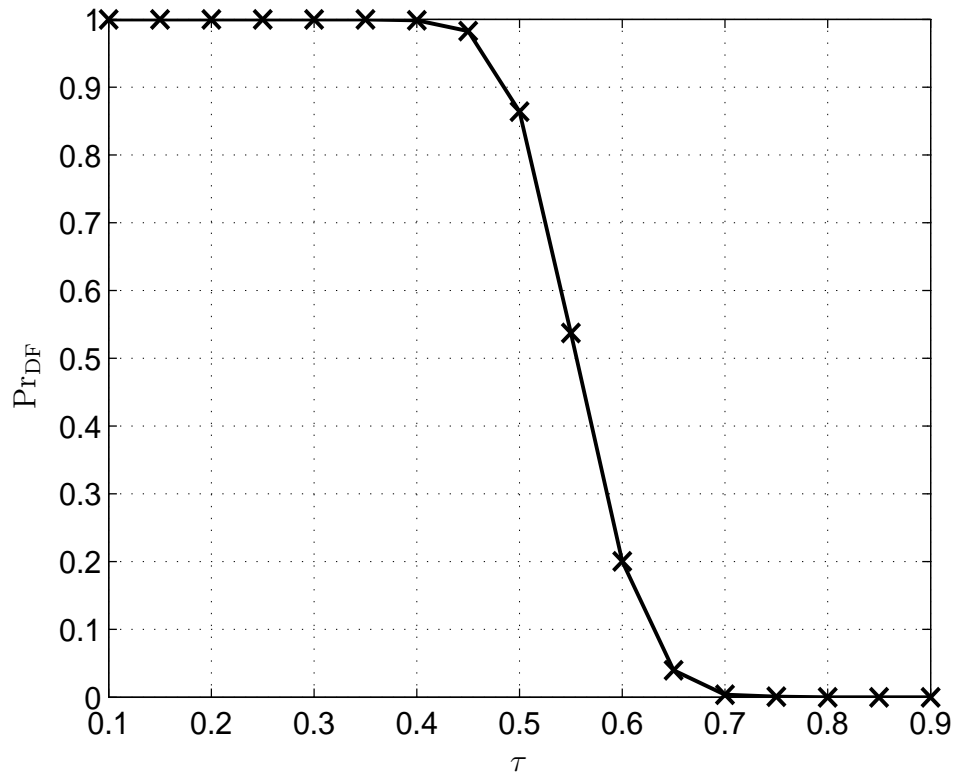


Figure 5.2: The solid curves marked by 'x' depicts the probability that the selection strategy chooses decode-and-forward model,  $\text{Pr}_{\text{DF}}$ , as a function of  $\tau$ .

case of sensor network as it requires that a GPS should be implemented at each sensor which increases the hardware complexity of the sensors. Therefore, the optimal selection strategy can be proved useful in optimizing the  $\text{Pr}(e)$  if the exact location of each relay is not available at the destination.

Finally, we remark that the optimal selection strategy has a major disadvantage that the strategy depends on the CSI of all the source-relay and relay-destination channels. Hence, if any node decides to join or leave the network, the

selection process needs to be recomputed for all the relay nodes which is not desirable in terms of computational complexity and processing delay.

### 5.2.2 Equivalent-channel Relay Selection Strategy

In this section, we present an alternative strategy for the optimal selection strategy presented in Sec. 5.2 based on the equivalent amplify-and-forward relay method presented in Sec. 4.1.3. This equivalent-channel based relay selection strategy, as it will be shown later, serves as a basis for developing the node-by-node basis selection strategy.

The main idea of the equivalent-channel selection strategy is to find a method to compare the maximum SNR attained by employing the optimal beamforming weights developed in Sec. 5.1.2 for the equivalent-channel relay model with that achieved with the amplify-and-forward model such that the destination  $\Pr(e)$  matches that attained by using the optimal selection strategy. In particular, we compare the maximum SNR

$$\gamma_{d,DF}^{\max} = \sum_{i=1}^L \frac{1}{(1 + \xi_{s_i}^{\text{eff}})(1 + \xi_{r_i}) - 1}. \quad (5.15)$$

attained by the equivalent amplify-and-forward model with the maximum SNR

$$\gamma_{d,AF}^{\max} = \sum_{i=1}^L \frac{1}{(1 + \xi_{s_i})(1 + \xi_{r_i}) - 1}. \quad (5.16)$$

We remark that we can not compare directly the values of  $\gamma_{d,AF}^{\max}$  and  $\gamma_{d,DF}^{\max}$  to determine the relay processing strategy. We first note that for the amplify-and-

forward relay model, the values of  $\gamma_{d,AF}^{\max}$  determines the values of the  $\Pr(e)$ , given the values of  $\xi_{r_i}$  and  $\xi_{s_i}$ , according to the following,

$$\Pr_{AF}(e|\xi_{s_i}, \xi_{r_i}) = Q(\sqrt{2\gamma_{d,AF}^{\max}}). \quad (5.17)$$

On the other hand, although the equivalent amplify-and-forward method provides an effective SNR for the decode-and-forward model, this effective SNR was mainly developed by matching the beamforming weights for the decode-and-forward relay model and its equivalent amplify-and-relay model at high average relay-destination SNR ( $\bar{\gamma}_r \rightarrow \infty$ ). Therefore, the  $\Pr(e)$  attained at the destination can not be represented directly as  $Q(\sqrt{2\gamma_{d,DF}^{\max}})$ . However, we can compare a skewed version of the equivalent-channel maximum SNR  $\gamma_{d,DF}^{\max}$  with the maximum SNR  $\gamma_{d,AF}^{\max}$  as follows

$$\gamma_{d,AF}^{\max} \underset{DF}{\overset{AF}{\gtrless}} \kappa \gamma_{d,DF}^{\max}. \quad (5.18)$$

where the constant  $\kappa$  can be optimized by matching the  $\Pr(e)$  values besides the  $\Pr_{DF}$  of the optimal selection strategy with the values obtained by using the above selection strategy. Using numerical techniques, we find that the value of  $\kappa$  that provide an almost the same  $\Pr(e)$  performance as the optimal selection strategy is equal to 2.9. Fig. 5.3 depicts the  $\Pr(e)$  destination as a function of  $\tau$  for  $L = 8$  and  $\bar{\gamma}_{sd} = 5\text{dB}$ . The solid curves marked by 'x' and 'o' depicts the  $\Pr(e)$  obtained using the optimal selection strategy and the equivalent-channel strategy, respectively. As the figure reveals, the two strategies provides the same destination  $\Pr(e)$  performance. Fig. 5.4 depicts the probability of using decode-and-forward model for the

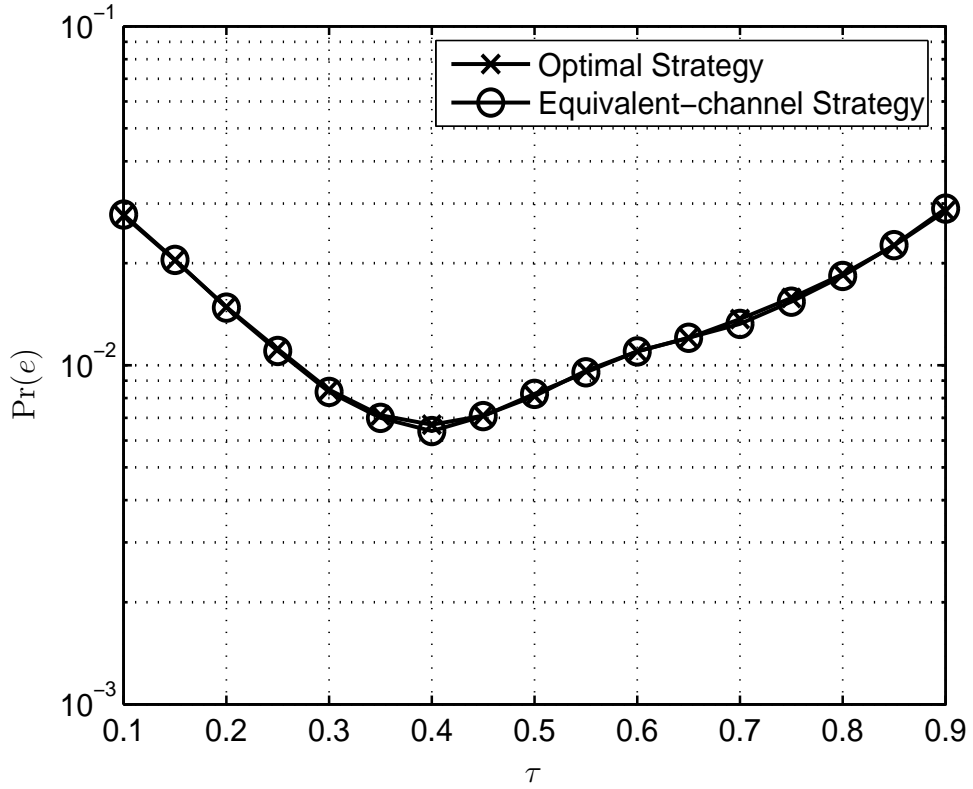


Figure 5.3: The solid curves marked by 'x' and marked by 'o' depicts the destination  $\Pr(e)$  for  $L = 8$  and  $\bar{\gamma}_{\text{sd}} = 5\text{dB}$  as a function of  $\tau$  for the case of optimal selection strategy and equivalent-channel selection strategy, respectively.

optimal selection strategy (marked by 'x') and equivalent-channel selection strategy (marked by 'o') as a function of  $\tau$  for  $L = 8$  and  $\bar{\gamma}_{\text{sd}} = 5\text{dB}$ . As the figure reveals, the  $\Pr_{\text{DF}}$  obtained by using the equivalent-channel method with  $\kappa = 2.9$  is equal to that obtained using the optimal selection strategy.

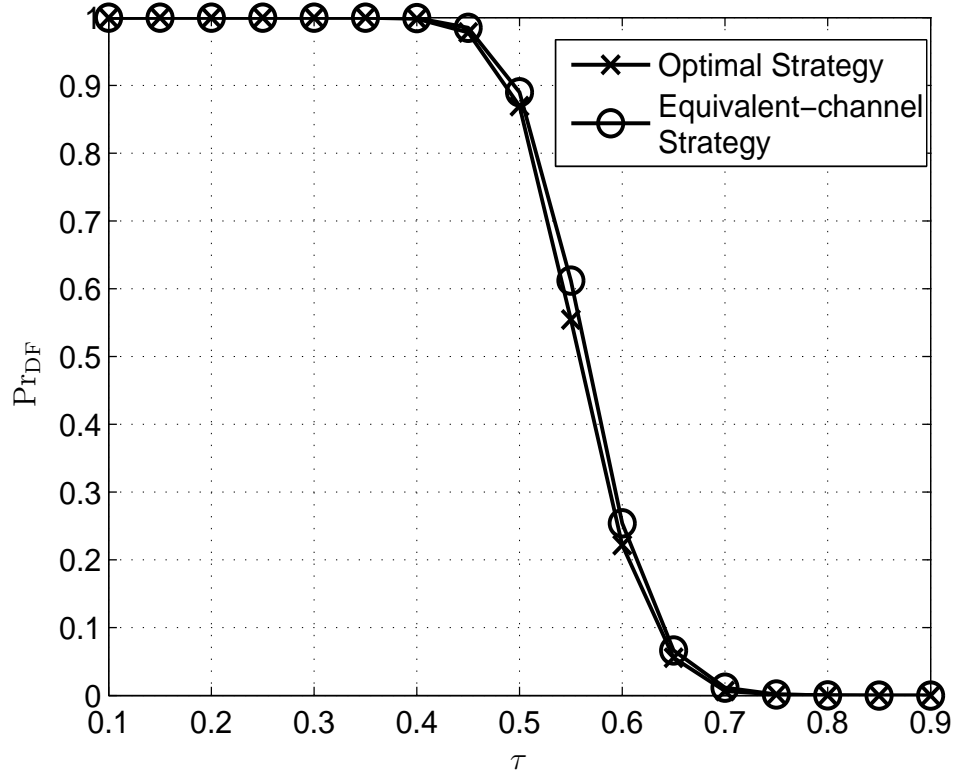


Figure 5.4: The solid curves marked by 'x' and 'o' depict the probability of employing decode-and-forward relaying,  $\Pr_{DF}$ , as a function of  $\tau$  for the case of optimal selection strategy and equivalent-channel selection strategy, respectively .

### 5.2.3 Node-by-Node Basis Relay Selection Strategy

In this section, we develop a node-by-node basis selection strategy based on the equivalent-channel selection strategy developed in Sec. 5.2.2. In particular, we develop a strategy where the destination selects for each node whether to amplify or decode independent of the type of processing at the other relays. This kind of strategy results in the formation of hybrid networks where the network are partitioned into two distinct networks with the first one employing amplify-and-forward model and the second is employing decode-and-forward model cooperating using beamforming to minimize the  $\Pr(e)$  at the destination.

By examining the maximum SNR expression defined in (5.13) attained by using the equivalent-channel for hybrid networks, we can deduce that using the optimal beamforming weights results in viewing the channels from the source to the destination as an equivalent  $L$  parallel channels each with maximum SNR value

$$\gamma_{i,AF}^{\max} = \left[ \frac{1}{(1 + \xi_{s_i})(1 + \xi_{r_i}) - 1} \right], \quad (5.19)$$

and

$$\gamma_{i,DF}^{\max} = \left[ \frac{1}{(1 + \xi_{s_i}^{\text{eff}})(1 + \xi_{r_i}) - 1} \right]. \quad (5.20)$$

for amplify-and-forward and decode-and-model, respectively. This suggest that selecting the maximum of the individual values of  $\gamma_{i,DF}^{\max}$  and  $\gamma_{i,AF}^{\max}$  yields in maximizing the combined SNR at the destination. However, as mentioned before, the effective SNR obtained by using the equivalent-channel model can not be used to find the

$\Pr(e)$ . Therefore, we compare  $\gamma_{i,\text{AF}}^{\max}$  with a skewed version of  $\gamma_{i,\text{DF}}^{\max}$  similar to the equivalent-channel selection strategy as follows,

$$\gamma_{i,\text{AF}}^{\max} \underset{\text{DF}}{\overset{\text{AF}}{\gtrless}} \kappa \gamma_{i,\text{DF}}^{\max}. \quad (5.21)$$

where the constant  $\kappa$  was determined for the equivalent-channel selection strategy to be equal to 2.9. As it is revealed by the above expression, the selection strategy selects the processing at each relay independent of the processing performed at the other relays as it depends on the CSI of its source-relay and relay-destination channels.

We next study the performance of the node-by-node basis strategy and compare it to the optimal selection strategy. Fig. 5.5 depicts the destination  $\Pr(e)$  as a function of  $\tau$  for  $L = 8$  and  $\bar{\gamma}_{\text{sd}} = 5\text{dB}$ . The solid curves marked by 'x' and 'o' depicts the  $\Pr(e)$  for the case of optimal strategy and node-by-node selection strategy. As the figure reveals, the node-by-node selection strategy incurs a very small loss compared to the optimal selection strategy. Fig. 5.6 depicts the  $\Pr_{\text{DF}}$  as a function of  $\tau$  for the optimal selection strategy (marked by 'x') and the equivalent-channel selection strategy (marked by 'o'). It is revealed by the figure that  $\Pr_{\text{DF}}$  using the node-by-node basis selection strategy approximates to a large extent the  $\Pr_{\text{AF}}$  provided by the optimal selection strategy. We remark that the above simulations verify the result that if the location of the relay node is below half of the distance to the source, then the decode-and-forward relaying should be selected. While for nodes located at more than half of the distance to the source, the amplify-and-forward



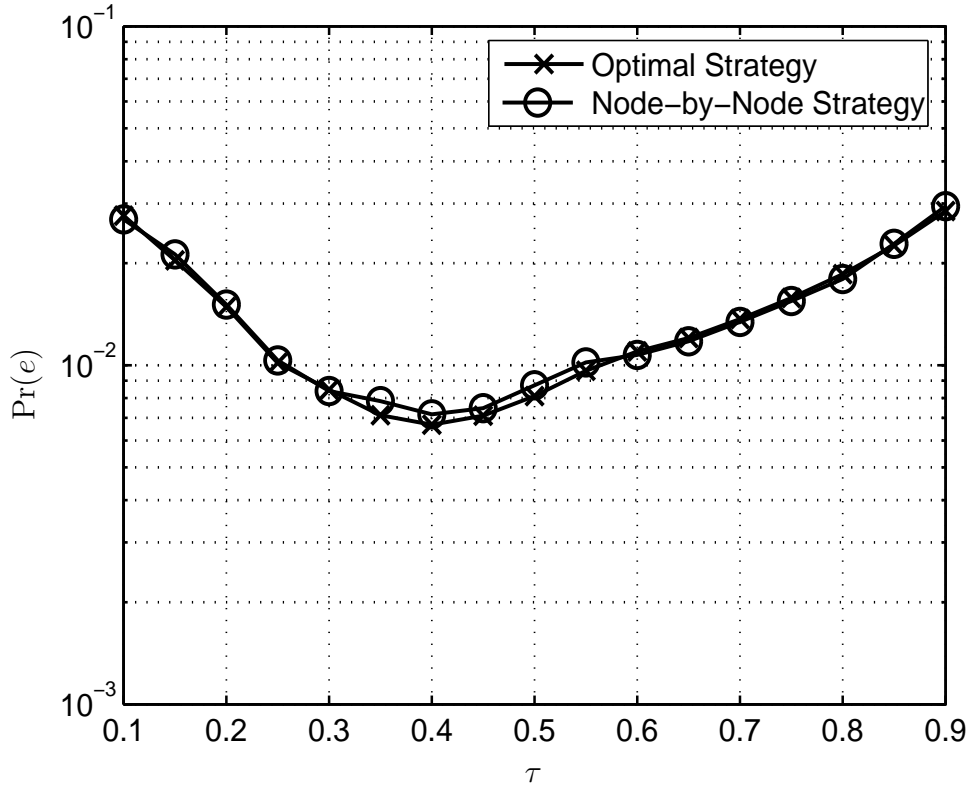


Figure 5.5: The solid curves marked by 'x' and marked by 'o' depicts the destination  $\Pr(e)$  for  $L = 8$  and  $\bar{\gamma}_{sd} = 5\text{dB}$  as a function of  $\tau$  for the case of optimal selection strategy and node-by-node selection strategy, respectively.

relaying is desirable.

We remark that if the location of the node is available upon joining the network is available at the destination, then it can select the optimal preprocessing model at the relays. However, for the case of mobile networks where the location information could be hard to estimate, the method defined by (5.21) determines the optimal processing strategy without the need for the knowledge of the location of

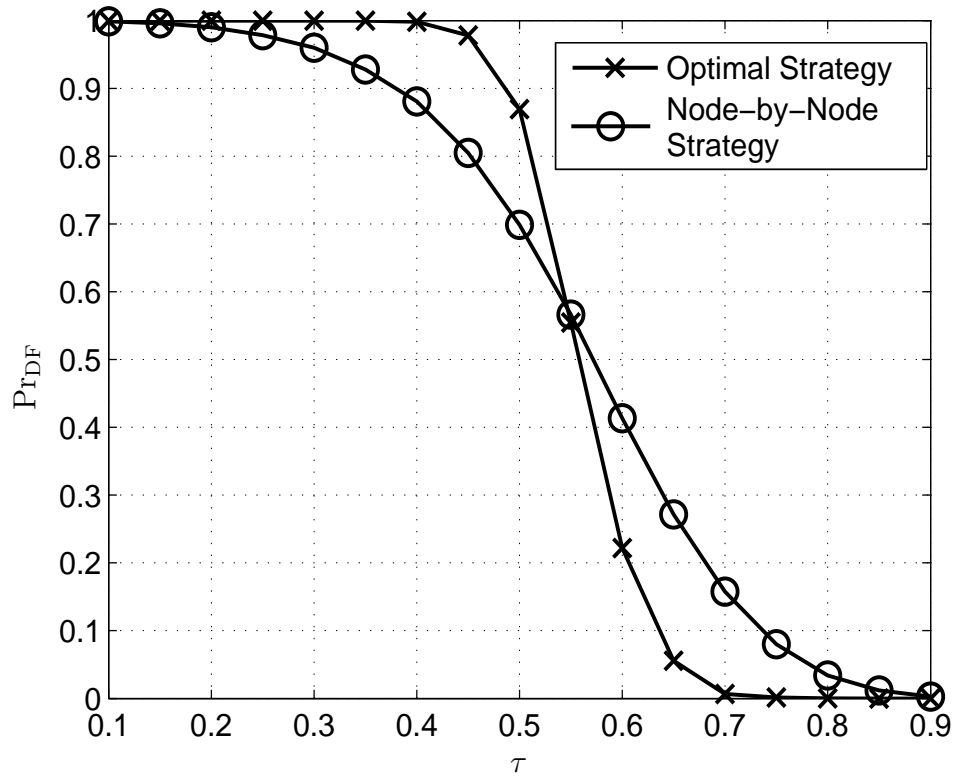


Figure 5.6: The solid curves marked by 'x' and 'o' depict the probability of employing decode-and-forward relaying,  $\Pr_{DF}$ , as a function of  $\tau$  for the case of optimal selection strategy and node-by-node selection strategy, respectively .

the relays at the destination.

We finally note that for the case of one-bit source relay-CSI quantizers are used at the relays, the same selection strategies can be used where the maximum SNR for the amplify-and-forward model is given by (3.33). While for the decode-and-forward relay model, the equivalent effective SNR is given by (4.29) where  $B_i$  is given by (4.31).

### 5.3 Relay-based Preprocessing Selection Strategy

In this section, we develop relay-based preprocessing selection strategy. In particular, we assume that the relays determine by themselves whether to use the AFB relay model or the DFB relay model. The selection is made at each relay based on its source-relay CSI. Specifically, if the source-relay CSI falls below a certain threshold  $\eta$ , the relay selects the AFB relay model, otherwise, it selects the DFB relay model. This selection has the advantage of eliminating the need for the destination to feedback to the relays the preprocessing strategies to be used. However, the relay-based selection strategy suffers from the disadvantage that each relay must only decide based on its source-relay CSI. This is in contrast to the destination-based method where the destination has the knowledge of each source-relay CSI and relay-destination CSI.

The relay-based selection strategy for a given threshold  $\eta$  can be expressed as follows,

$$\gamma_{s_i} \underset{\text{AFB}}{\overset{\text{DFB}}{\gtrless}} \eta. \quad (5.22)$$

Our objective is to determine the optimal value of  $\eta$  that optimize the destination  $\text{Pr}(e)$  performance at any given location. Our approach in finding the optimal threshold is to find the threshold that provides almost the same of behavior of  $\text{Pr}_{\text{DF}}$  as a function of  $\tau$  shown in fig. 5.6. Using exhaustive search techniques, we find that the optimal threshold  $\eta$  that optimizes the  $\text{Pr}(e)$  value using the relay-based strategy at any given location is equal to 0.45 .

Fig. 5.7 compares the  $\text{Pr}(e)$  performance of the relay-based selection strategy for  $\eta = 0.45$  with the  $\text{Pr}(e)$  performance of the AFB and DFB relay model. As the figure reveals, the  $\text{Pr}(e)$  attained by using the relay-based selection strategy incur a small loss compared to the  $\text{Pr}(e)$  performance attained by the AFB relay model if the relays are close to the source and similarly for the DFB relay model. Also, it is evident that the destination-based selection strategy provides a better  $\text{Pr}(e)$  performance compared the relay-based selection strategy on the expense of using additional feedback bandwidth.

Fig. 5.8 depicts the probability of using the DFB relay model,  $\text{Pr}_{\text{DF}}$  as a function of  $\tau$ . As the figure reveals, the  $\text{Pr}_{\text{DF}}$  values attained by using relay-based selection strategy does not exactly match that attained by using the destination-based selection strategy. For example, when the value of  $\tau = 0.9$ , the relay-based strategy

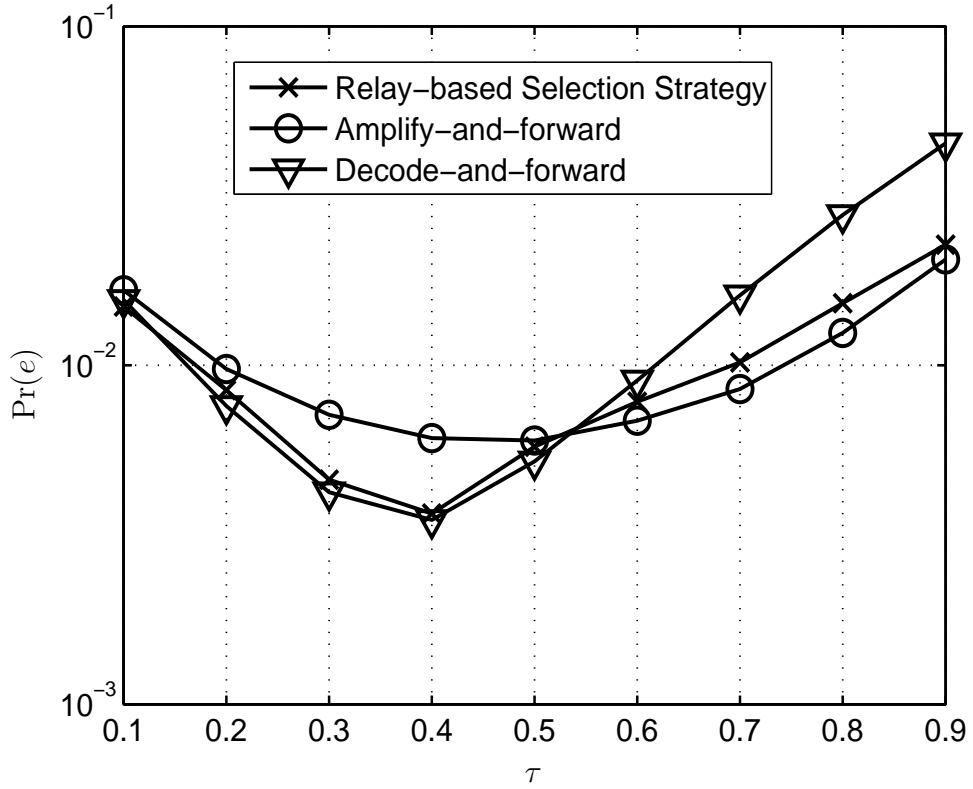


Figure 5.7: The solid curves marked by 'x', 'o' 'v' depict the destination  $\Pr(e)$  for  $L = 10$  and  $\bar{\gamma}_{sd} = 5\text{dB}$  as a function of  $\tau$  for the case of relay-based selection strategy, employing AFB relay model, and employing DFB relay model, respectively.

allows for 10% of the nodes to use DFB relay model while for the destination-based strategy, the probability of using DFB relay model is almost zero. This explains why the relay-based selection strategy does not provide the minimum  $\Pr(e)$  at any given relative relay location.

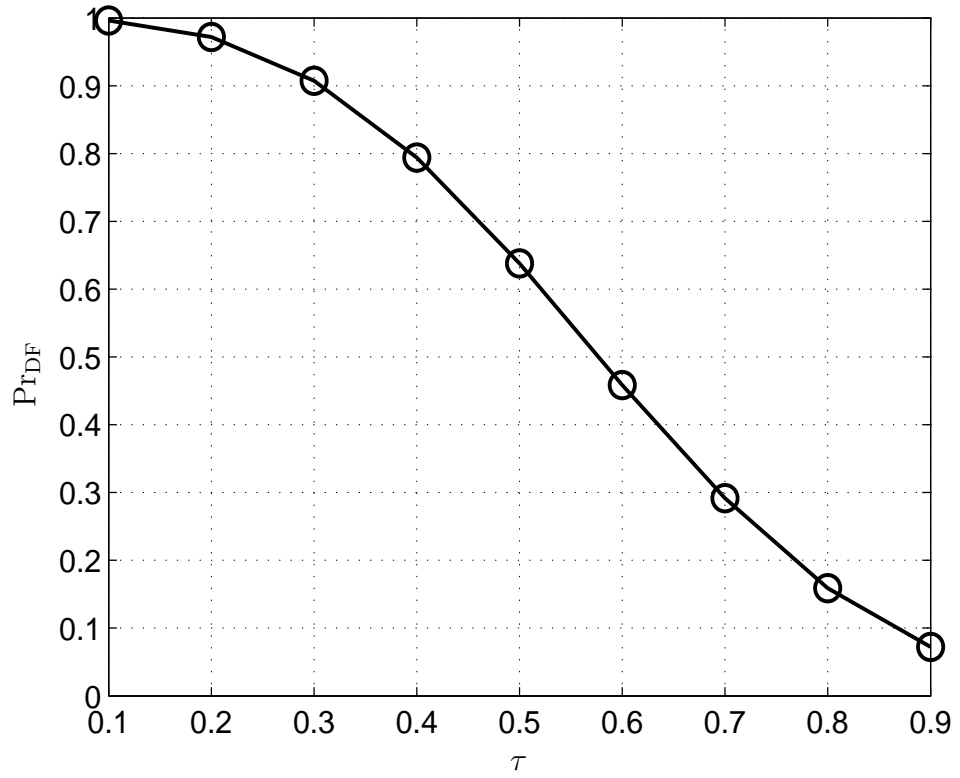


Figure 5.8: The solid curve depicts the probability of employing decode-and-forward relaying,  $\text{Pr}_{\text{DF}}$ , as a function of  $\tau$  for the case of relay-based selection strategy.

## Chapter 6

# Beamforming Algorithms for Multi-hop Networks

In this chapter, we develop beamforming algorithms for networks that involve multi-hop relaying. We develop extensions for the beamforming algorithms presented in Chaps. 3 and 4. Multi-hop relaying is attractive in high dense networks where, due to the limited power constraint, nodes can only transmit reliably to the neighboring nodes that fall within its proximity. In addition, multi-hop relaying minimizes the interference in the network as it limits the need to use extra power to achieve successful transmission between a source and a far destination.

In delivering the data per hop, we consider a hierarchal clustering approach. In particular, excluding the first broadcast data hop, each set of nodes is divided into number of groups. Each group consists of a communication set of transmitting nodes and receiving nodes. In the clustering approach, the communication set represents a cluster where the receiving nodes transmit its data to a one receiving node denoted

as the cluster head (CH).

Clustering has been proved resource-efficient useful for information propagation and data fusion. In particular, clustering reduces the amount of energy for transmitting the data across the network. In addition, it reduces the overall bandwidth as it minimizes the communication overhead among the nodes. A variety of clustering algorithms have been developed with the objective of achieving better energy efficiency and minimizing the number of the clusters that covers the whole network [32–34]. We remark that there exists other techniques to perform data aggregation in multi-hop relaying such as the case where multiple transmitting nodes are communicating to multiple receiving nodes. We did not consider these techniques in our study as it requires a lot of coordination between the relay nodes. This coordination is usually difficult to implement in large-scale networks.

Although the hierarchal clustering approach suggests the use of beamforming methods, designing these beamforming weights properly for each cluster poses many challenges that has been addressed in this chapter. We develop methods for effectively capturing the channel state information (CSI) at each relay. Based on these effective CSI, we present methods to construct the beamforming weights locally for each cluster which optimize the  $\Pr(e)$  at the destination. For the case of using optimized one-bit descriptions of the source-relay CSIs, we determine the optimal quantizer to be used at each relay and its associated beamforming weight. We also determine the type of relay preprocessing model to be employed at each



hop. Finally, we develop algorithms for finding the optimal locations for any given number of hop networks as well as the associated preprocessing relay model.

This chapter is organized as follows. We first present a system model for a multi-hop network involving hierarchal clustering. We then develop algorithms to select the beamforming weights at each hop for the amplify-and-forward and decode-and-forward relay models. For the case of using one-bit quantizers, we show how to select the quantizer threshold at each hop for each relay preprocessing type. Finally, we develop an algorithm to find the optimal location of the relay nodes for any given multi-hop network and the associated data preprocessing relay model.

## 6.1 System Model

We consider a setting of multi-hop relaying. The setting in its simplest form is shown in Fig. 6.1 where first the data broadcasted from the source are beamformed to a set of cluster heads (CHs) then the CHs form a cluster that beamforms the received data to the destination. This setting includes two levels of clustering. In general,  $M$ -level of clustering corresponds to  $M+1$  levels of hops. We assume that at the  $i$ th level of clustering, the nodes are divided into  $\mathcal{C}_i$  clusters. We assume that the number of nodes per cluster is equal and given by  $L$  and the power allocated to each cluster at the same level is equal and denoted by  $P_{h_i}$ . The number of clusters formed at each level of clustering is given by

$$\mathcal{C}_i = L^{M-i} \quad \forall i = 1, 2, \dots, M \quad (6.1)$$

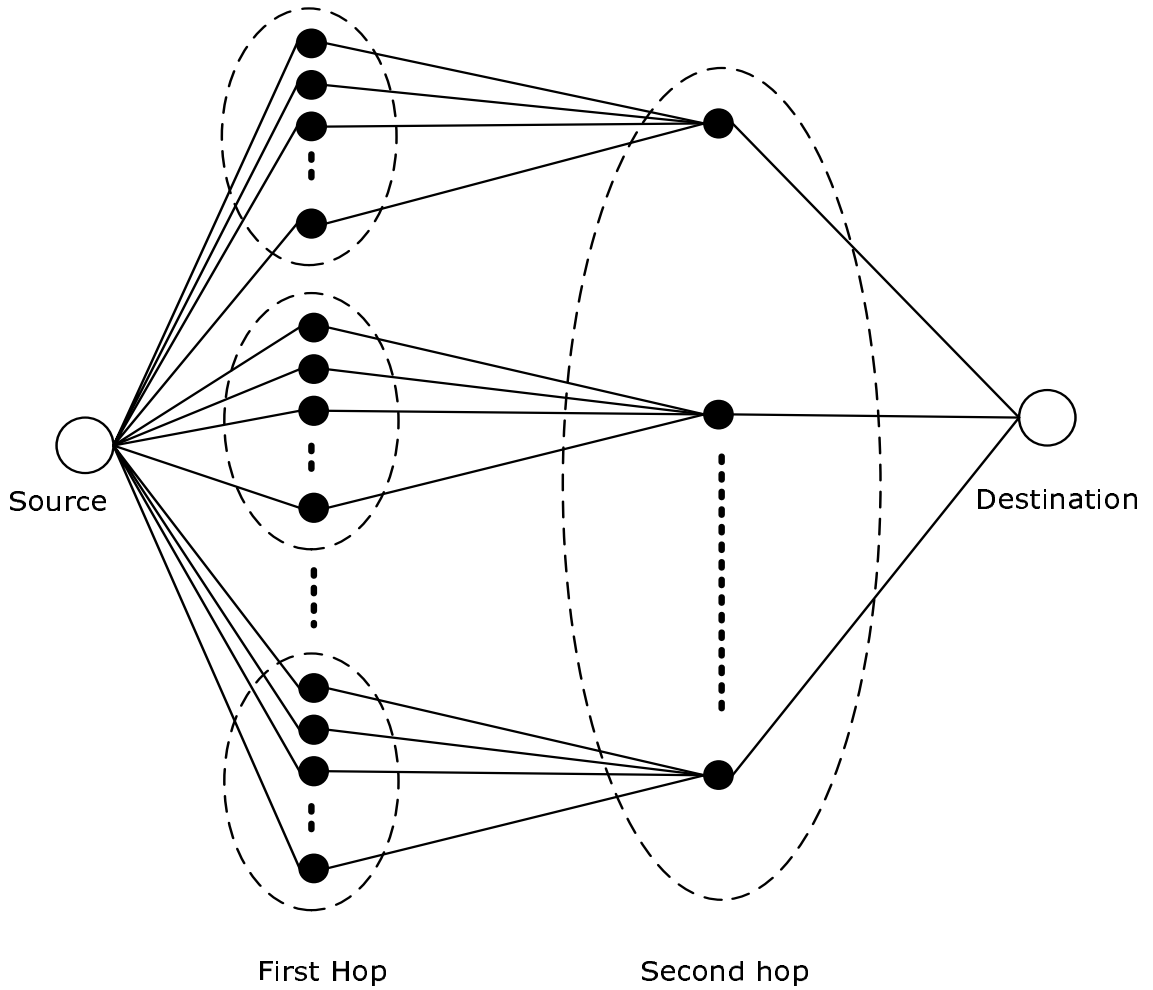


Figure 6.1: A system model for a three-hop network.

with the total number of nodes used per hop is given by  $\mathcal{C}_i L = L^{M+1-i}$ .

The system model that involves the source communicating to the level-1 CHs is modeled similar to that developed in Chap. 2 for both amplify-and-forward and decode-and-forward relay models. We next develop a concatenated index to label the received signal at each relay. In particular, we assume that the signal received at the destination is denoted by  $y_d$ . For the relay nodes at the last hop, the received

signals are denoted as  $y_1, y_2, \dots, y_L$ . Now for the previous hop, the relays transmitting to the second cluster, its received signals are denoted as  $y_{21}, y_{22}, \dots, y_{L2}$ . Hence, we define a concatenated index  $\zeta$  which labels the received signal at each relay. For a given relay, the index  $\zeta$  for a given relay determines the path of data from this relay to the destination. Hence, for an arbitrary index  $\zeta$ , the received signal  $y_\zeta[n]$  can be expressed, using (2.11), as follows,

$$y_\zeta[n] = \sum_{i=1}^L \alpha_{i\zeta} \beta_{i\zeta} z_{i\zeta}[n] + w_\zeta[n] , \quad (6.2)$$

where  $\alpha_{i\zeta}$  and  $\beta_{i\zeta}$  denote the channel fading coefficient and the complex beamforming weight, respectively, between the  $i$ th relay and its cluster head determined by the index  $\zeta$ . We assume that all the channels involved in communication are modeled as mutually independent quasi-static Rayleigh fading channels with equal variance  $\sigma_{i\zeta}^2$ . The term  $w_\zeta$  represents the noise and interference term and is modeled as white Gaussian noise with zero mean and unit variance. The term  $z_{i\zeta}$  denotes the output preprocessed signal of the  $i$ th relay for the  $\zeta$ th CH. The term  $z_{i\zeta}$  is determined by the type of the relay preprocessing model employed at the  $i$ th relay and effective CSI computed at this relay.

Specifically, we can exploit the fact that the received signal at the  $i$ th relay can be viewed as being transmitted on a single channel between the source and the  $i$ th relay with effective aggregate SNR  $\gamma_{i\zeta}^{\text{agg}}$ . This aggregate SNR combines all the effects that the source signal encounters while being transmitted to the relay. To explain how the aggregate SNR is computed, we first develop the aggregate SNR

for the communication system between the source and the CH labeled by the index  $\zeta$ . Based on the expression (6.2), the aggregate SNR  $\gamma_\zeta^{\text{agg}}$  can be represented as follows,

$$\gamma_\zeta^{\text{agg}} = \frac{|\sum_{i=1}^L \beta_{i\zeta} \alpha_{i\zeta} E[z_{i\zeta}]|^2}{\sum_{i=1}^L |\beta_{i\zeta}|^2 |\alpha_{i\zeta}|^2 (E[|z_{i\zeta}|] - E[|z_{i\zeta}|^2]) + \sigma_{w_\zeta}^2}. \quad (6.3)$$

The term  $z_{i\zeta}$  is given by  $z_{a_i}$  defined in (2.6) or  $z_{d_i}$  defined in (2.8) for the amplify-and-forward and decode-and-forward relay models, respectively. Hence, the communication system between the source and the  $i$ th cluster head can be alternatively viewed as a single channel with aggregate SNR  $\gamma_\zeta^{\text{agg}}$  (or equivalently its inverse  $\xi_{i\zeta}^{\text{agg}}$ ). Thus, for the case if amplify-and-forward model is employed at the cluster head, the received sequences in (6.2) after proper scaling can be rewritten as follows,

$$z_{i\zeta}[n] = \frac{1}{\sqrt{1 + \xi_{i\zeta}^{\text{agg}}}} x[n] + \frac{\sqrt{\xi_{i\zeta}^{\text{agg}}}}{\sqrt{1 + \xi_{i\zeta}^{\text{agg}}}} \bar{v}_i[n] \quad (6.4)$$

Similarly, for the decode-and-forward relay model, the equivalent channel can be represented as follows,

$$z_{i\zeta}[n] = e_{i\zeta}[n] x[n] \quad (6.5)$$

where  $e_{i\zeta}[n]$  denotes the IID error sequences given by

$$e_{i\zeta}[n] = \begin{cases} 1, & \text{with probability } 1 - p_{i\zeta} \\ -1, & \text{with probability } p_{i\zeta} \end{cases}, \quad (6.6)$$

where  $p_{i\zeta}$  is the bit error values associated with the equivalent channel between the source and the cluster heads labeled by the index  $\zeta$ . The values of  $p_{i\zeta}$  are determined based on the processing employed at the relays. In particular, if amplify-and-forward

is used, then  $p_{i\zeta}$  is determined as follows

$$p_{i\zeta} = Q\left(\sqrt{2\gamma_{i\zeta}^{\text{agg}}}\right), \quad (6.7)$$

while for the decode-and-forward model,  $p_{i\zeta}$ , can be determined by using equation (A.8) as shown in App. A. Similarly, as the data flow through the network, the communication channels between the source and the cluster heads are combined in a single channel with effective aggregate SNR determined by the type of processing employed at the relays, the number of nodes per cluster, the number of clusters combined and the power allocated to each cluster. We remark that to compute the aggregate SNR, each cluster head requires only the knowledge of the aggregate SNR computed at the previous cluster heads rather than the individual SNRs of all the communication channels up to this cluster head. This has the advantage of limiting the communication overhead required to compute the beamforming weights at each cluster.

## 6.2 Beamforming algorithms

In this section, we compute the beamforming weights selected for the clusters at each hop so as to optimize the destination  $\Pr(e)$ . In particular, our objective is to select the weights that aggregate information efficiently from the source to the destination. Specifically, at a given hop, the beamforming weights are selected to minimize the  $\Pr(e)$  computed at the  $\zeta$ th cluster head by maximizing the aggregate

SNR,  $\gamma_\zeta^{\text{agg}}$ . The beamforming weights at each hop can then be computed based on the methods developed in Sec. 3.1 and Sec. 4.1 for the amplify-and-forward model and the decode-and-forward model, respectively. This is due to the fact that these methods are mainly based on the instantaneous channel realizations of the source-relay and relay-destination channels. Hence, for the case of multi-hop networks, to compute the beamforming weights at each hop, it is only required to find the aggregate SNR,  $\gamma_\zeta^{\text{agg}}$ , from the source to the relays at this hop.

We first consider the case where full knowledge of the aggregate SNR at the relays is available to its cluster head. For the amplify-and-forward model, the beamforming weights at the  $i$ th cluster head that maximizes the SNR can be expressed using (3.7) and  $\xi_{i\zeta}^{\text{agg}}$  instead of  $\xi_{s_i}$  as follows,

$$\beta_i \propto \frac{\sqrt{\xi_{i\zeta}^{\text{agg}} + 1}}{\alpha_{r_i} [(\xi_{i\zeta}^{\text{agg}} + 1)(\xi_{r_{i\zeta}} + 1) - 1]}. \quad (6.8)$$

where  $\xi_{r_{i\zeta}} = \left(P_{h_i} \alpha_{i\zeta} / \sigma_{w_\zeta}^2\right)^{-1}$ . Similarly, for the decode-and-forward model, we select the beamforming weights by using the equivalent channel method developed in Sec. 4.1.3. In particular, the effective SNR of the aggregate SNR at each relay is computed using (4.29) with  $B_i$  is given by

$$B_i = \log \left( \frac{1 - p_{i\zeta}}{p_{i\zeta}} \right) \quad (6.9)$$

where  $p_{i\zeta}$  is determined based on the processing performed at the previous hop as mentioned before.

We next consider the case where the one-bit quantizers are employed at the

relays. For such case, we need to compute the beamforming weights along with the quantizer threshold for the relays at each hop. For the amplify-and-forward model, the beamforming weights developed in Sec. 3.1.2 can be used to find the optimized weights at each hop. However, we note that the computation of the value of  $a_i$  and  $c_i$  in (3.30) depends on the probability distribution function of the aggregate SNR computed at each relay. As a result, the values of  $a_i$  and  $c_i$  must be recomputed at each hop as the information flows through the network. Similarly, for the decode-and-forward model, the effective SNR at each hop depends on the values of  $f_i = E [p_{i\zeta} | p_{t\zeta} < p_{i\zeta}]$  which requires the knowledge of distribution function of  $p_{i\zeta}$  at each relay. Therefore, the effective SNR must be recomputed at each hop as the distribution function of  $p_{i\zeta}$  varies at each hop. We note that the computed parameters  $a_i$ ,  $c_i$  and  $f_i$  at each hop remains fixed as the average SNR of all the channels in the network is constant or equivalently the location of the nodes remains fixed. Hence, this process of selecting the quantizer threshold can be performed offline as long as the nodes have fixed locations.

To find the quantizer threshold for the amplify-and-forward model, we find the value that maximize the average quantized SNR defined in (3.36) at each hop. It is evident that the values of the threshold varies at each hop, therefore the expression  $\mathcal{C}_{AF}$  in (3.37) does not necessarily approximate the value of the threshold at each hop given that the average SNR in (3.37) is replaced with the average aggregate SNR,  $\bar{\gamma}_{i\zeta}^{\text{agg}} = E [\gamma_{i\zeta}^{\text{agg}}]$ . This is due to the fact that the distribution function of  $\gamma_{i\zeta}^{\text{agg}}$

varies at each hop not only its average value. Similarly, for the decode-and-forward model, the quantizer threshold must be recomputed at each hop by minimizing the  $\Pr(e)$  expression (A.8) developed in App. A. Also, the expression  $\mathcal{C}_{\text{DF}}$  in (4.32) needs to be recalculated at each hop. As it will be shown in our simulations, that simple relations can be obtained via simulations to compute the threshold at each hop for both relay preprocessing models.

## 6.3 Performance Analysis and Power Allocation Strategy

In this section, we perform Monte-Carlo simulations to study the performance of the beamforming algorithms developed in Sec. 6.2. We focus our attention on the case where one-bit quantizers are employed at the relays. In particular, our objective is to find the quantizer threshold to be employed at the relays of each hop for both the decode-and-forward and the amplify-and-forward relaying models. Then, we study the  $\Pr(e)$  performance using the obtained quantizer thresholds and compares it to the  $\Pr(e)$  performance attained by using full knowledge of the aggregate SNR at the cluster heads.

In our simulations, we consider a network setting of four level of clustering or equivalently five hops where the number of nodes per cluster,  $L_c = 3$ . Since we assume that the clusters are of equal size, then the number of clusters formed at



each hop is given as follows

$$\mathcal{C}_1 = 27, \quad \mathcal{C}_2 = 9, \quad \mathcal{C}_3 = 3, \quad \text{and} \quad \mathcal{C}_4 = 1. \quad (6.10)$$

We assume that the values of the variances of the channel coefficients are set to  $\sigma_{i\zeta}^2 = 1$ .

We next consider a strategy for allocating the total power  $P$  among the clusters at different hops. As it was shown in Chaps. 3, 4, for the case of two-hop networks, the optimum power allocation for equal average source-relay and relay-destination SNR is to distribute the power equally between the source and the relays. As a result, for the multi-hop network, our objective is to develop a power allocation strategy that provides equal power distribution for each cluster and take into consideration the effect of information aggregation across the network.

Taking these conditions into consideration, we develop a power allocation strategy which can be explained through the following example. We consider a three-hop networks where the number of nodes per cluster is given by  $L$ . We first allocate power  $P_{h_2}$  to the single cluster at the last hop. We then select the power allocated to the  $L_c$  clusters at the first hop as well as the source such that the average aggregate SNR  $\bar{\gamma}_{i\zeta}^{\text{agg}}$  at the second hop is equal to  $\bar{\gamma}_{r_i\zeta} = P_{h_2}/\sigma_{w_\zeta}^2$ . This power allocation strategy can be adequately generalized for multi-hop network with any number of hops. Using this power allocation strategy and under the given assumption, we find that the following power allocation results in  $\text{Pr}(e)$  values close to the optimal values,

$$P_{h_i} = \left(\frac{2}{L}\right)^{M-i} P_o \quad \forall i = 1, 2, \dots, M \quad (6.11)$$

where  $P_o$  is obtained based on the following expression,

$$P = \sum_{i=1}^M C_i \left(\frac{2}{L}\right)^{M-i} P_o = \sum_{i=1}^M 2^{M-i} P_o. \quad (6.12)$$

We remark that this power allocation strategy provides more power as the CHs get closer to the destination. This is advantageous in terms of the practical requirements of the hierarchial clustering approach where the cluster heads closer to the destination are assumed to be nodes with better capabilities in terms of battery life compared to the nodes away from the destination.

We first focus our attention on the amplify-and-forward relay model where we determine the quantizer threshold to be employed at the relays of each hop so as to minimize the  $\Pr(e)$  at each cluster head. Due to the hierarchal clustering approach, the quantizer threshold can be optimized at each cluster in a sequential order. In particular, the optimal quantizer threshold at the first hop can be selected by maximizing the average quantized aggregate SNR in (3.36) at the first cluster head. Then, we can view the channels from the source to the cluster heads at the first hop as effectively single channels with combined aggregate SNR computed using the obtained quantizer threshold. These combined channels can be used to determine the quantizer threshold at the cluster heads of the second hop where optimizing this threshold will not affect that computed for the first hop. This process can be computed at each hop to determine the optimized quantizer thresholds. We remark

that for illustration purposes, it is convenient to introduce the notion of normalized total power  $P_N$  defined as follows,

$$P_N = \frac{P}{\sum_{i=1}^M \mathcal{C}_i}. \quad (6.13)$$

or equivalently the average amount of total power  $P$  allocated per cluster. For the rest of the chapter, we present our simulation results in terms of  $P_N$ .

Table 6.1 lists, for each hop, the value of the quantizer threshold normalized to the mean of the aggregate SNR computed ( $\gamma_{t_{i\zeta}}/\bar{\gamma}_{i\zeta}^{\text{agg}}$ ) at this hop for various values of a normalized SNR  $\bar{\gamma}_N = P_N/\sigma_w^2$ . As the table reveals, the values of normalized quantizer threshold gets closer to the value of 0.7 as the data flows across the hops. As it was shown in Fig. 3.5, the  $\text{Pr}(e)$  performance incurs a negligible amount of loss within range of 2 dB of the optimal threshold, then normalized quantizer threshold can be approximated well by setting its value to the 0.7.

We then study the probability density function (pdf) of the aggregate SNR  $\gamma_{i\zeta}^{\text{agg}}$  at each hop. At the first hop, given the assumption of using quasi-static Rayleigh fading channel, the pdf of the SNR  $\gamma_{1\zeta}^{\text{agg}}$  is an exponential distribution with mean  $\bar{\gamma}_{1\zeta}^{\text{agg}} = P_s\sigma_{i\zeta}^2/\sigma_{w\zeta}^2$ . Fig. 6.2 depicts the exponential distribution for  $\bar{\gamma}_{1\zeta}^{\text{agg}} = 10$  dB. Fig. 6.3 depicts the pdf of the aggregate SNR at the second, third, fourth hop and the destination. As the figure reveals, the pdf of  $\gamma_{i\zeta}^{\text{agg}}$  converges to a Gaussian distribution as the information flows across the hop. This result can be explained by the fact that employing beamforming algorithms result in constructive adding of the signals at each hop. As our simulations reveal, we have central-limit

$\bar{\gamma}_N$	1	2	3	4
5 dB	0.4006	0.6234	0.7511	0.7893
10 dB	0.2073	0.5423	0.6711	0.7209
15 dB	0.1020	0.4995	0.6858	0.6817

Table 6.1: The optimal quantizer thresholds normalized to the mean of the aggregate SNR,  $\gamma_{t_{i\zeta}}/\bar{\gamma}_{i\zeta}^{\text{agg}}$ , computed via Monte-Carlo simulations at each hop for a four multi-hop network employing amplify-and-forward relaying.

theorem type of performance so we can deduce that as more number of signals are added constructively across the hops, the pdf converges to Gaussian. As it is also shown by the figure, the mean and the variance of the aggregate SNR changes as the number of hop increases.

We then study the  $\Pr(e)$  performance of the one-bit quantized beamforming algorithms using the optimized quantizer thresholds. Fig. 6.4 depicts the  $\Pr(e)$  performance of the one-bit (solid curves) and infinite-bit (dashed-curves) beamforming algorithms, respectively, at the first, second, third hop and the destination as a function of  $\bar{\gamma}_N$ . As the figure reveals, that employing an optimized one-bit beamforming algorithms incur a small amount of loss in terms of  $\Pr(e)$  compared to the infinite-bit beamforming algorithms (equivalent to the full knowledge of the aggregate SNR at the cluster heads). Also shown by the figure, that the  $\Pr(e)$  values for both beamforming algorithms decreases as the information flow across the hop.

We next turn our attention to the decode-and-forward relay model. We first

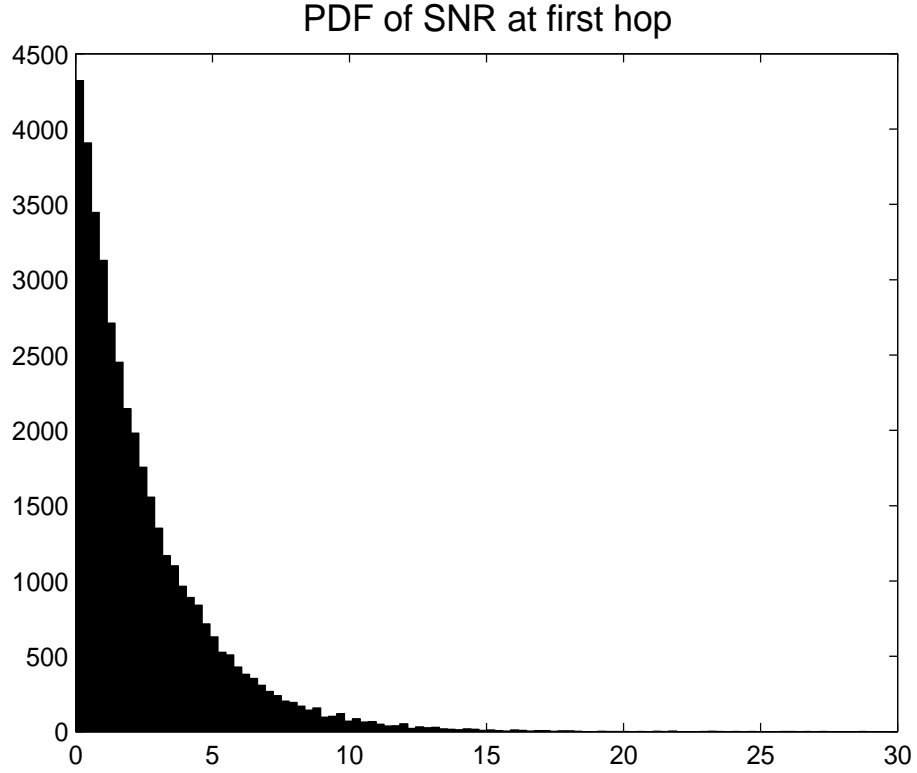


Figure 6.2: The exponential probability density function of the SNR at the first hop.

$\bar{\gamma}_N$	1	2	3	4
5 dB	0.8383	0.9809	0.8917	0.9041
10 dB	0.7246	0.9399	1.0213	1.0474
15 dB	0.5425	0.8692	0.9970	0.9661

Table 6.2: The optimal quantizer thresholds normalized to the mean of the aggregate SNR,  $p_{t_{i\zeta}}/\bar{p}_{i\zeta}$ , computed via Monte-Carlo simulations at each hop for a four multi-hop network employing decode-and-forward relaying.

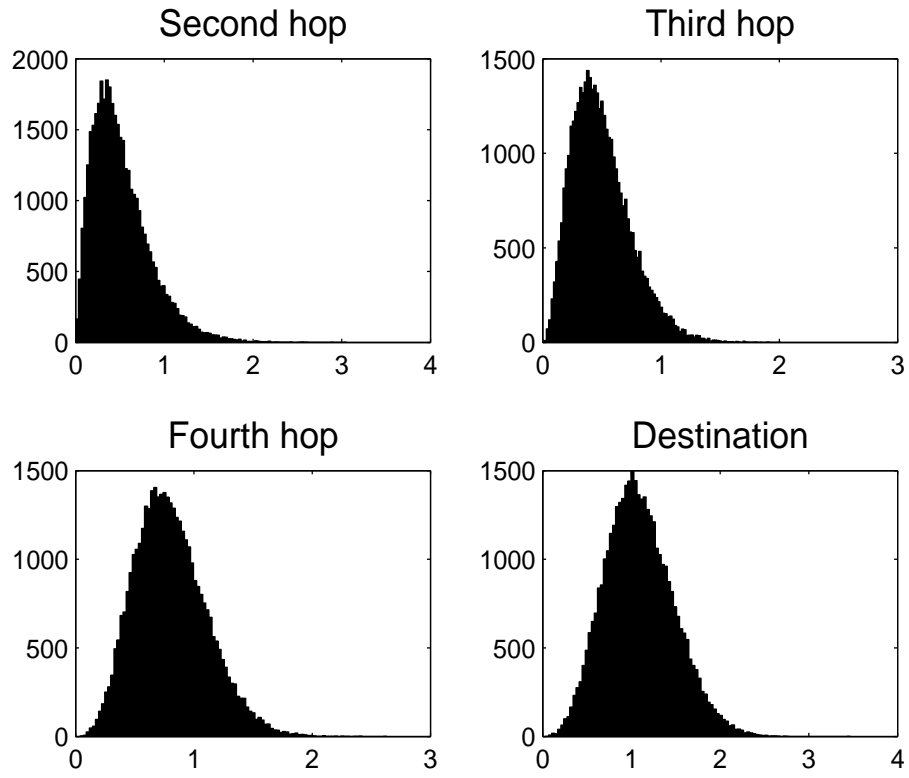


Figure 6.3: The probability density function of the aggregate SNR at each hop for an amplify-and-forward relaying system that employs optimized one-bit quantizers at the relays.

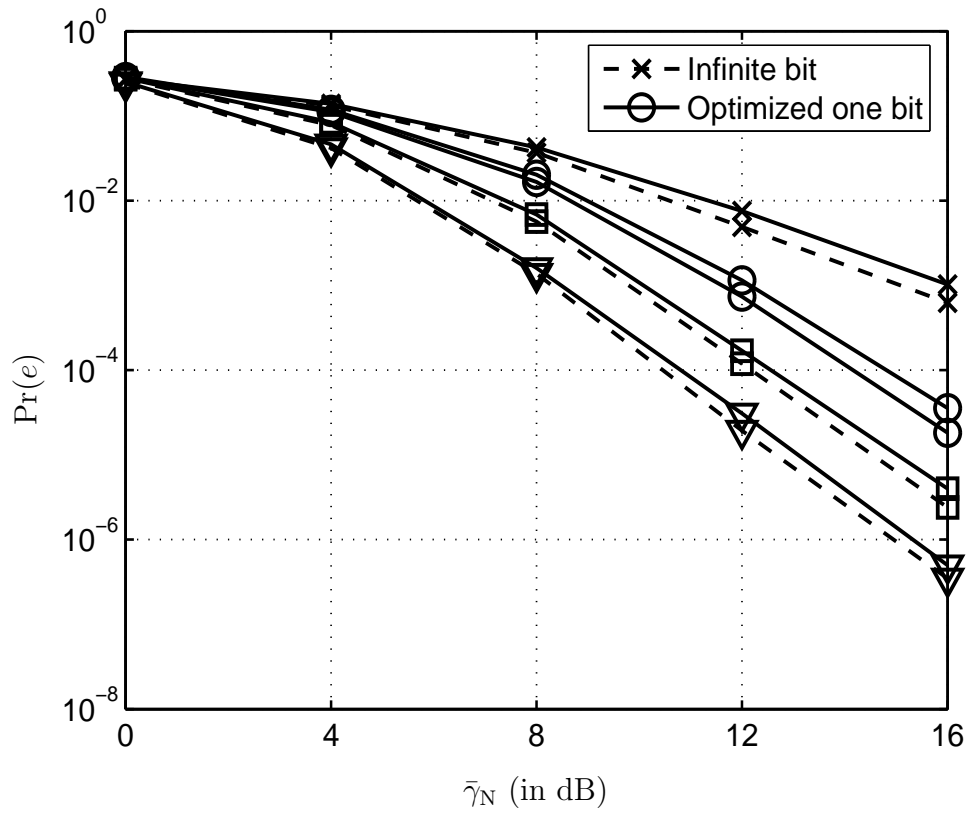


Figure 6.4: The successively lower solid curves and the dashed curves depict the destination  $\Pr(e)$  performance of the optimized *one-bit* and infinite-bit amplify-and-forward beamforming algorithms, respectively, at the first, second, third and fourth hop.

determine the optimized quantizer thresholds normalized to the mean of average probability of error values at this hop  $p_{t_{i\zeta}}/\bar{p}_{i\zeta}$  at each hop. Table 6.2 lists the values of the normalized quantizer thresholds computed via simulations at different hops and for different power values. As the table reveals, that the optimal quantizer threshold can be well approximated to the average probability of error at this hop  $p_{i\zeta}$  as the number of hops increase. Fig. 6.5 depicts the pdf of the aggregate SNR at each hop for the case of one-bit beamforming algorithms are used. The figure also shows that the pdf of the aggregate SNR converges to Gaussian as the number of hop increases. Finally, Fig. 6.6 shows that the one-bit beamforming algorithms at the different hops provides  $\Pr(e)$  performance very close compared to the  $\Pr(e)$  values attained by using full knowledge of aggregate SNR.

For the purpose of comparing the  $\Pr(e)$  performance of the amplify-and-forward and decode-and-forward relaying strategy attained at each hop, Fig. 6.7 shows that the decode-and-forward model outperforms the amplify-and-forward model starting from the second hop to the destination. This is mainly due to the fact that the mean of the aggregate SNR at each hop is increasing compared to the average SNR from the relay at this hop to the destination which allows better  $\Pr(e)$  performance for the decode-and-forward model.



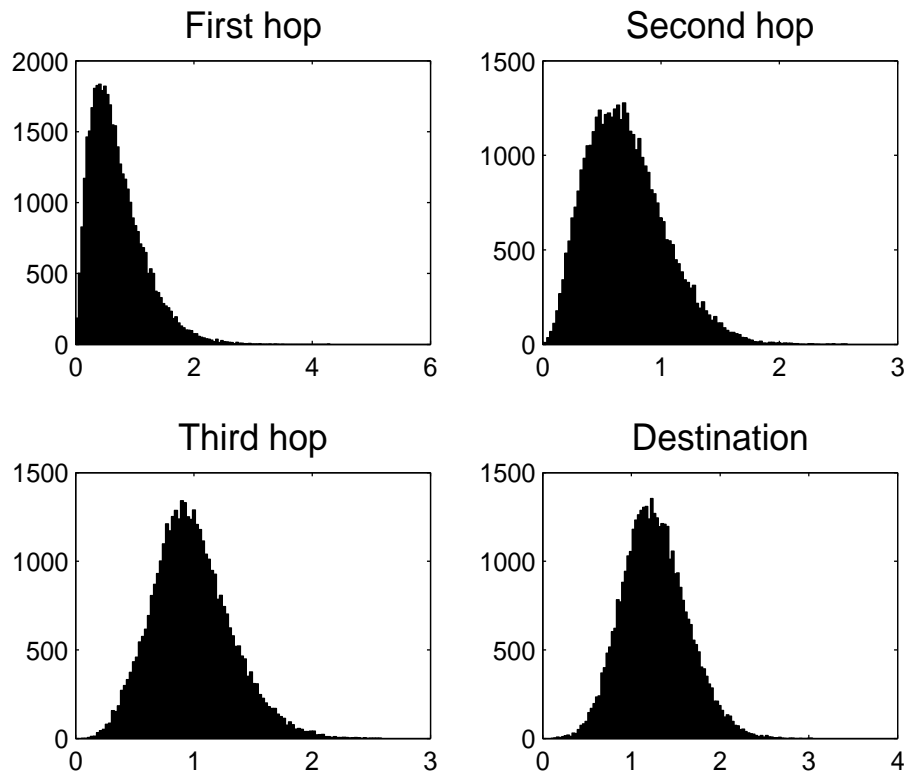


Figure 6.5: The probability density function of the aggregate SNR at each hop for an decode-and-forward relaying system that employs optimized one-bit quantizers at the relays.

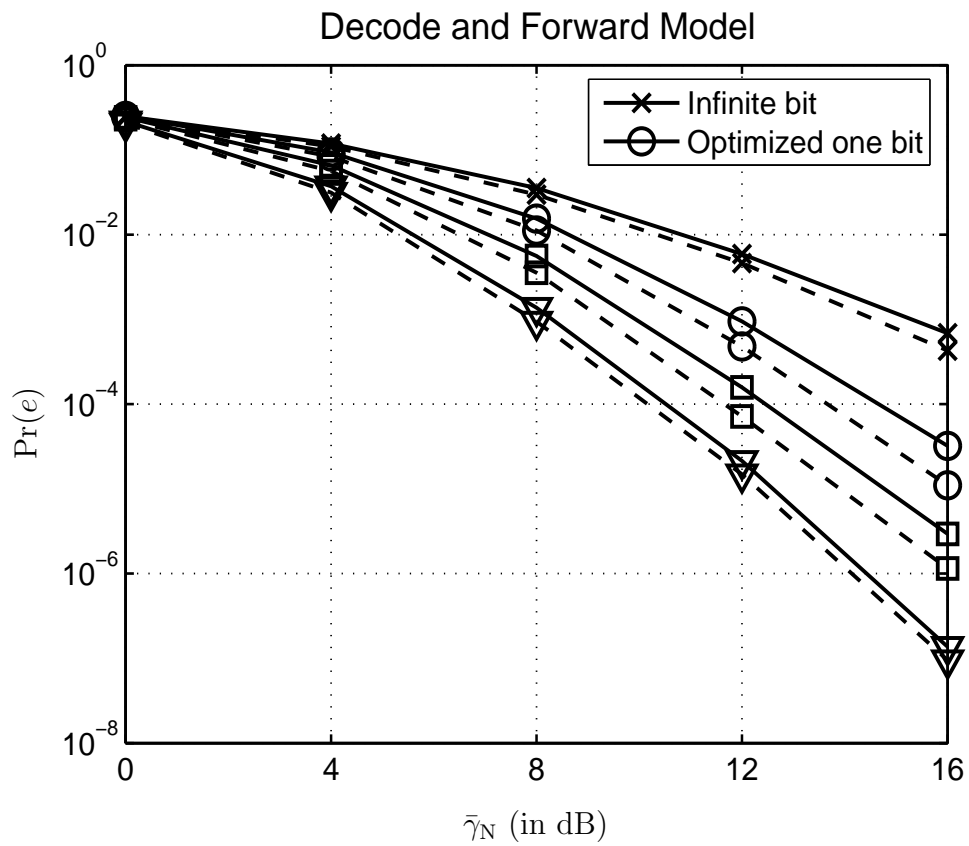


Figure 6.6: The successively lower solid curves and the dashed curves depict the destination  $\text{Pr}(e)$  performance of the optimized *one-bit* and infinite-bit decode-and-forward beamforming algorithms, respectively, at the first, second, third and fourth hop.

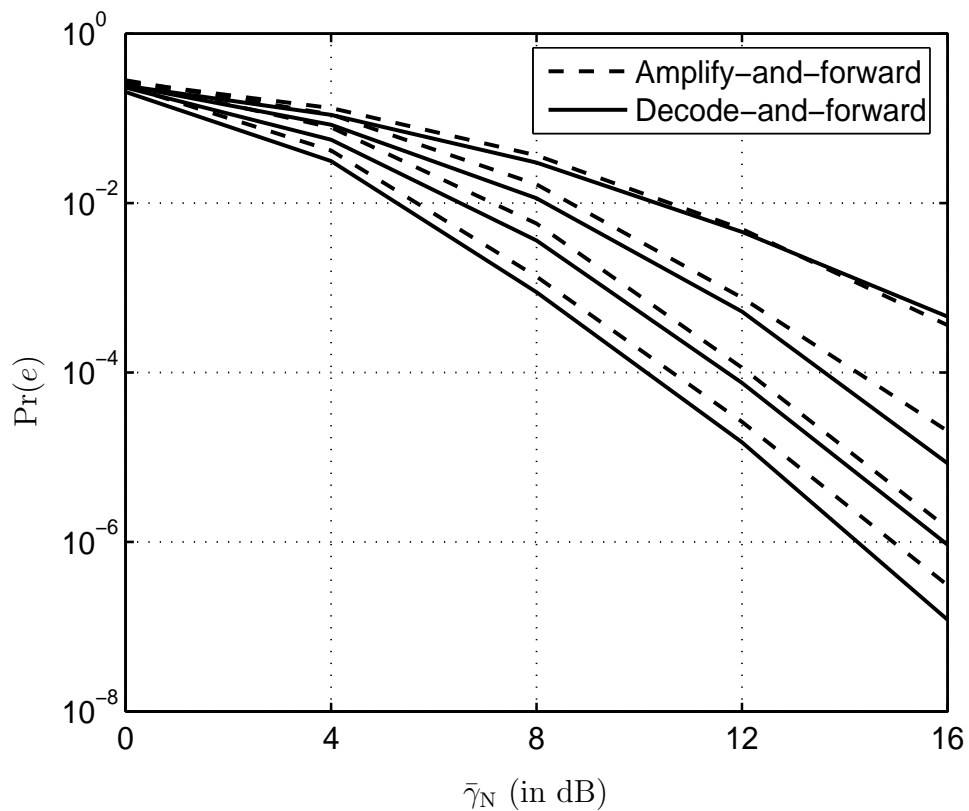


Figure 6.7: The successively lower solid curves and the dashed curves depict the destination  $\Pr(e)$  performance of using amplify-and-forward and decode-and-forward relaying algorithms, respectively, at the first, second, third hop and destination.

## 6.4 Relay Location Strategy

In this section, we develop algorithms to determine the optimal location of the relays for each hop for the amplify-and-forward and decode-and-forward model. We consider the case where full knowledge of the aggregate SNR is available at each cluster head. We define the average channel variances between the source and the relays at the first hop as follows,

$$\sigma_{\text{sh}_1}^2 = \frac{K}{(d_{\text{sh}_1})^\nu}, \quad (6.14)$$

while the average channel variances between the relays at the  $i$ th hop and  $(i + 1)$ th hop as follows,

$$\sigma_{i\zeta}^2 = \frac{K}{(d_{\text{h}_i, i+1})^\nu}, \quad (6.15)$$

and finally the average channel variances between the relays at the last  $M$  hop and the destination as

$$\sigma_{\text{d}}^2 = \frac{K}{(d_{\text{d}})^\nu}. \quad (6.16)$$

Throughout our simulations, we set  $K = 1$  and  $\nu = 3$ . Our objective is to determine the optimal values of the distances associated with each relay processing type.

To this end, we develop a simple yet effective algorithm for determining the optimal location by exploiting the hierarchal clustering approach. Based on the results developed in Chap. 3 and Chap. 4, we determine the optimal location for the two hop network. In particular, we show that the optimal location for the amplify-and-forward model is half the distance between the source and the destination or

equivalently  $\tau = 0.5$ . While, for the decode-and-forward model, the optimal  $\tau$  is equal 0.35. Let us consider the case for three hop network where we need to determine the optimal distance ratios

$$\tau_h = d_{h_{1,2}}/d_{sh_1} \quad \text{and} \quad \tau_d = d_d/d_{sd}. \quad (6.17)$$

Based on the results obtained from the two-hop network and given the hierarchal clustering approach, the optimal value of  $\tau_h$  can be set to 0.5 for the amplify-and-forward model and 0.35 for the decode-and-forward model independent of the parameter  $\tau_d$ . This reduces the complexity of the problem in the sense that we need only to find the value of  $\tau_d$  that minimize the  $\Pr(e)$ . This optimization process can be adequately generalized for multi-hop networks as it can be performed in a sequential manner to find the optimal location for each hop.

We next determine via simulations the optimal value of  $\tau_d$  for the case of the amplify-and-forward and decode-and-forward model. Fig. 6.8 depicts the  $\Pr(e)$  performance for the amplify-and-forward model (solid curve) and the decode-and-forward model (dashed curve) for  $\bar{\gamma}_N = 10$  dB assuming a two hop networks as a function of  $(1 - \tau_d)$ . As the figure reveals, the optimal value of  $\tau_d$  is 0.2 and 0.3 for the amplify-and-forward and decode-and-forward, respectively. Also, it is clear that the location of the relays at the second hop gets closer, the decode-and-forward model performs better than the amplify-and-forward model and vice versa.

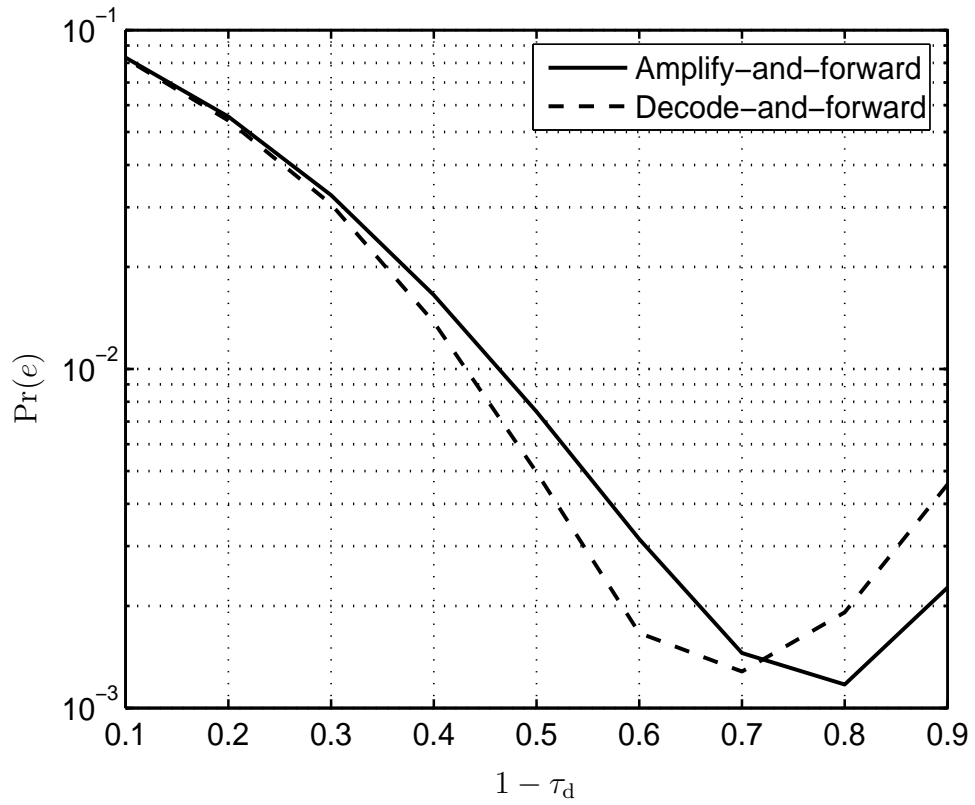


Figure 6.8: The destination  $\Pr(e)$  as a function of  $1 - \tau_d$  assuming three hop networks and full knowledge of aggregate SNR available at the CHs. The solid curve represents the amplify-and-forward model while the dash curve represents the decode-and-forward model.

## Chapter 7

# Conclusion and Future Directions

In this dissertation we developed a class of beamforming algorithms for information relaying in wireless networks under bandwidth constraints. We considered a network setting whereby a source is communicating to a destination via the aid of low-power low-cost nodes. To amount for the bandwidth limitations in these networks, we assumed that the relay nodes are communicating to the destination over a shared nonselective fading channel. We considered two types of relay data-preprocessing strategy. The first is amplify-and-forward via beamforming (AFB) for which the received signals at the relays are first scaled to achieve unit-power form prior to forwarding via beamforming to the destination. The second is decode-and-forward via beamforming (DFB) where the nodes are first decoded (using matched filter followed by a slicer) then scaled using beamforming weights. The beamforming weights are formed based on the composite relays-destination channel state information (CSI) and  $m$ -bit descriptions of the source-relay CSI.

For both the AFB and the DFB relay models, we presented methods for optimizing the beamforming algorithms designed at the destination and the m-bit quantizer function used at the relays to encode their data quality. We developed rule-of-thumb expressions for the quantizer threshold that proved via simulations to provide the optimal threshold value. The resulting  $\Pr(e)$  values at the destination even when an one-bit description of the source-relay channel CSI is available at the destination, are slightly higher than the ones attained by beamforming algorithms exploiting an full knowledge of the quality of the individual relay data.

We determined the effect of the relative relay location on the destination  $\Pr(e)$  performance for the AFB and DFB relay models. In particular, we showed that if the relays are closed to the source, then it is advantageous in terms of  $\Pr(e)$  to employ DFB relay model, while AFB relay model gives favorable  $\Pr(e)$  performance if the relay nodes are closer to the destination. Based on our findings, we develop locally-optimized adaptive data pre-processing algorithms at the relays. These adaptive algorithms provide the best attainable  $\Pr(e)$  performance at any given relay location.

We developed extensions involving multi-hop networks with hierarchal cluster-based relaying. In particular, we presented methods for systematically selecting the beamforming weights at the relays of each cluster. We showed that the beamforming algorithms optimize the  $\Pr(e)$  performance at each hop and thus at the destination. We developed power allocation strategies that determine the amount of power to



be allocated to each cluster at each hop. We finally show the optimal relative relay locations with respect to the source and the destination as well as the associated relay preprocessing strategy to be used at each relay. As our simulations reveal, the probability of using the DFB relay model increases considerably in comparison to the AFB relay model as the data processing gets closer to the destination.

## 7.1 Future Directions

In this section, we discuss fruitful research extensions to the problems addressed in this dissertation. The beamforming algorithms developed in this dissertation mainly focused on uncoded communication system. However, these algorithms can be readily integrated with any coding schemes like space-time coding or Turbo coding to achieve

A one important extension to our work is to investigate the case of the feedback channel with limited bandwidth. In particular, a lossy yet efficient representation of the beamforming weights must be constructed to make efficient use of the broadcast feedback channel. For instance, it was assumed that full representation of the complex beamforming weights are feedback to the relays. Alternatively, we can consider cases where only the phases of the weights are transmitted fully back to the relays, while the amplitudes of the weights are quantized efficiently. There is a lot of vector quantization efficient techniques that can be used to represent the amplitude of the weights. Our beamforming algorithms provide a lower bound on

the  $\Pr(e)$  performance attained by any vector quantization technique.

Channel estimation and prediction at the destination is a key design parameter for beamforming techniques as the quality of the channel estimates affects the level of output SNR attained at the destination. In this dissertation, we focused on pilot-based techniques where pilot signals are transmitted on a periodic basis so as to allow the destination obtain estimates of the individual relay-destination channels. Using pilot tones has the disadvantage of training overhead, which limits the effective data rate over time-varying channels. In order to limit the use of pilot tones, there is a need to employ efficient joint data-aided detection and channel estimation methods. It is important to remark that the quality of the predicted channel estimates is also affected by the beamforming vectors employed at the relays. As a result, the beamforming vectors have to be chosen so as to achieve the following closely coupled goals:

- Desired level of output SNR at the destination for the current frame;
- Reliable relay-destination predicted channel estimates as these affect the attainable SNR level in future data frames.

As an important extension, we can investigate the problem of developing new beamforming techniques for correlated relay-destination channels that allow efficient joint data detection and reliable channel prediction at the destination. There exists a trade off in achieving these closely-coupled objectives. In particular, there exists a trade off in maximizing the output SNR and obtaining reliable channel estimates.

This can be illustrated by assuming an  $L$ -relay network setting where all the relays have the same information-bearing signal and where the relay-destination channels remain constant for a data frame of length  $M$ . Then, given the initial channel estimates, the beamforming vector developed in this dissertation can be chosen to maximize the output SNR for all time slots within a frame. However, such selection allows only accurate prediction of a linear sum of the signal paths received at the destination, but not the individual relay channels. Hence, such selection provides no information to improve the channel estimates and, as a result, the output SNR for the subsequent frame can not be maximized. Therefore, there is a need to develop new techniques for beamforming that provide reliable joint data detection and channel estimation.

## Appendix A

# $\Pr(e)$ Analysis for Decode-and-forward Relay Model

In this appendix, we obtain an expression for computing the  $\Pr(e)$  at the destination for the decode-and-forward via beamforming model assuming full knowledge of the source-relay CSIs at the destination. For convenience we omit the dependence of random process on the time-index  $n$ . The desired  $\Pr(e)$  quantity can be expressed in the following form

$$\Pr(e) = E_{\boldsymbol{\alpha}_r, \mathbf{p}_s} [\Pr(e|\boldsymbol{\alpha}_r, \mathbf{p}_s)] \quad (\text{A.1})$$

where

$$\mathbf{p}_s = \begin{bmatrix} p_{s_1} & p_{s_2} & \dots & p_{s_L} \end{bmatrix}^T \quad (\text{A.2})$$

and  $\boldsymbol{\alpha}_r$  is given by (3.20). Furthermore, assuming that  $x = 1$  is sent,

$$\Pr(e|\mathbf{p}_s, \boldsymbol{\alpha}_r) = \sum_{\mathbf{z}_d \in \mathcal{Z}} \Pr(\mathbf{z}_d) \Pr(e|\mathbf{z}_d, \mathbf{p}_s, \boldsymbol{\alpha}_r) \quad (\text{A.3})$$

where  $\mathbf{z}_d = [z_{d_1} z_{d_2} \dots z_{d_L}]^T$ , with  $z_{d_i}$  given by (2.7) and  $\mathcal{Z}$  is the (size  $2^L$ ) domain size  $2^L$  of the  $\mathbf{z}_d$ . In addition,

$$\Pr(\mathbf{z}_d) = \prod_{i=1}^L (1 - p_{s_i})^{\binom{1+z_{d_i}}{2}} p_{s_i}^{\binom{1-z_{d_i}}{2}}, \quad (\text{A.4})$$

and

$$\Pr(e|\mathbf{z}_d, \mathbf{p}_s, \boldsymbol{\alpha}_r) = \mathcal{Q}\left(\sqrt{2} \mathcal{R}(\delta)\right) \quad (\text{A.5})$$

where

$$\delta = \frac{(\sum_i \beta_i \alpha_{r_i} z_{d_i})}{\sigma_w} \quad (\text{A.6})$$

can take both positive or negative values, depending on the error patterns that occur at the relays. Eqn. (A.5) can also be conveniently expressed as follows,

$$\Pr(e|\mathbf{z}_d, \mathbf{p}_s, \boldsymbol{\alpha}_r) = \mathcal{Q}\left(\sqrt{2\delta^2}\right) \mathcal{I}(\delta \geq 0) + \left(1 - \mathcal{Q}\left(\sqrt{2\delta^2}\right)\right) \mathcal{I}(\delta < 0) \quad (\text{A.7})$$

where  $\mathcal{I}(\cdot)$  denotes the indicator function. Substituting (A.4) and (A.5) in (A.3), we obtain

$$\Pr(e|\mathbf{p}_s, \boldsymbol{\alpha}_r) = \sum_{\mathbf{z}_d \in \mathcal{Z}} \left[ \prod_{i=1}^L (1 - p_{s_i})^{\binom{1+z_{d_i}}{2}} p_{s_i}^{\binom{1-z_{d_i}}{2}} \right] \left[ \mathcal{Q}\left(\sqrt{2\delta^2}\right) \mathcal{I}(\delta \geq 0) + \left(1 - \mathcal{Q}\left(\sqrt{2\delta^2}\right)\right) \mathcal{I}(\delta < 0) \right], \quad (\text{A.8})$$

which, when substituted in (A.1) provides an expression for computing the desired  $\Pr(e)$  quantity.

## Appendix B

# $\Pr(e)$ Analysis for Decode-and-Forward Relay Model at High Relay-destination Average SNR

In this appendix, we obtain a closed-form expression for the  $\Pr(e)$  in the decode-and-forward via beamforming relay model that is valid in the infinite relay-destination SNR limit. We may express  $\ell$  in (4.1) as follows

$$\ell = \sum_{i=1}^L \lambda_i z_i = \sum_{i=1}^N \mu_1 z_i + \sum_{i=1}^{L-N} \mu_2 z_i, \quad (\text{B.1})$$

where

$$\mu_i = \log \left( \frac{1 - f_i}{f_i} \right), \quad (\text{B.2})$$

$$f_1 = E [p_{s_i} | p_{s_i} < p_t] = \frac{e^{-\frac{\gamma_t}{\gamma_s}} Q(\sqrt{2\gamma_t}) - \tau Q(\sqrt{\frac{2\gamma_t}{\tau}})}{\delta_o}, \quad (\text{B.3})$$

$$f_2 = E [p_{s_i} | p_{s_i} > p_t] = (\bar{p}_s - f_1 \delta_o) / (1 - \delta_o), \quad (\text{B.4})$$

$\tau = \sqrt{\frac{\bar{\gamma}_s}{\bar{\gamma}_s + 1}}$ , and  $N$  denotes the number of “poor-data-quality” relay nodes, *i.e.*, relay nodes with source-relay CSI satisfying  $p_{s_i} < p_t$ . The  $\Pr(e)$  of the optimal linear detector can be expressed as follows

$$\Pr(e) = \sum_{k=0}^L \Pr(e|N = k) \Pr[N = k] \quad (\text{B.5})$$

where  $\Pr[N = k]$  denotes the probability that  $k$  out of  $L$  nodes have poor-quality data (*i.e.*, have  $p_{s_i} < p_t$ ), and is given by,

$$\Pr[N = k] = \binom{L}{k} \delta_o^k (1 - \delta_o)^{(L-k)} \quad (\text{B.6})$$

with

$$\delta_o = \Pr[p_{s_i} < p_t] = \exp\left(-\frac{\gamma_t}{\bar{\gamma}_s}\right). \quad (\text{B.7})$$

The term  $\Pr(e|N = k)$  denotes the bit error rate given that  $k$  (out of  $L$ ) nodes have  $p_{s_i}$ 's below  $p_t$ . Given that  $r$  out of the  $N = k$  “poor-data-quality” nodes and  $m$  out of the  $L - N = L - k$  “good-data-quality” nodes have decoded the source data correctly, an error is made by the linear detector exploiting  $\ell$  in (B.1), if  $\ell x < 0$ , or, equivalently, if

$$r\mu_1 + m\mu_2 < \frac{N\mu_1 + (L - N)\mu_2}{2}. \quad (\text{B.8})$$

By applying Bayes' rule and exploiting (B.8),  $\Pr(e|N = k)$  can be expressed as follows,

$$\Pr(e|N = k) = \sum_{i=0}^{r_{\max}(k)} \sum_{j=0}^{m_{\max}(k,i)} \Pr(e|N = k, r = i, m = j) \Pr(r = i, m = j|N = k)$$

where, due to (B.8),

$$r_{\max}(k) = \min \left\{ k, \left\lfloor \frac{k}{2} + \frac{L-k}{2} \frac{\mu_2}{\mu_1} \right\rfloor \right\}$$

and

$$m_{\max}(k, r) = \min \left\{ L - k, \left\lfloor \frac{k - 2r}{2} \frac{\mu_1}{\mu_2} + \frac{L-k}{2} \right\rfloor \right\} .$$

Finally, by exploiting the symmetry of error events corresponding to the same  $(r, m)$  pairs, we obtain

$$\Pr(e|N = k) = \sum_{i=0}^{r_{\max}(k)} \sum_{j=0}^{m_{\max}(k,i)} \binom{L-k}{L-k-j} \binom{k}{k-i} f_1^{k-i} (1-f_1)^i f_2^{L-k-j} (1-f_2)^j \quad (\text{B.9})$$

where  $f_1$  and  $f_2$  are given by (B.3), and (B.4), respectively. Substituting (B.6) and (B.9) in (B.5) yields the desired expression.



## Bibliography

- [1] I. F. Akyildiz, W. Su, Y. Sankarasubramaniam, and E. Cayirci, “A survey on sensor networks,” *IEEE Communication Magazine*, pp. 102–114, August 2002.
- [2] S. Kumar, F. Zhao, and D. Sheperd, “Special issue on collaborative signal and information processing in microsensor networks,” in *IEEE Signal Processing Mag.*, vol. 19, March 2002.
- [3] M. Yeddanapudi, Y. Bar-Shalom, and K. R. Pattipati, “IMM estimation for multitarget multisensor air traffic surveillance,” *IEEE Trans. Signal Processing*, vol. 85, no. 1, pp. 80–94, January 1997.
- [4] S. Simic and S. Sastry, “Distributed environmental monitoring using random sensor networks,” in *Proc. Information Processing in Sensor Networks*, April 2003, pp. 582–592.
- [5] Z. Chair and P. Varshney, “Optimal data fusion in multiple sensor detection systems,” *IEEE Trans. Aerospace Elec. Sys.*, vol. 22, no. 1, pp. 98–101, January 1986.

- [6] M. Kam, X. Zhu, and P. Kalata, "Sensor fusion for mobile robot navigation," *IEEE Trans. Signal Processing*, vol. 85, no. 1, pp. 108–119, January 1997.
- [7] T. M. Cover and A. A. E. Gamal, "Capacity theorems for the relay channel," *IEEE Trans. Inform. Theory*, vol. it-25, no. 5, September 1979.
- [8] P. Gupta and P. R. Kumar, "The capacity of wireless networks," *IEEE Trans. Inform. Theory*, vol. 46, pp. 388–404, March 2000.
- [9] M. Grossglauber and D. N. Tse, "Mobility can increase the capacity of wireless networks," in *IEEE INFOCOM, Anchorage, Alaska*, April 2001.
- [10] M. Gastpar and M. Vetterli, "On the capacity of wireless networks: The relay case," in *IEEE Infocom*, 2002.
- [11] P. Gupta and P. R. Kumar, "Towards an information theory of large networks: An achievable rate region," *IEEE Trans. Inform. Theory*, vol. 49, no. 8, August 2003.
- [12] A. Sendonaris, "Advanced techniques for next-generation wireless systems," Ph.D. dissertation, Rice University, Houston, Texas, August 1999.
- [13] J. N. Laneman and G. W. Wornell, "Energy-efficient antenna sharing and relaying for wireless networks," in *Wireless Communications and Networking Conference, WCNC*, WCNC, Ed., vol. 1. IEEE, 2000, pp. 7–12.

- [14] —, “Distributed space-time-coded protocols for exploiting cooperative diversity in wireless networks,” *IEEE Trans. Inform. Theory*, vol. 49(10), pp. 2415–2425, October 2003.
- [15] A. Ribeiro, X. Cai, and G. B. Giannakis, “Symbol Error Probabilities for General Cooperative Links,” in *IEEE Transactions on Wireless Communications*, vol. 4, May 2005, pp. 1264–1273.
- [16] M. Abdallah and H. Papadopoulos, “Sequential Signal Encoding and Estimation Strategies for Wireless Sensor Networks,” in *Proc. Int. Conf. Acoust. Speech, Signal Processing*, May 2001.
- [17] B. Chen, R. Jiang, T. Kasetkasem, and P. K. Varshney, “Channel aware decision fusion in wireless sensor networks,” in *IEEE Trans. Signal Processing*, Dec 2004, pp. 3454– 3458.
- [18] D. Chen and J. N. Laneman, “Modulation and Demodulation for Cooperative Diversity in Wireless Systems,” *IEEE Trans. Wireless Comm.*, June 2005.
- [19] J. N. Laneman, D. N. C. Tse, and G. W. Wornell, “Cooperative diversity in wireless networks: Efficient protocols and outage behavior,” *IEEE Trans. Inform. Theory*, vol. 50, pp. 3062–3080, Dec. 2004.
- [20] P. Viswanath, D. Tse, and R. Laroia, “Opportunistic beamforming using dumb antennas,” vol. 48, June 2002, pp. 1277–94.

- [21] J. Chen, L. Yip, J. Elson, H. Wang, D. Maniezzo, R. Hudson, K. Yao, and D. Estrin, “Coherent acoustic array processing and localization on wireless sensor networks,” in *IEEE Proceedings*, vol. 91, August 2003, pp. 1154–1162.
- [22] G. Barriac, R. Mudumbai, and U. Madhow, “Distributed Beamforming for Information Transfer in Sensor Networks,” in *Information Processing in Sensor Networks, IPSN’04*, April 2004.
- [23] M. Abdallah and H. Papadopoulos, “Beamforming Algorithms for Amplify-and-Forward Relaying in Wireless Networks,” in *43rd Allerton Conf. Commun. Control Comput.*, Oct. 2005.
- [24] —, “Beamforming Algorithms for Information Relaying in Wireless Sensor Networks,” in *Submitted to IEEE Transactions on Signal Processing*, March 2006.
- [25] Z. Wang and G. B. Giannakis, “A Simple and General Parametrization Quantifying Performance in Fading Channels,” in *tcomm*, vol. 51, August 2003, pp. 1389–1398.
- [26] M. Abdallah and H. Papadopoulos, “Beamforming Algorithms for Decode-and-Forward Relaying in Wireless Networks,” in *Conference of Information Sciences and Systems (CISS’05)*, March 2005.

- [27] A. Sendonaris, E. Erkip, and B. Aazhang, "User Cooperation Diversity - Part II: Implementation Aspects and Performance Analysis," in *IEEE Trans. Commun.*, vol. 51, Nov 2003, pp. 1939–1948.
- [28] J. G. Proakis, *Digital Communications*, 4th ed. McGrawHill, 2001.
- [29] N. Patwari, A. O. Hero, M. Perkins, N. S. Correal, and R. J. O'Dea, "Relative Location Estimation in Wireless Sensor Networks," in *IEEE Trans. on Signal Processing*, Nov 2002.
- [30] M. Youssef, M. Abdallah, and A. Agrawala, "Multivariate Analysis for Probabilistic WLAN Location determination systems," in *MobiQuitos*, July 2005.
- [31] Y. Gwon, R. Jain, and T. Kawahara, "Robust Indoor Location Estimation of Stationary and Mobile Users," in *IEEE INFOCOM*, March 2004.
- [32] C. R. Lin and M. Gerla, "Adaptive Clustering for Mobile Wireless Networks," in *IEEE J. Select. Areas Commun.*, vol. 15, September 1997, pp. 1265–1275.
- [33] A. D. Amis, R. Prakash, T. H. P. Vuong, and D. T. Huynh, "Max-Min D-Cluster Formation in Wireless Ad Hoc Networks," in *IEEE INFOCOM*, March 2000.
- [34] O. Younis and S. Fahmy, "HEED: A Hybrid, Energy-Efficient, Distributed Clustering Approach for Ad Hoc Sensor Networks," in *IEEE Trans. on Mobile Computing*, vol. 3, Oct-Dec 2004, pp. 366–379.